sys anal

1019

# FINAL REPORT
# SMALL SOLAR ELECTRIC SYSTEM COMPONENTS DEMONSTRATION

AUGUST 20, 1980

WORK PERFORMED UNDER JPL CONTRACT 955279

FOR

JET PROPULSION LABORATORY
CALIFORNIA INSTITUTE OF TECHNOLOGY
4800 Oak Drive
Pasadena, CA 91103

SANDERS ASSOCIATES, INC.
ENERGY SYSTEMS CENTER
95 Canal Street
Nashua, New Hampshire 03061

## ABSTRACT

In order to be economically viable, distributed point focus air Brayton systems will require highly effective recuperators. The use of recuperators with effectiveness of .9 can reduce the energy required to run the Brayton engine by a factor of two or more. This translates into a substantial cost reduction when the reduced size of the parabolic dish, receiver and tracking and support mechanism are taken into account.

Metal recuperators can be designed to provide high effectiveness. These devices, however, seriously reduce the mean-time-between failures for the Brayton systems because the thermal stresses experienced by the recuperator exceed the creep stress of the metals used in the construction. After a limited number of cycles the stress induced distortion leads to metal fatigue and failure. Sanders has proposed a Brayton conversion system where the recuperator is replaced by a pair of thermal storage modules (TSM's) and associated valving, which act as a regenerator. By operating these TSM 's at low air velocities, a sharp temperature gradient (thermocline) can be propagated through the ceramic. The use of this thermocline mode of operation allows the design of a recuperator system with an effectiveness over .9 and with very low pressure drops. An air cycle Brayton system using these TSM's as valved regenerators will have a thermal-to-mechanical conversion efficiency of 40%.

The goals of this program were to demonstrate the thermocline propagation in the TSM's, to measure the steepness of the thermocline, and to measure the effectiveness of the TSM's when used in a Brayton system. In addition, a high temperature valve suitable for switching the TSM at temperatures to 1700°F was to be designed, built and tested.

A thermal storage module was designed, built and tested. Test results confirm the existence of a sharp thermocline under design conditions. The thermal profile was steeper than expected and was insensitive to air density over the range of the test conditions;

| | |
|---|---|
| Air Flow | 0.2 - 0.6 lb/sec |
| Inlet Temperature | 100°F - 1700°F |
| Pressure | 1 - 3 atmospheres |

Experiments were performed which simulated the airflow of a small Brayton engine, 20 KWe, having a pair of thermal storage modules acting as efficient recuperators. Low pressure losses, averaging 12 inches of water, and high effectiveness, 93% for a 15 minute switching cycle, were measured. The insulation surrounding the ceramic core limited thermal losses to approximately 1 KWt.

The hot valve was operated over 100 cycles and performed well at temperatures up to 1700$^{o}$F.

Additional testing is required to characterize the high mass flow performance of the TSM's to determine where the onset of thermocline degradation occurs. In addition, more cycling is required on the high temperature valve to determine how the valve will perform under extended service conditions and to measure the advantages and problems associated with different high temperature coatings on the sealing surfaces.

TABLE OF CONTENTS

TABLE OF CONTENTS (Cont'd.)

## LIST OF ILLUSTRATIONS

LIST OF ILLUSTRATIONS (Cont'd.)

LIST OF ILLUSTRATIONS (Cont'd.)

## LIST OF TABLES

## SECTION 1
## INTRODUCTION

Since the onset of the oil crises in 1973, there has been a great interest in both solar electric systems and in high efficiency fossil fired generation. Point focus distributed solar thermal systems using recuperated open cycle Brayton engines have the potential for providing an economically viable alternative to conventional fossil fired systems. In addition, the efficiency of a fossil fired Brayton cycle system can be significantly increased by lowering the pressure ratio and adding a recuperator with a high effectiveness. A well designed recuperated Brayton engine can yield efficiencies over 40% for 20KW sizes and over 50% for machines delivering above one MW.

Recuperators having a long service life are not available. The metal recuperators have a limited life caused by metal fatigue. The exhaust temperature of a Brayton engine approaches the inlet temperature during start-up. This temperature ~ $1700^{o}F$ is applied to the recuperator inlet resulting in thermal expansion which exceeds the elastic limit of the material causing a permanent deformation each time the machine is started. After a limited number of cycles, failure occurs.

The solar system described in this report is based on an Air Cycle Brayton Engine recuperated with a novel ceramic Thermal Storage Module (TSM). The TSM is designed to allow the ceramic core to move in response to thermal stresses. This movement eliminates the failure mechanism of metal recuperators and should allow the recuperator to have a long service life.

The Sanders thermal storage module performs two distinct functions in the Brayton cycle, Figure 2-2. The first function is to store the thermal energy collected by the solar receiver. In this capacity it is paired with another module and each is switched in sequence between the Brayton power loop and the solar collection loop. While in the solar collection loop it is charged with hot air from the solar collector. When fully charged it is switched into the Brayton power cycle to heat the turbine air. The test program simulated the solar collection cycle by measuring the TSM performance at temperatures to 1700$^{o}$F under pressurized and unpressurized conditions. Under these conditions the thermocline passes completely through the TSM and the module is used to its maximum thermal storage capacity.

The second function of the TSM is to perform the recuperation function in a low pressure ratio Brayton engine. In this capacity a pair of TSM's alternately add heat to the compressor exhaust air and recover heat from the turbine exhaust. To optimize recuperator effectivenes, the switching times occur before the TSM has been either fully charged or discharged. Furthermore, an optimized system might well have different size storage modules for the storage of solar energy and for the Brayton recuperation function. The TSM design, Figure 2-4, consists of an insulated, pressurized shell approximately 1.2 meter in diameter and 2.2 meters high (4 ft. by 7 ft.). Each TSM contains internal air ducts and a large array of cordierite refractory storage material. The ceramic storage material has a honeycomb structure which forms a large number of individual flues through which air can flow. Heat is alternately stored in or removed from the ceramic during the various phases of the operating cycle. Thermal energy is stored as sensible heat in solid materials and later is delivered at a constant temperature, as required for efficient turbine operation. This is accomplished by a combination of the following methods: (a) a step propagation (thermocline) effect, and (b) automatically activated valves which switch the TSM positions to maintain high system efficiency. The thermal step effect occurs when an airflow channel is in close thermal contact with an adjacent channel of substantial thermal mass. If the coupling between airstream and solid is sufficiently strong and the individual elements comprising the total thermal mass are weakly coupled, an input step in temperature can propagate an identifiable front or thermocline.

The program was divided into three phases. Phase I was a preliminary sizing of the TSM to insure that the experimental model would not be sized so small that surface effects (thermal losses through the walls) would distort the data obtained on the thermocline propagation.

During Phase II a complete Solar Brayton System was designed. The design considered the impact of the receiver,heat transport system, TSM's for transferring the energy from the solar loop to the engine and TSM's as the recuperator. The system was sized and the required TSM's were designed. The calculated thermocline propagation characteristics were used to predict the effectiveness of the TSM's when used as a recuperator. Operating characteristics for each of the TSM's were determined and a test program was designed to simulate the system operation for each TSM position.

During Phase III, one TSM and one four way valve were built and assembled into a test system consisting of a propane fired burner, controls and instrumentation needed to test the performance of both the TSM and the valve. A series of tests were run to measure the TSM performance characteristics and the effectiveness of a TSM pair when used as a recuperator. Various switching periods and flow rates were used to determine the sensitivity to operating conditions.

This report details the design effort, the details of the experimental system, the test results, and recommendations for additional testing.

SECTION 2
SYSTEM DESCRIPTION

## 2.1 DESIGN CONCEPT

The Small Solar Power system designed under Phase II uses a Brayton engine and 36' diameter concentrator as shown in Figure 2-1. Novel features are:

- Heat is transferred from the focal point of the collector to the thermal storage area in the base of the collector using air as the working fluid.
- Heat collection and power generation are accomplished in separate, independent air flow loops.
- Since heat to the power generation system is always delivered from storage, the power generation system is decoupled from the solar power input which can be efficiently collected even with deep fluctuations of the insolation.
- The system rejects waste heat directly to the ambient thus eliminating the need for water cooling.
- The use of thermal storage modules for storage and recuperation significantly increases the efficiency of the system.

### 2.1.1 System Design Concept

Figure 2-2A is a schematic of the concept for power generation. A set of four thermal storage modules (TSM) is switched in pairs between Positions I and IIA and between positions IIB and III, Figure 2-2B. The first pair transfers solar energy to the engine, while the second pair act as a recuperator.

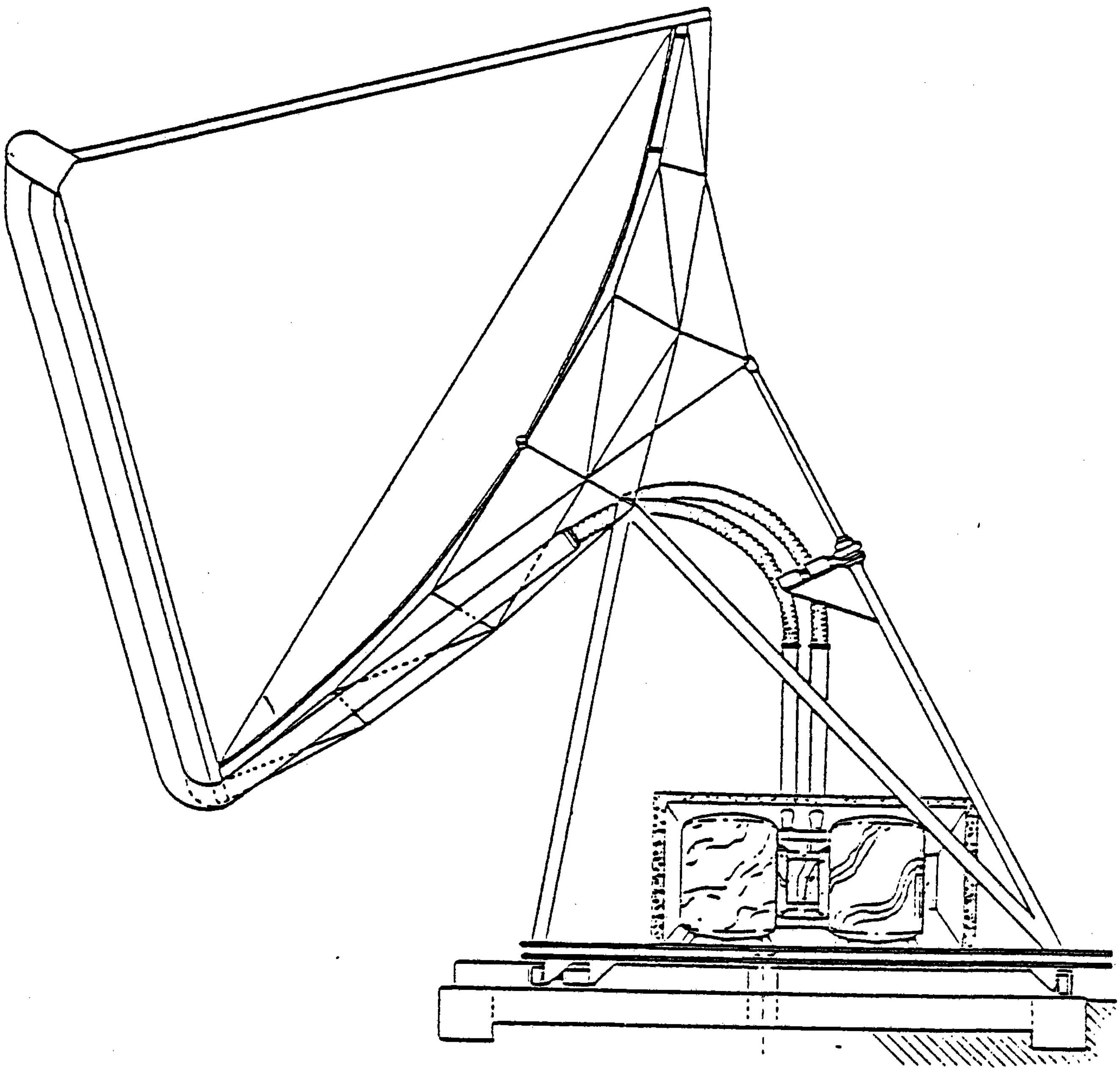

FIGURE 2-1

SOLAR ELECTRIC SYSTEM
WITH 4 TSM POWER MODULE

I - IIA - I
IIB - III - IIB

4 TSM WITH PAIRED SWITCHING

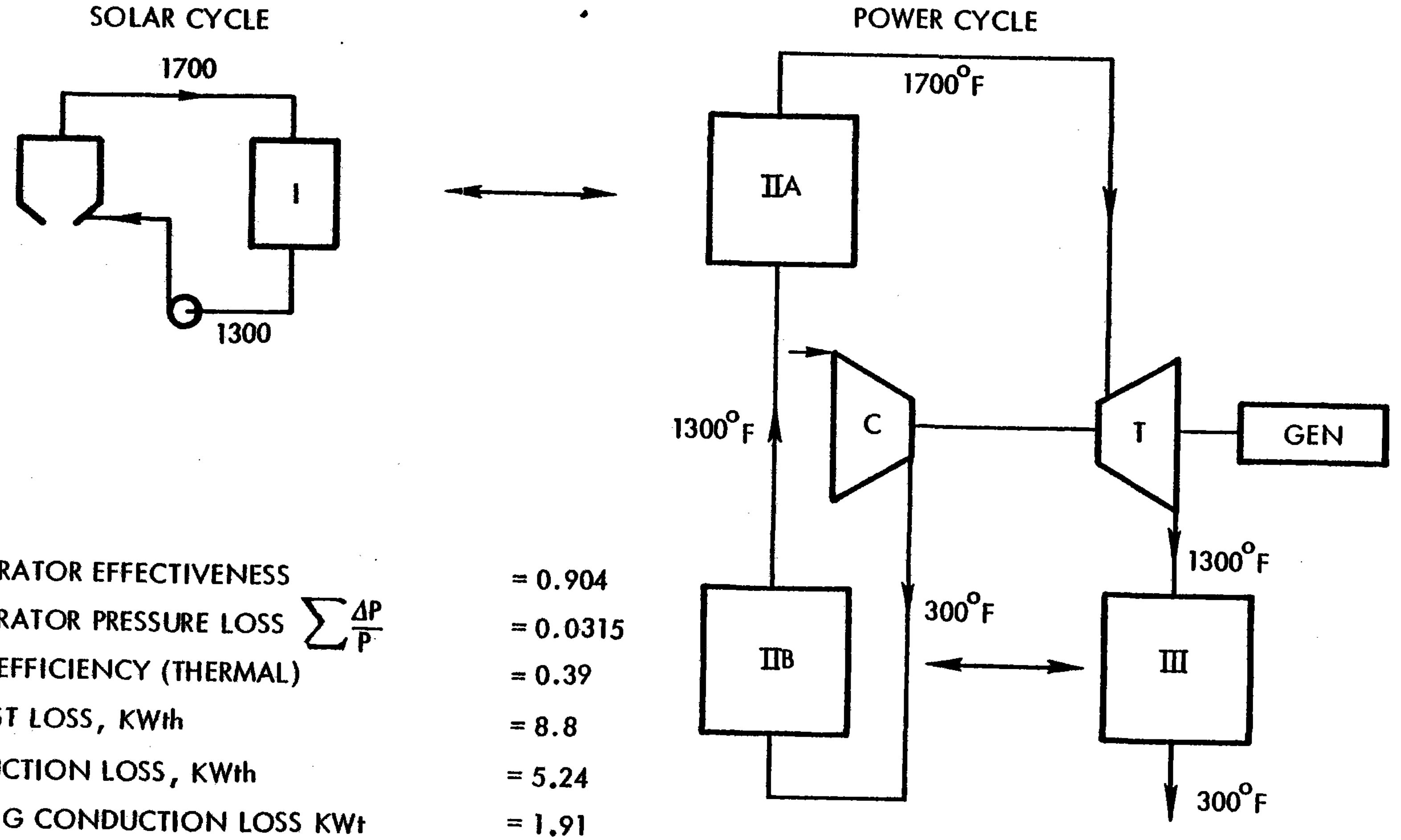


| | |
|---|---|
| RECUPERATOR EFFECTIVENESS | = 0.904 |
| RECUPERATOR PRESSURE LOSS $\sum \frac{\Delta P}{P}$ | = 0.0315 |
| CYCLE EFFICIENCY (THERMAL) | = 0.39 |
| EXHAUST LOSS, KWth | = 8.8 |
| CONDUCTION LOSS, KWth | = 5.24 |
| DUCTING CONDUCTION LOSS KWt | = 1.91 |
| TOTAL HEAT ADDED, KWth | = 69.3 |

04259-18

FIGURE 2-2A

**BRAYTON CYCLE ANALYSIS**

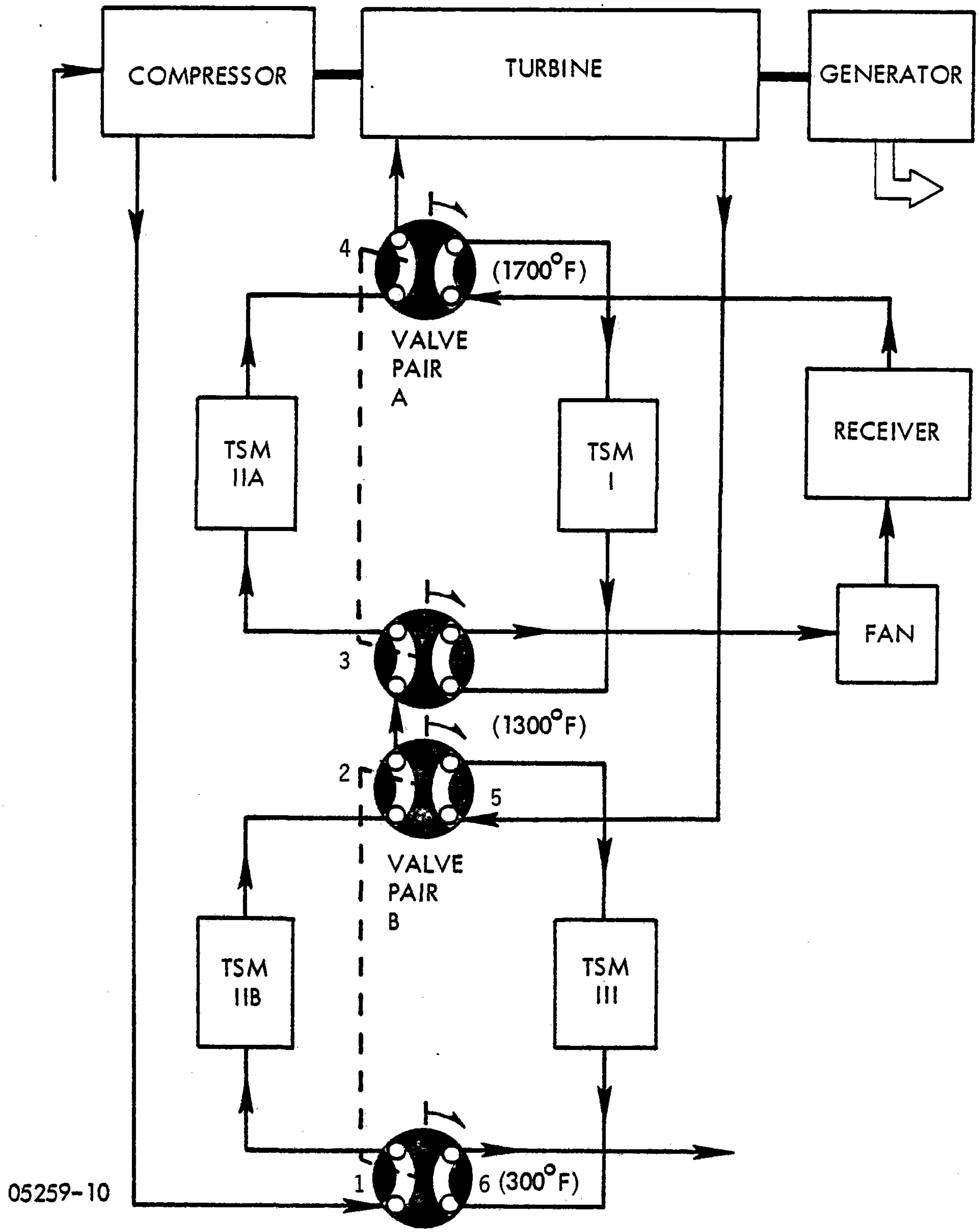


FIGURE 2-2B

# SOLAR POWER SYSTEM SCHEMATIC

The solar Brayton power module is shown in Figure 2-3. All power generation and storage functions are accomplished from a centrally located platform on the ground. Only the receiver is located at the focus of the concentrator and the air is ducted between the receiver and the power module via flexible insulated ducts.

The TSM selected for this experiment consists of an insulated, pressurized shell approximately 4 feet in diameter and 6 feet high. Each module contains internal air ducts in a porous ceramic matrix. The ceramic material forms a large number of individual air passages. Heat is alternately stored in or removed from the ceramic during the various phases of the operating cycle. Thermal energy is stored as sensible heat in the ceramic material at a constant temperature, as required for efficient turbine operation.

The heat collection loop transfers the collected energy to a sensible heat storage module, TSM I in Figure 2-2A. When this module is fully charged, it is valved into the power generation loop (TSM IIA) to run a low pressure ratio Brayton gas turbine generator.

The Brayton engine uses a pair of TSM's to act as periodic heat exchangers between the nominal temperatures of $300^{\circ}F$ and $1300^{\circ}F$. One of the TSM's (Position III) recovers waste heat from the turbine when the other TSM is adding heat to the compressor exhaust (Position IIB).

During the design analysis phase of this program the Williams Research Corp. Brayton engine was identified as the most appropriate selection for the system design because of its availability and low cost potential. This engine designated WR-34-14 when modified for the solar application has the following characteristics:

| | |
|---|---|
| Max. Turbine Inlet Temperature | $1700^{\circ}F$ |
| Engine Shaft Speed | 98,427 rpm |
| Output Shaft Speed | 3600 rpm |
| Compressor Pressure Ratio | 2.88 |
| Output Shaft Power | 27 HP |
| Fuel Flow (Propane) | 30 lb/hr |
| Thermal to Mechanical Efficiency | 12% |

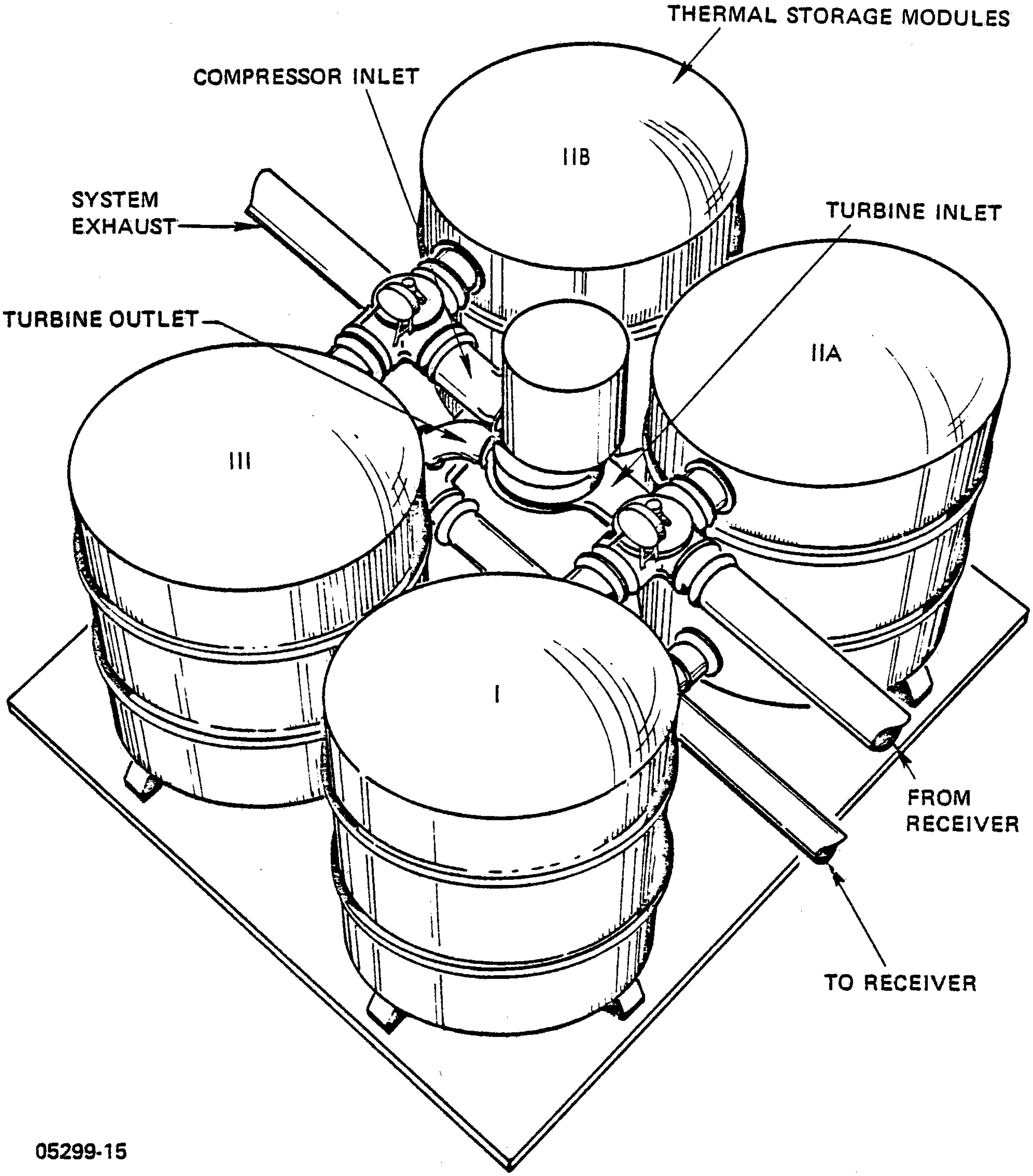


FIGURE 2-3

SOLAR BRAYTON POWER MODULE

| | |
|---|---|
| Compressor Exhaust Temperature (50$^{O}$F day) | 295$^{O}$F |
| Turbine Exhaust Temperature | 1293$^{O}$F |
| Airflow | 0.423 lb/sec |

This engine was used as the basis for the system design and determined the temperature ranges over which thermocline measurements were to be made.

Two thermal storage modules containing a ceramic matrix are used as a periodic regenerator. When air velocity entering the ceramic matrix is less than 10 ft/sec, a sharp thermocline develops which allows for efficient engine operation. For instance, the pair of TSM's used as recuperator have an effectiveness in excess of 90%. This modification allows an engine efficiency for the recuperated version to increase to 40% compared with the 12% for the unrecuperated version.

### 2.1.2 TSM Design Concept

The energy storage and recuperator system, schematically defined in Figure 2-2A, is composed of the following subassemblies:

- Thermal Storage Modules (TSM)
- Inlet and Outlet Manifolds
- Automatic Valving
- Valve Drive Mechanism
- Controls and Sensors

The concept uses four equal size TSM's physically oriented as shown in Figure 2-3, two to transfer the solar collected energy to the turbo machinery, and two to act as a recuperator to recover the energy in the turbine exhaust.

The TSM is a heat exchanger device similar to a checker stove used by the glass and steel industries to supply large quantities of air at constant high temperatures. The TSM design, Figure 2-4, consists of an insulated, pressurized shell approximately 1.2 meters in diameter and 2.2 meters high (4 ft. x 7 ft.) containing internal air ducts and cordierite refractory storage material. The ceramic storage material

SANDERS ASSOCIATES, INC.
ENERGY SYSTEMS CENTER

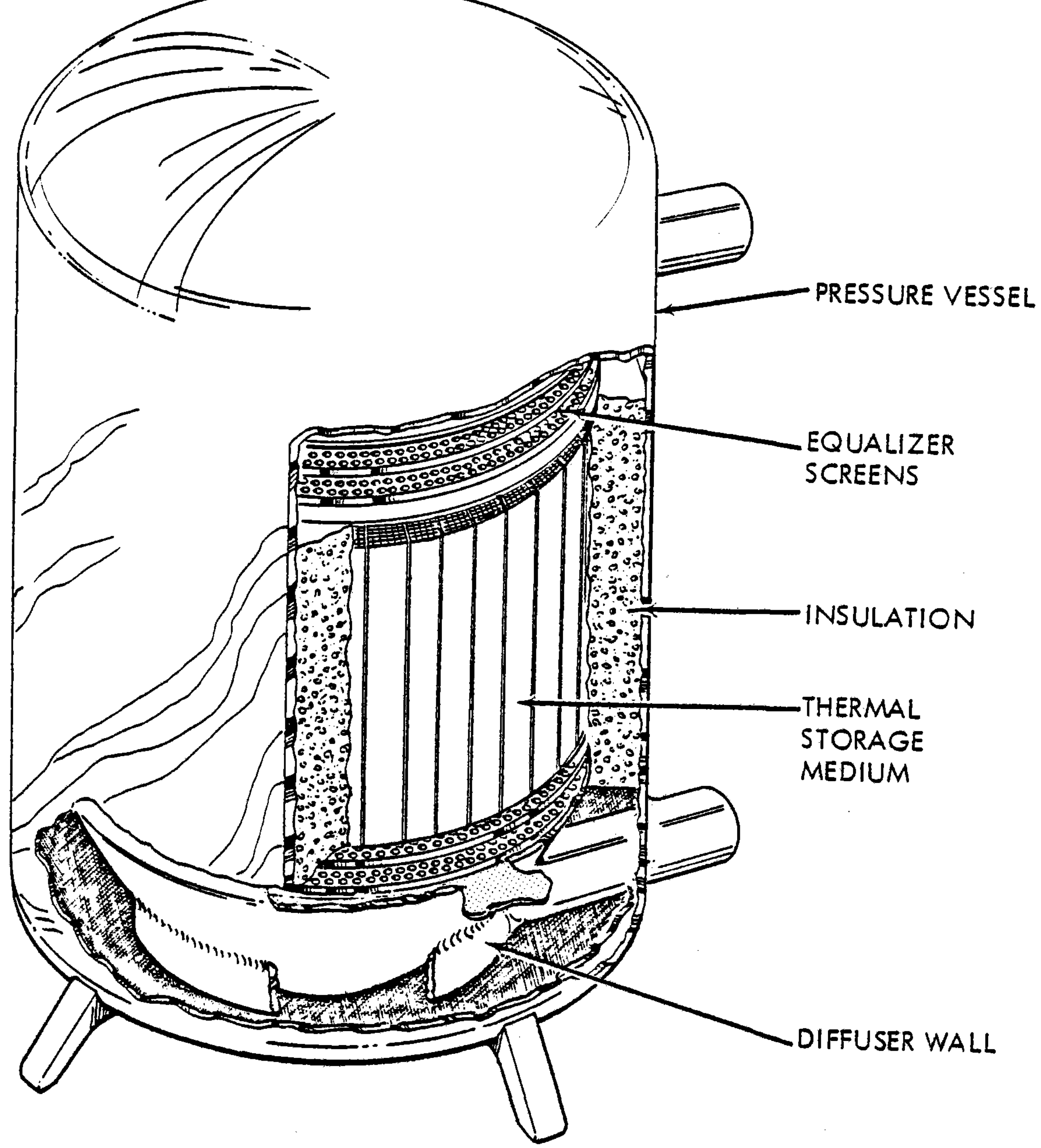


05309-37

FIGURE 2-4

THERMAL STORAGE MODULE (TSM)
WITH RADIAL SIDE ENTRY

has a honeycomb structure which forms a large number of individual flues through which air can flow. Heat is alternately stored in or removed from the ceramic during the various phases of the operating cycle.

During operation, a TSM's temperature history cycles through the following positions:

I. Raised from 1300°F to 1700°F while accepting heat from the solar collector.

IIa. Reduced from 1700°F to 1300°F as energy is used to drive the turbine.

IIb. Reduced from 1300°F to 300°F when transferring the waste heat to the turbine loop and preheating the air going to TSM IIa.

III. Raised from 300°F to 1300°F while accepting waste heat from the turbine.

Thermal energy is stored as sensible heat in solid materials and later is delivered at a constant temperature, as required for efficient turbine operation. This is accomplished by a combination of the following methods, (a) a step propagation (thermocline) effect, and (b) automatically activated valves which switch the TSM positions to maintain high system efficiency. The thermal step effect occurs when an airflow channel is in close thermal contact with an adjacent channel of substantial thermal mass. If the coupling between airstream and solid is sufficiently strong and the individual elements comprising the total thermal mass are weakly coupled, an input step in temperature can propagate an identifiable front or thermocline.

An array of high temperature thermocouples distributed through the storage stoves provides useful information on the status of charge as well as position and thickness of the thermocline. In addition, the temperature data provides notification of cycle end points and can be used to activate the automatic valve switching sequence.

The key to the high system efficiency is the TSM which allows the recovery and storage of turbine exhaust heat and its re-introduction into the inlet air stream with very high effectiveness and low pressure drop. The high effectiveness is achieved by the propagation of a sharp thermocline (a region within the ceramic core which contains the thermal gradient between the hot and cold regions).

The modules designed for this program, Figure 2-4, have a ceramic core, a diffusing section at the top and bottom, air passages with a hydraulic diameter of .044 inches, and 12,000 square feet of heat transfer surface area. Five inches of Johns-Mansville cerafiber insulation surrounds 1 inch of Min-K insulation which encloses the ceramic core to minimize thermal conduction losses.

The thermal step effect occurs when an airflow channel is in close thermal contact with an adjacent channel of substantial thermal mass. If the coupling between airstream and solid is sufficiently strong and the individual elements comprising the total thermal mass are weakly coupled, an input step in temperature can propagate an identifiable front or thermocline.

The thermal mass of the surrounding insulation has been shown to affect the thermocline slope. The seriousness of this effect depends on the ratio of insulation mass to matrix mass. The larger the diameter of storage, the less pronounced the influence of the insulation material.

### 2.1.3 Hot Valve Design Concept

The switching function needed to reverse the flow between a pair of TSM's is accomplished by utilizing two four-way valves. Since the switching should occur simultaneously, the simplest and most reliable method is to use a single actuator connected by a shaft to the two four-way valves. The concept for a four-way valve, Figure 2-5, consists of a rotatable spherical center section with two $90^{o}$ channels cast within the sphere. Spring mounted conical seals ride on the surface of the ball as it turns and provides a gas seal. A cross-sectional view, Figure 2-6, shows the flow paths within the ball. One of these valves was evaluated as part of the TSM testing.

SA SANDERS ASSOCIATES, INC.
ENERGY SYSTEMS CENTER



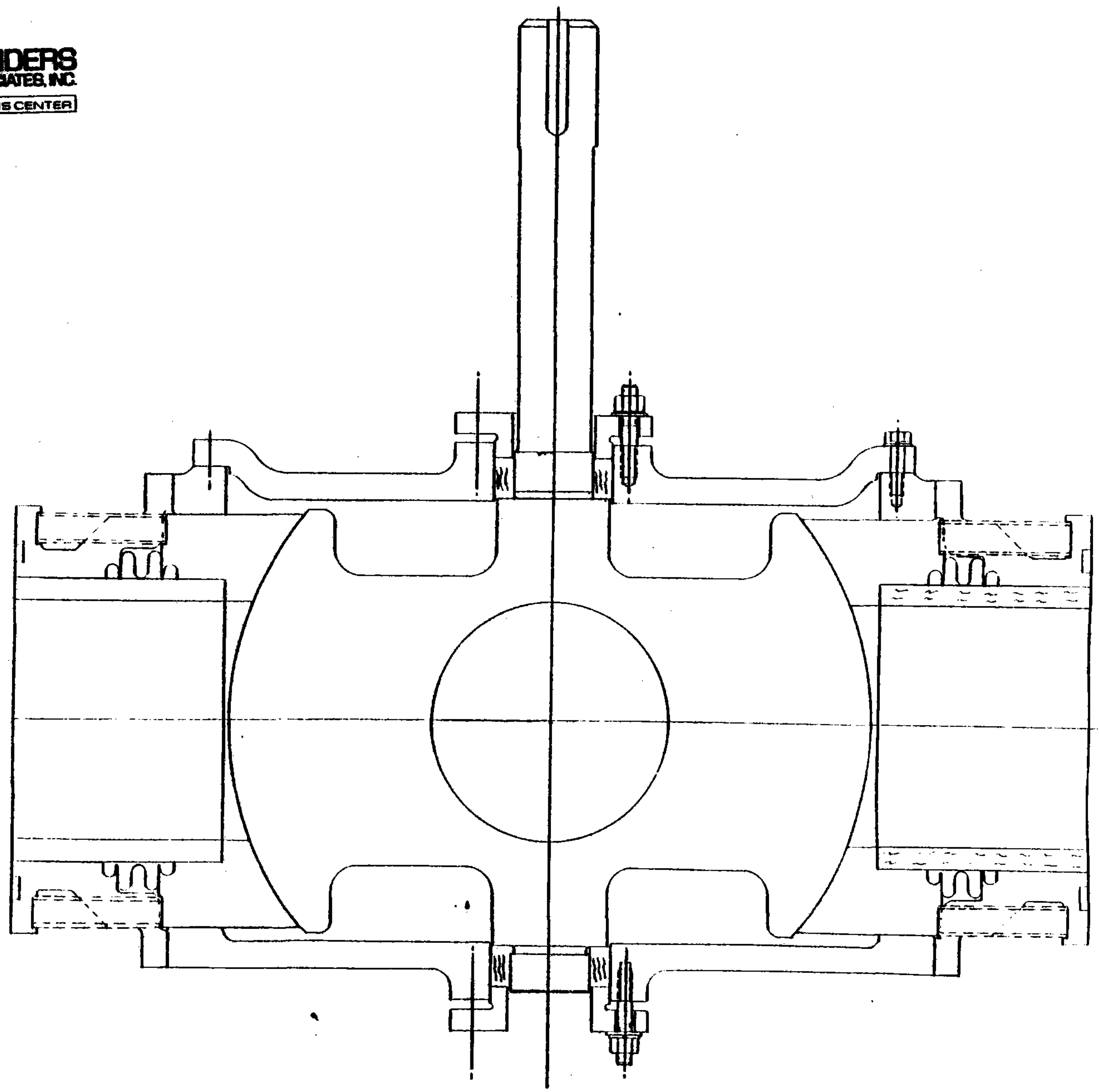

05309-38

FIGURE 2-5

# FOUR WAY VALVE

SANDERS ASSOCIATES, INC.
ENERGY SYSTEMS CENTER

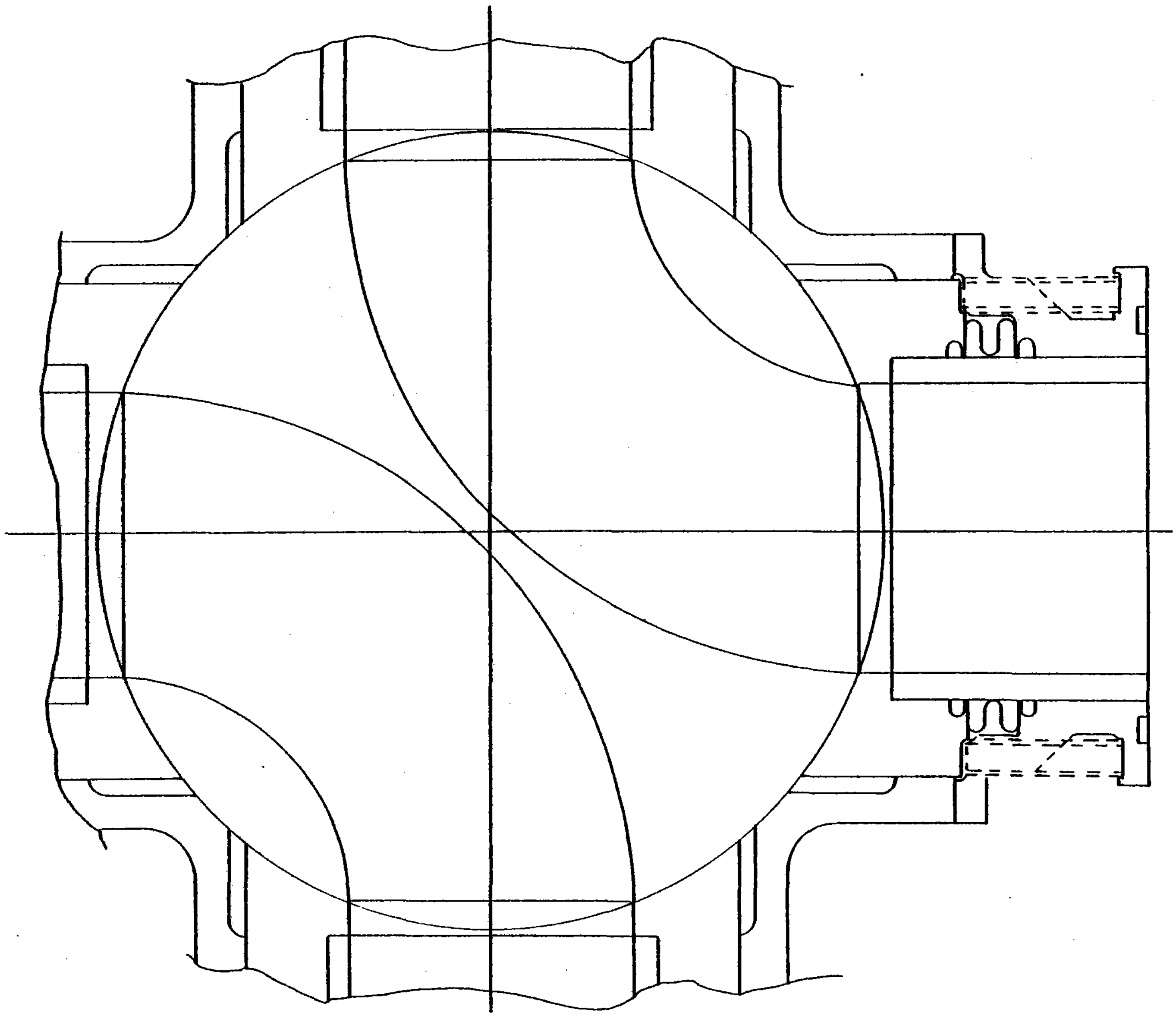

05309-40

FIGURE 2-6

VALVE CROSS SECTION SHOWING FLOW PATHS

## 2.2 TSM ANALYSIS

The thermal analysis system developed at Sanders, using ANSYS* software, was used in two ways as follows:

1) To support the detail design of the TSM by simulating the performance of the TSM for several promising potential configurations.

2) To support the overall system design tradeoffs for several simulated Brayton engine recuperation cycles to determine system performance.

The approximations in the analysis replace a whole storage module with a single fictitious pipe having an inside perimeter equal to the total perimeter of the actual tube bundle. The effective hydraulic diameter is the same as the average cell in the honeycomb; the wall mass per unit length is the same as the total honeycomb mass per unit length. The insulation is in contact with the outside of this pipe. For numerical analysis, the heat transfer equations are solved at discrete nodes along the axis to yield temperatures and heat flow results.

A typical thermocline representation in the TSM is shown in Figure 2-7, where the temperature variation with time is shown for 3 locations in the TSM core. The steeper these curves are, the more efficient the storage system. In this curve the total thermal gradient occurs within less than half the core length.

Figure 2-7 shows the thermal response of the core as developed by the analytical model introduced at 1295°F and 295°F (charge and discharge cycle respectively). The time required for the thermocline to pass through the TSM is 17.5 minutes regardless of the flow direction, i.e. charge or discharge cycle.

On the basis of these computations and the desire to have a conservative design for the first full scale test, a cylinder of honeycomb ceramic matrix 36" in diameter

---

*ANSYS - A Computer Code for Finite Element Analysis. Developed by: Swanson Analysis Systems, Inc., Elizabeth, Pa.

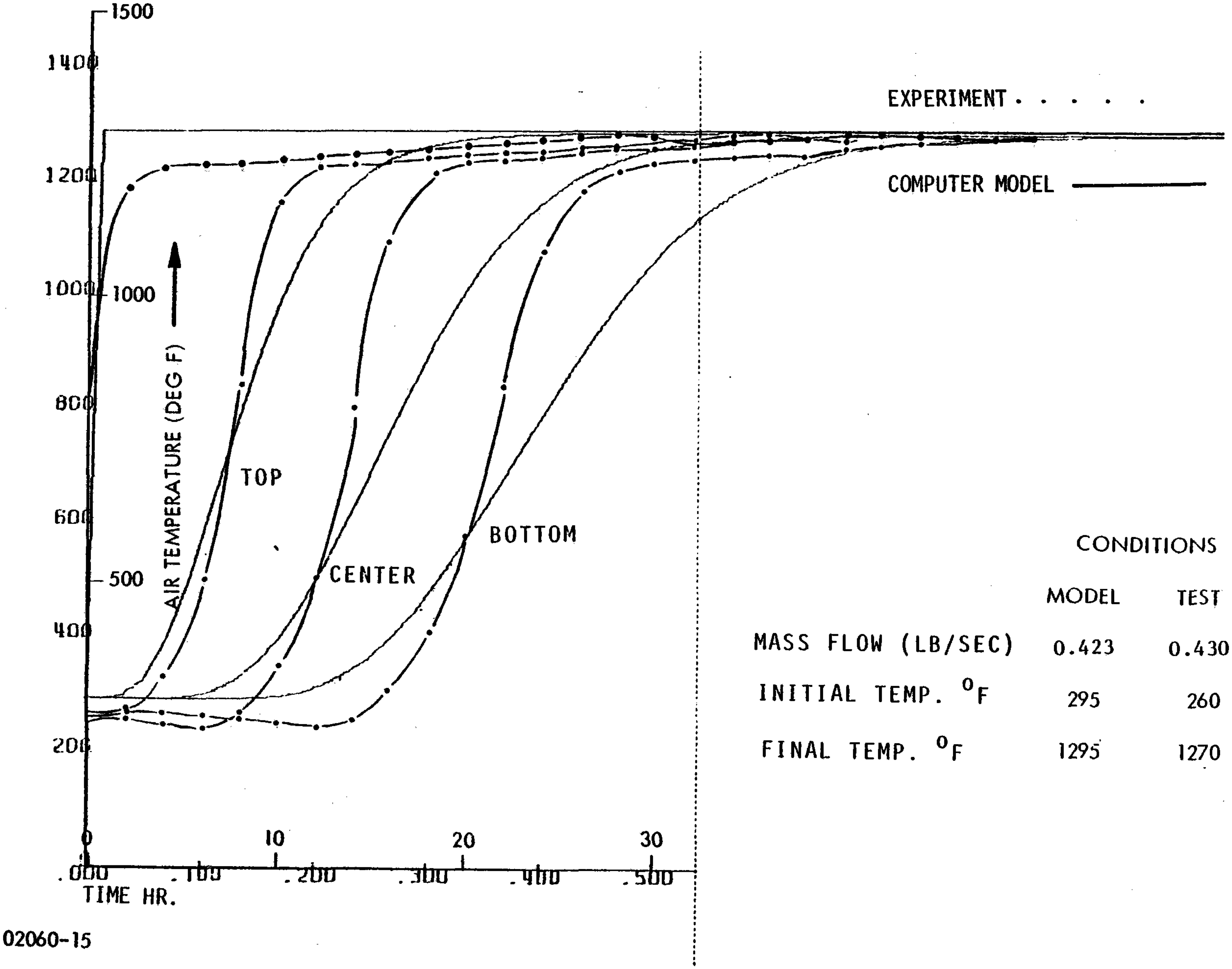


FIGURE 2-7

**'SINGLE SHOT' THERMOCLINE PROPAGATION TEST**

and 31" long was selected for construction. This size was selected to limit airflow velocities to less than 10 ft/sec into the TSM and to provide 15 minutes of storage time between switching points.

When a pair of TSM's are operated as a periodic heat exchanger for a Brayton cycle engine, an optimum cycle time must be selected for switching air flow from position IIB, pressurized air entering the bottom at 295$^{o}$F, to position III, unpressurized air entering the top at 1295$^{o}$F. This is determined using a simulation program, which uses the final conditions of one cycle to initialize the next cycle. Many cycle simulations are needed before a stable oscillating thermal profile has been established mathematically. Only at this point can the effectiveness be determined. By making many runs with different switching times, the switching time which leads to the highest effectiveness can be determined.

The effectiveness of any heat exchanger is a measure of how well it can transfer energy from one heat flow path to another. In the case of the TSM pairs acting as a heat exchanger in the Brayton cycle, the effectivness is defined as:

$$\varepsilon = \frac{Q_{TE} - Q_L}{Q_{TE}}$$

where: $Q_{TE}$ = Turbine exhaust energy at temperatures above the compressor exhaust temperature.

$Q_L$ = Energy exhausted to atmosphere at temperature above the compressor exhaust temperature + conduction wall losses.

This information can be readily obtained by integrating the areas under the thermocline curves as represented in Figure 2-8. After sufficient cycling, the cycle conditions for the TSM reach a steady state and the exhaust power remains constant from cycle to cycle. Having the compressor output temperature as the datum, the thermocline curves are integrated over the cycle time to arrive at the effectiveness of the storage modules by the following expression:

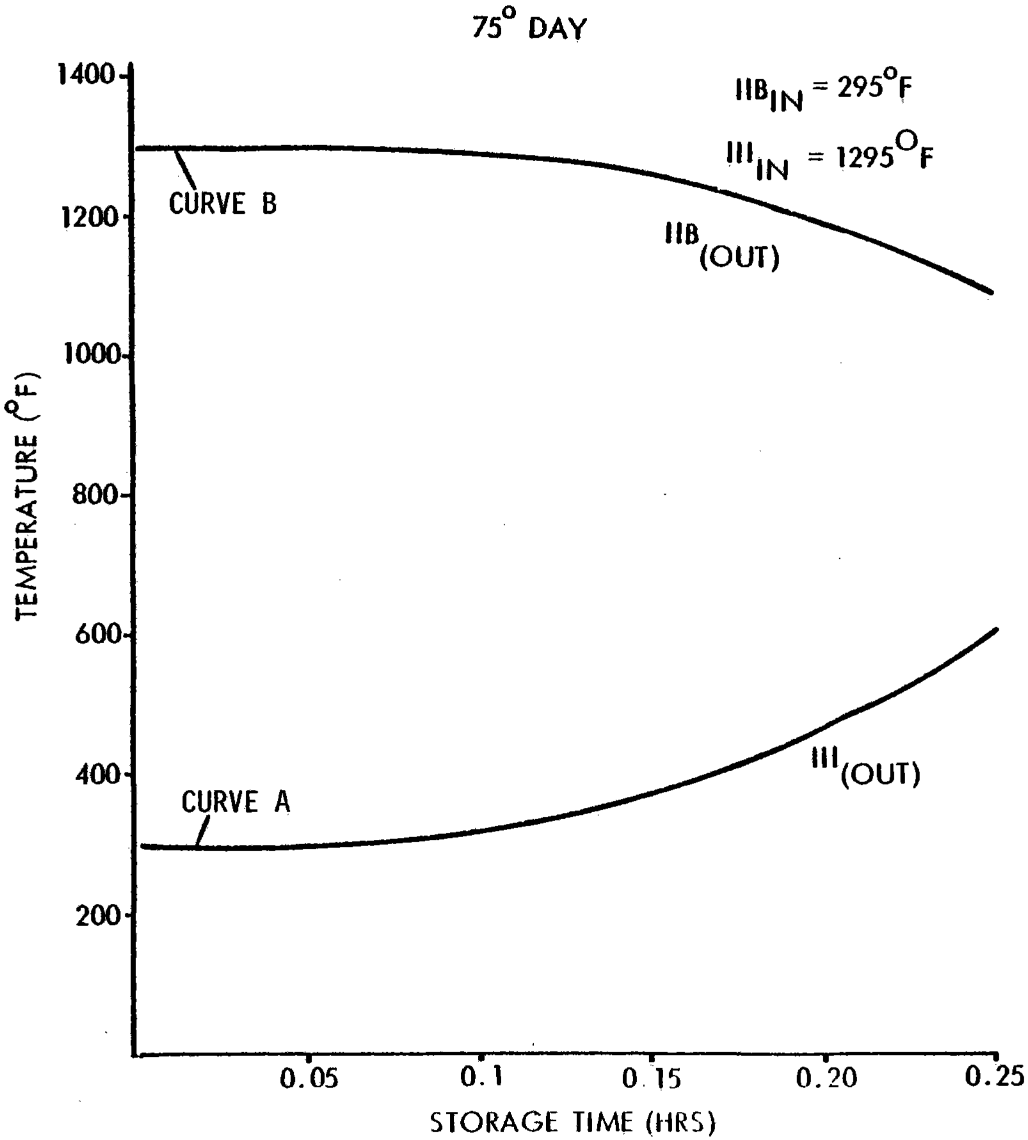


FIGURE 2-8

CALCULATED THERMAL PROFILES FOR STORAGE MODULES

$$\varepsilon = \frac{\dfrac{\int T_{H_o}\,dt}{\int dt} - \dfrac{\int T_{C_o}\,dt}{\int dt}}{\dfrac{\int T_{H_i}\,dt}{\int dt} - \dfrac{\int T_{C_i}\,dt}{\int dt}} = \frac{T_{H_o} - T_{C_o}}{T_{H_i} - T_{C_i}}$$

where: $T_{H_o}$ = Temperature of the outlet air in position IIB.

$T_{H_i}$ = Temperature of the inlet air in position III.

$T_{C_i}$ = Temperature of the inlet air in position IIB.

$T_{C_o}$ = Temperature of the exhaust air in position III.

Integration is carried out over the cycle time (e.g. 15 minutes).

The curves of Figure 2-8 represent the sixth cycle of 15 minutes simulated switching. Curve A represents the output of the TSM in Position III, Figure 2-2, and Curve B represents the IIB position. In the Brayton cycle this series of temperature profiles represents a recuperator effectiveness of 90%.

Equations and engine performance parameters used in calculating system losses are summarized in Tables 2-1 and 2-2.

## 2.3 TSM DESCRIPTION

### 2.3.1 Thermal

The thermal storage module is designed to operate at temperatures to 1700°F and pressures to 3 atmospheres with air flow rates from 0.2 lb/sec to 0.6 lb/sec.

Two diffent types of insulation were used within the tank to minimize thermal losses and to protect the outside steel pressure vessel. The first insulation layer, next to the ceramic core, is 1" thick Min-K followed by a 5" layer of cerafiber. The properties of both insulation materials are shown in Table 2-3. The objective in choosing the insulation was to minimize the conduction losses, yet to hold a reasonable size tank. Min-K and cerafiber offer sufficiently low conductivity that

TABLE 2-1
SYSTEM LOSSES

Thermal Exhaust

$$Q_a = \dot{m} \int_{t_1}^{t_2} \left[ \int_{T_{DATUM}}^{T(x)} c_{p_a} (T)\ D\ T \right] dt$$

Compression

$$Q_{comp} = \frac{c_v V}{R} \Delta P$$

where:
$L$ = length
$r$ = radius
$V$ = volume of air in TSM
$c_v$ = 0.1714 BTU/lb $^oF$
$R$ = 53.3 $\frac{ft/lb}{lb\ ^oF}$ (gas constant)

De-compression (Thermal Venting)

$$Q_{VENT} = \frac{P_2 V_2}{R} C_V \left[ 1 - \frac{P_1}{P_2} \right]^{\frac{K-1}{K}}$$

Pressure Drop Losses

$$\Delta P = 4f \frac{L}{D} \rho \frac{V^2}{2g} \quad \text{(psf)}$$

Required Fan Power

$$W_f = \frac{\dot{m}\Delta P}{\rho \eta_{fan}} \quad \frac{1}{(778)\ (3413)} \quad \text{(KWt)}$$

Conduction Losses

$$q = \frac{2\pi KL}{\ell n(\frac{2}{1})} \Delta T \quad \text{cylindrical surface}$$

$$q = \frac{KA\Delta T}{L} \quad \text{for flat surfaces}$$

| | |
|---|---|
| COMPRESSOR INLET TEMP. | 50°F |
| TURBINE INLET TEMP. | 1700°F |
| COMPRESSOR PRESSURE RATIO | 2.92 |
| MASS FLOW RATE | 0.423 (LB/SEC) |
| COMPRESSOR ADIABATIC EFFICIENCY | 0.80 |
| TURBINE ADIABATIC EFFICIENCY | 0.85 |
| ENTHALPY RISE BETWEEN COMPRESSOR OUTPUT & TURBINE INLET | 374.3 BTU/LBS. |

TABLE 2-2

## CONSTANT PARAMETERS FOR CYCLE ANALYSES

## INSULATION PROPERTIES

| | Cerafiber & Cerablanket | MIN-K |
|---|---|---|
| Service Temperature | 2300 | 1800 |
| Color | White | White |
| Density ($lb/ft^3$) | 8 | 20 |
| Chemical Analysis | 47% Alumina<br>52.8 Silica | |
| Compressive Strength (psi) | - | 170 |
| Thermal Conductivity ($BTU\text{-}in/ft^2\text{-}hr\text{-}F$) | | |
| $500^{o}F$ | 0.38 | |
| $800^{o}F$ | 0.8 | 0.28 |
| $1000^{o}F$ | 1.2 | 0.31 |
| $1200^{o}F$ | 1.6 | 0.35 |
| $1400^{o}F$ | 2.0 | 0.41 |
| $1600^{o}F$ | 2.4 | 0.50 |
| Specific Heat (BTU/lb-F) | | |
| 400 | 0.214 | 0.23 |
| 800 | 0.24 | 0.25 |
| 1200 | 0.258 | 0.27 |
| 1600 | 0.268 | 0.27 |

TABLE 2-3

the tank surface temperature will remain below 300$^{o}$F while operating the TSM core at 1700$^{o}$F. The headers of the tank are similarly insulated with 6" of cerafiber.

Heat loss from the TSM is a direct function of core temperature. Since the temperature in the TSM varies as the thermocline passes through the core, steady state conduction losses are calculated for an equilibrium cycle based on the average core temperature.

The TSM core material with overall dimensions of 3' dia. x 31" long is isolated from the containment vessel by 6" of insulation, and undergoes a temperature change as high as 1700$^{o}$F depending on the cycle position of Figure 2-2. When used as a recuperator, each TSM cycles between 300 and 1300$^{o}$F with an average core temperature of 800$^{o}$F. When operated in Position IIA as a heat source, the temperature range is between 1300 and 1700$^{o}$F with an average core temperature of 1500$^{o}$F.

The heat losses through the cylindrical walls and the ends of the TSM pressure vessel are given by:

$$q_{cylinder} = \frac{T_i - T_o}{\frac{\ln r_2/r_1}{2\pi L k_a} + \frac{\ln r_3/r_2}{2\pi L k_b} + \frac{1}{2\pi L\ r_3 h_o}}$$

$$q_{end} = \frac{T_i - T_o}{\frac{1}{Ah_e} + \frac{x_b}{k_b A}}$$

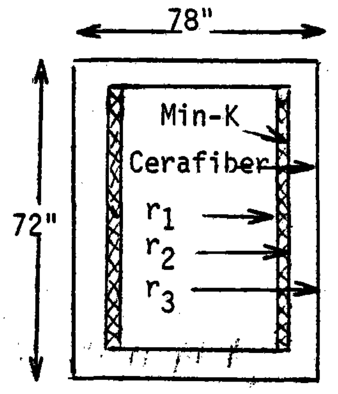


where: $r_1$ = 18 inches
$r_2$ = 19 inches
$r_3$ = 24 inches

$L$ = 6 (ft.)
$x_b$ = 0.5 (ft.)
$h$ = 1 (BTU/hr.ft$^2$F) (natural convection)
$k$ = Conduction coefficients from Table 2-3.

Corresponding to average temperatures of 480$^{o}$F and 875$^{o}$F for Positions IIB and III), the loss during the recuperation cycle is calculated to be 1 kwt and during position I and IIA the loss is 3 kwt.

When the TSM is used in a Brayton cycle system as shown in Figure 2-2, the modules are switched from one position to the next in pairs at 15 minute invervals. The heat transfer rate and stored energy has been calculated in Table 2-4 for the positions in the power loop.

## 2.3.2 Mechanical

The TSM design and associated test setup piping have been designed and fabricated based on ASME pressure vessel codes. Internal insulation in the tank allowed the use of carbon steel in the construction of the pressure vessel.

The minimum required thickness of the pressure vessel is given by:

$$t_m = \frac{PD_o}{2SE - 1.2P}$$

where:

| | | | |
|---|---|---|---|
| where: | $t_m$ | = | Min. required thickness of shell (inches) |
| | P | = | Design pressure = 30 psi |
| | S | = | Max. allowable stress, 13,750 psi |
| | E | = | Longitudinal weld joint factor .85 |
| | D | = | Outside diameter of shell 48" |

Based on these inputs, the minimum required thickness is calculated to be .06". A search on available pressure vessel headers indicated that 0.25" thick units were readily available. The mid section is a 0.25" thick cylindrical piece that interfaces with two spherical headers bolted to the cylinder. Three inch diameter inlet and outlet ports are located on the headers, Figure 2-9. The ceramic core is suspended at the mid section of the tank. Diffusers located in each header have screens and turning ducts designed to provide uniform air velocity into the core regardless of the direction of flow. A total pressure drop of less than 2 inches of water is expended in the diffusers for the highest volumetric air flow expected using the Brayton engine.

MODULE HEAT TRANSFER RATE
AND
STORED ENERGY

| POSITION | IIA | IIB | III |
|---|---|---|---|
| HEAT TRANSFER RATE (KWT) | | | |
| IN | 98 | 0 | 113.68 |
| OUT | 167 | 98 | 8.8 |
| STORED ENERGY (KW-HR) | | | |
| INITIAL | 63 | 37 | 11 |
| FINAL | 45 | 11 | 37 |

TABLE 2-4

SANDERS ASSOCIATES, INC.
ENERGY SYSTEMS CENTER

# THERMAL STORAGE MODULE, TSM

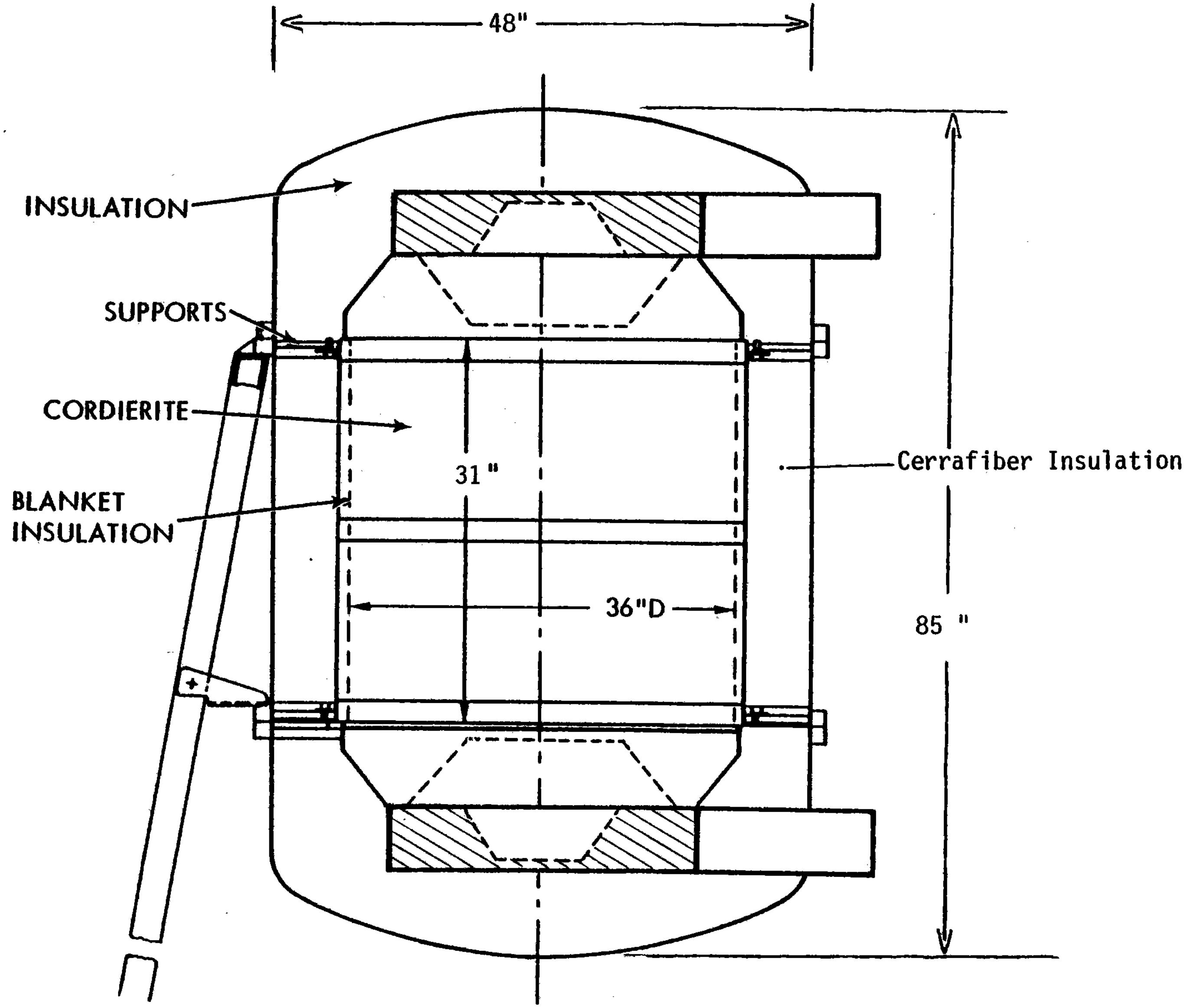


10229-19

FIGURE 2-9

### 2.3.3 Ceramic Core

The cordierite honeycomb core material has a large surface area per unit volume, excellent thermal shock resistance, high strength, chemical inertness and high temperature capabilities, see Table 2-5 for the physical characteristics.

The ceramic core was fabricated from commercial extruded cordierite logs 4.50 inches in diameter and 31 inches long which were cut with a number of cross-sections in order to assemble a nearly cylindrical core shape. In assembly, a thin layer of insulation is placed between neighboring ceramic sections to provide a compliant contact surface and prevent rubbing between the sections as temperatures fluctuated. Min-K insulation is wrapped around the core assembly and the sections are held together by three high temperature alloy spring loaded bands surrounding the Min-K. The applied preload on the springs at ambient temperature was sufficient to support the center sections of the core at elevated temperatures.

### 2.3.4 Assembly

The core is suspended in the tank by 2 sets of 4 equidistant cantilevered Hastelloy supports, one at each end of the core, bolted to the tank flanges on the cylindrical part of the tank. Top and bottom sections of the tank contains diffusers for directing the air uniformly across the ceramic core.

## 2.4 SYSTEM EFFICIENCY

To arrive at system efficiency, the component heat losses and pressure drops must be included in the Brayton cycle computations:

1) The thermal exhaust losses due to heat rejection to the atmosphere from the TSM while it is acting as a recuperator is by far the greatest contributor to system losses.

2) The conduction losses are the second major source of thermal leakage, and are a function of internal TSM temperature.

CORDIERITE CHARACTERISTICS
(CORNING GLASS WORKS)

| | |
|---|---|
| Maximum Use Temperature ($^oF$) | 2450 |
| Cell Density (Holes/$in^2$) | 300 |
| Cell Shape | Square |
| Cell Size (in) | 0.044 x 0.044 |
| Wall Thickness (in) | 0.012 |
| Hydraulic Diameter (in) | 0.044 |
| Open Frontal Area | 65% |
| Geometrical Surface Area ($in^2/in^3$) | 55 |
| Bulk Density ($lb/ft^3$) (Corning Spec. on Code 9475) | 40 |
| Bulk Density ($lb/ft^3$) (Measured by Sanders on 4"x 3" x 30" section) | 36.4 |
| Thermal Conductivity (BTU-in/hr $ft^2$ F) | 10 |
| Coef. of Thermal Expansion in/in/$^oF$ | $2.1 \times 10^{-6}$ |
| Specific Heat (BTU/lb-$^oF$) | |
| $500^oF$ | 0.240 |
| $750^oF$ | 0.267 |
| $1000^oF$ | 0.285 |
| $1500^oF$ | 0.308 |
| $1750^oF$ | 0.31 |

TABLE 2-5

3) Compression losses represent the incremental work that the compressor must do to pressurize a TSM from a low pressure to a higher pressure state. The decompression (thermal venting) losses occur in expanding the high pressure, high temperature air to a lower pressure and temperature.

4) The pressure drops in the TSM and the associated ducting and valves which degrade the available pressure to the turbine.

5) The parasitic losses associated with the fan which circulates the air through TSM 1 and the receiver.

The first step in the cycle analysis was a parametric study to determine the optimum duct size in the solar loop to minimize the thermal and pumping losses. Conduction and pumping losses through a 100 ft. duct at various duct diameters are shown in Figure 2-10. With an average internal temperature of $1500^{\circ}$F and 6 inches of insulation, the optimum duct diameter was determined to be 4.5". Below the optimum diameter the pumping losses predominate due to the high pressure drops, while above it the conduction losses take over due to increased surface area.

To determine the effect of pressure drops on the thermodynamic cycle efficiency, the pressure drops during heat rejection were plotted in Figure 2-11 against cycle efficiency with $\Delta P/P$ during heat addition as a parameter. The heat addition path runs from the compressor inlet to turbine inlet while the heat rejection path is from turbine outlet to exhaust.

Trial design points, A, B and C show the effect of duct and valve sizes on cycle efficiency. The B design condition, 4.5" valves and 4.5" ducts, offers the highest efficiency. Design A has a higher pressure drop and a 1.2% lower efficiency but a considerable reduction in manufacturing cost. Using 3" ducts and 3" valves, Design C results in the lowest cycle efficiency of 36.8% . Selection of Design B has a projected cycle efficiency of 39.5% compared with 40.2% for the A design.

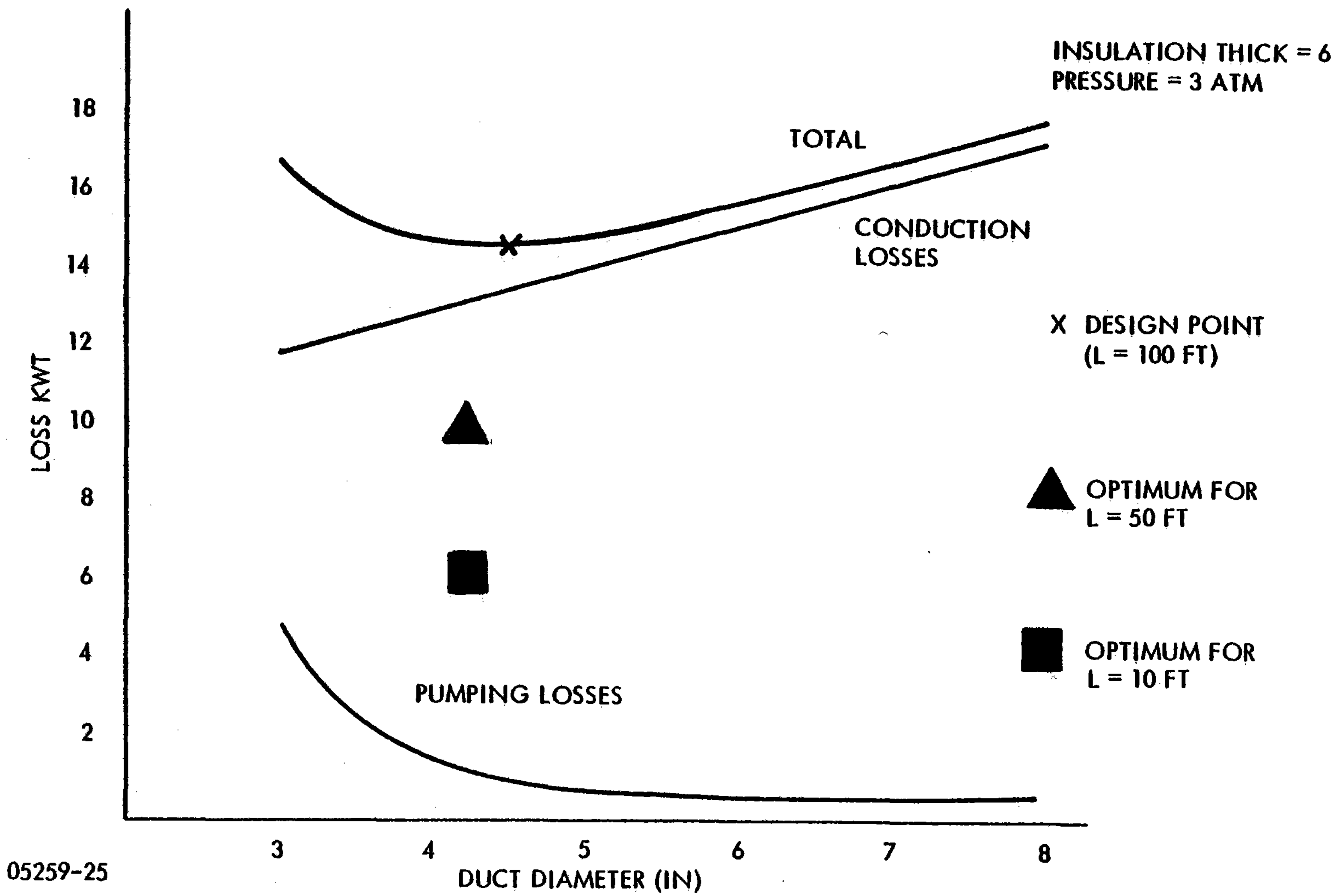


FIGURE 2-10

**SOLAR LOOP DUCT SIZE OPTIMIZATION**

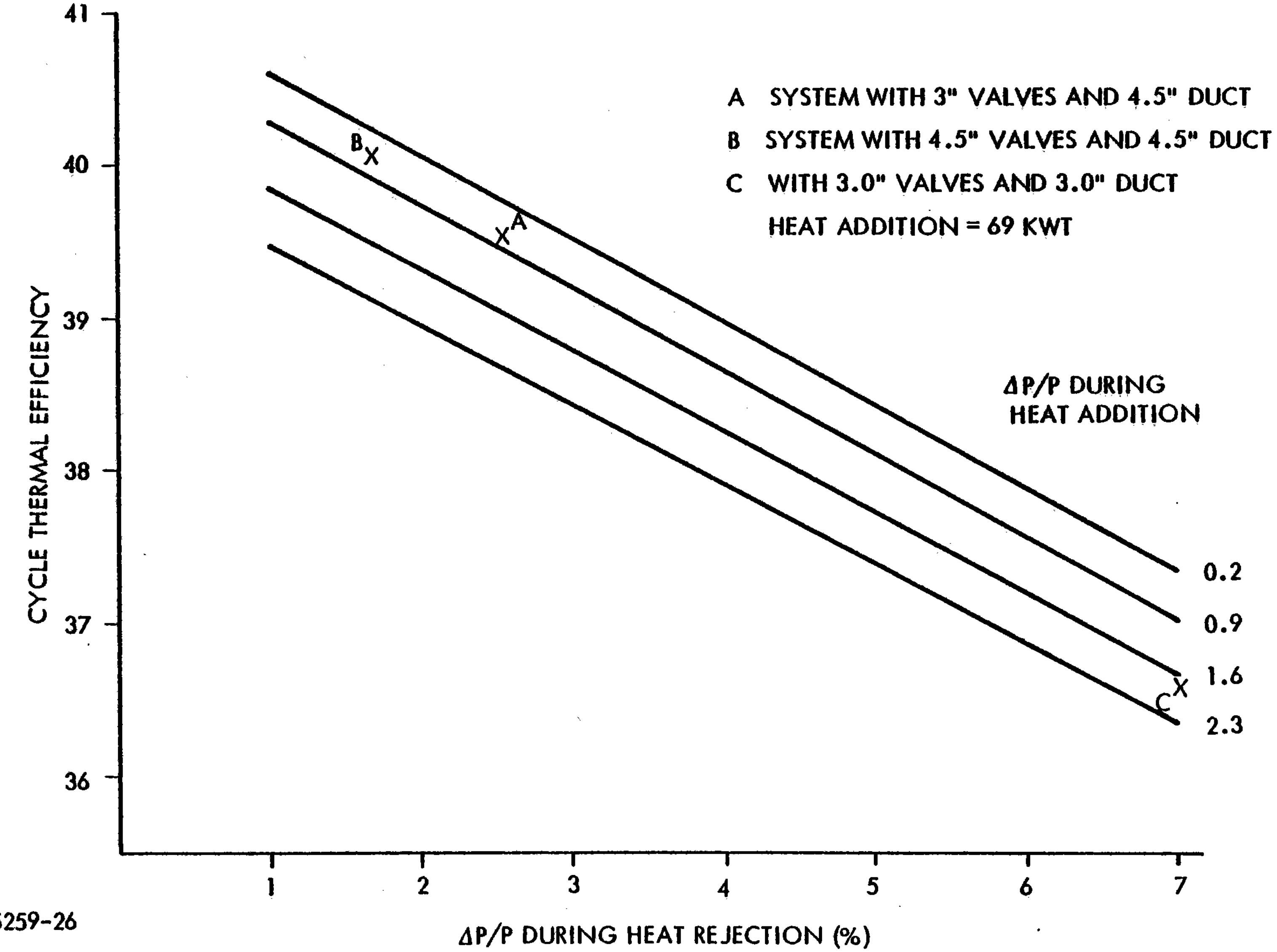


05259-26

FIGURE 2-11

**BRAYTON CYCLE THERMAL EFFICIENCY AS FUNCTION OF PRESSURE DROPS**

Details of the system efficiency calculations are summarized in Tables 2-6, 2-7 and 2-8 based upon the B design concept. Tables 2-6 and 2-7 show the pressure drops and heat losses in the power loop. The $\Delta P$ of 96 psf in the loop is divided between the heat addition and heat rejection paths with 0.65% and 2.5% of operating pressures respectively. The exhaust losses (above the compressor output datum) from TSM III, represent half the power loop losses. This is due to the quality of thermocline propagating down in TSM III. For a perfect thermocline, there would be no losses, and the TSM's would switch between IIB and III at the edge of the thermal front. Conduction losses through the wall represent the other half of the losses.

The calculated thermal and pressure drop losses for the solar loop are shown in Table 2-8 for the various components in the loop. Assuming a 100 ft. travel to concentrator focus and back to the power module 1.56 kw of fan power is required to move the air through the receiver. Receiver losses and pressure drops have been calculated using data from previous tests of Sanders Air Cycle Solar Receiver.

Table 2-9 summarizes the performance of the power loop under design operating conditions. A cycle thermal efficiency of 39% is obtained based on turbine and compressor adiabatic efficiencies of 85% and 80% respectively and heat addition rate of 155.54 BTU/lb. of air or 69.3 KWt.

System performance is examined in Table 2-10 versus solar loop duct length. Power modules located 10 feet from the concentrator focus have an efficiency of 23.3% which is degraded to 20% by 100 ft. of ducting. The output power is 21.3 KWe for a compressor inlet air temperature of $50^{\circ}F$.

Cycle performance is summarized in the bar chart, Figure 2-12, which is a percentage of insolation at the various junctions in the system cycle. Starting with 11.6 meter concentrator of 0.9 reflectivity, a 105.7 KWt solar input corresponds to 95 KWt at the receiver aperture. Using the 94% efficiency of the Sanders receiver, a useful thermal energy of 82 KWt is available at the receiver exit. Deducting conduction losses of 13.1 KWt, useful energy of 69 KWt is available for TSM IIA in the power loop. This energy is added to the 98 KWt recuperated from the turbine exhaust, for a total of 167 KWt at the turbine inlet.

| PRESSURE DROP | IIA | IIB | III | SUMMATION |
|---|---|---|---|---|
| CERAMIC CORE (psf) | 9.23 | 4.63 | 13.46 | 27.32 |
| DUCTS, BENDS, VALVES (psf) | | | | 69 |
| TOTAL (psf) | | | | 96.32 |
| $(\Delta P/P)_{HEAT\ ADDITION}$ | .0065 | | | |
| $(\Delta P/P)_{HEAT\ REJECTION}$ | .025 | | | |

TABLE 2-6
RESULTS OF PRESSURE DROP COMPUTATIONS

| HEAT LOSSES | IIA | IIB | III |
|---|---|---|---|
| WALL LOSSES ($KW_{th}$) | 3.2 | 1. | 1. |
| EXHAUST ($KW_{th}$) | - | - | 8.79 |
| VENT ($KW_{th}$) | - | 0.11 | - |
| $Q_{TOT}$ (W. DUCTING) ($KW_{th}$) | | 16.04 | |

TABLE 2-7
RESULTS OF HEAT LOSS COMPUTATIONS

| | HEAT LOSSES (KWT) | PRESSURE DROP (PSF) |
|---|---|---|
| RECEIVER | 1.4 | 0.653 |
| STORAGE I | 3.2 | 9.23 |
| DUCTING | 8.2 | 51 |
| VALVES | 0.3 | 8.94 |
| TOTAL | 13.1 | 70 |

FAN POWER REQUIREMENT 1.56 KW (SHAFT)

05299-16

TABLE 2-8

RESULTS OF SOLAR LOOP LOSS COMPUTATIONS

| PERFORMANCE | POWER LOOP |
|---|---|
| $\sum \Delta P/P$ | .0315 |
| TURBINE EXHAUST (BTU/LB) | 254.8 |
| RECUPERATOR LOSS (BTU/LB)<br>EXH. + COND. + VENT) | 24.25 |
| EFFECTIVENESS | 0.904 |
| TOTAL HEAT LOSS (BTU/LB) | 35.95 |
| COMPRESSION LOSS (BTU/LB) | 0.64 |
| COMPRESSOR WORK (BTU/LB) | 54.53 |
| TURBINE WORK (BTU/LB) | 115.74 |
| HEAT ADDITION (BTU/LB) | 155.45 |
| CYCLE THERMAL EFFICIENCY | .390 |

04209-10

TABLE 2-9

RESULTS OF BRAYTON ENGINE CYCLE COMPUTATIONS

| PRESSURIZED (3 ATM) SOLAR LOOP DUCT LENGTH | CONCENTRATOR DIAMETER | | HEAT INPUT TO CONCENTRATOR | OUTPUT POWER | OVERALL EFFICIENCY |
|---|---|---|---|---|---|
| (FT) | (M) | (FT) | KWT | KWE | |
| 100 | 11.6 | 38 | 105.7 | 21.31 | 0.201 |
| 50 | 11.37 | 37.3 | 101.6 | 21.81 | 0.230 |
| 10 | 11.18 | 36.6 | 98.3 | 22.21 | 0.233 |

TABLE 2-10
EFFECT OF SOLAR LOOP DUCTING LENGTH ON CYCLE PERFORMANCE

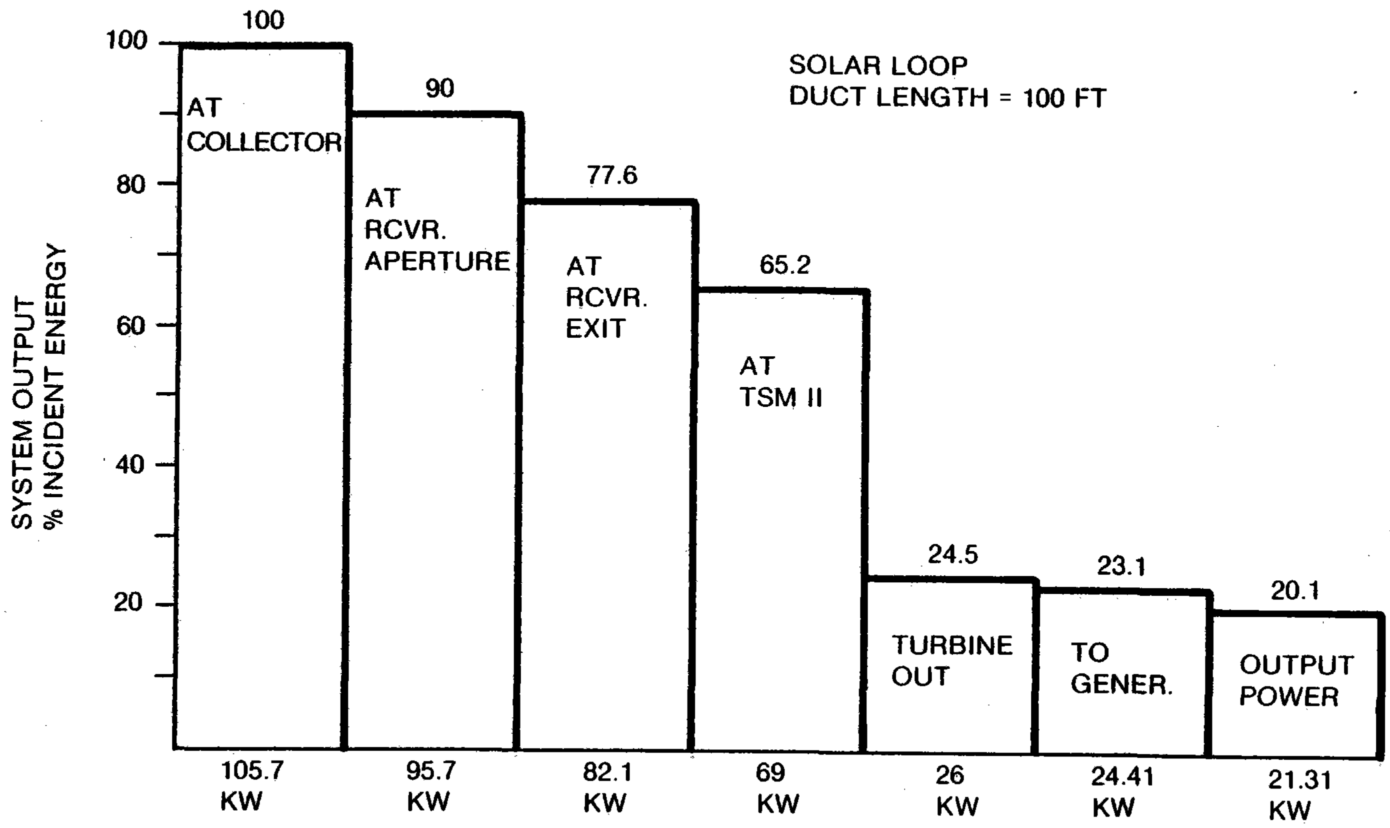


FIGURE 2-12

SOLAR BRAYTON ELECTRIC POWER SYSTEM PERFORMANCE CHART

Based on the Brayton cycle analyses, a net output of 26 KW is the useful work available from the engine. Deducting the parasitic losses of the fan in the solar loop, 24.4 KW is available to be converted to electric power. Assuming gear losses and generator efficiency of 94% and 87%, respectively, the output power is 21.31 KWe, resulting in an overall solar to electric efficiency of 20%.

## 2.5 VALVE DESCRIPTION

To accomplish the switching mechanism between the two pairs of storage modules, either an extensive manifolding, piping and valving mechanisms must be designed or two pairs of 4-way valves can be used for system operation. Extensive manifolding of single-on-off valves was discarded after evaluating the pressure drops and heat losses associated with such a scheme. One supplier of a suitable 4-way valve was found but because of an unacceptable cost and delivery quotation, one valve was built and tested by Sanders.

The design shown in Figure 2-13 has a 9" diameter ball with two 3" passageways that turn the flow 90$^{o}$. It is made of high temperature cast iron called Meahnite. This material has three times the strength of stainless steel at 1700$^{o}$F. Four conical stainless steel seats are spring loaded against the ball with 17 - 4PH springs and sealed with 321 stainless steel bellows to maintain a continuous line contact with each of the four ports of the valve. The valve housing is also made of Meahanite. The completed valve weighs about 200 lbs.

The final system design will have four such valves to establish the individual functions of each TSM, as shown in Figure 2-2. Each pair of TSM's has an assembly of two valves, one for the upper and one for the lower manifolds. Each valve will be activated by a pneumatic actuator operating through a bell crank. Since the upper and lower valve assemblies for a given TSM pair must operate in unison, the actuator for each pair will be coupled.

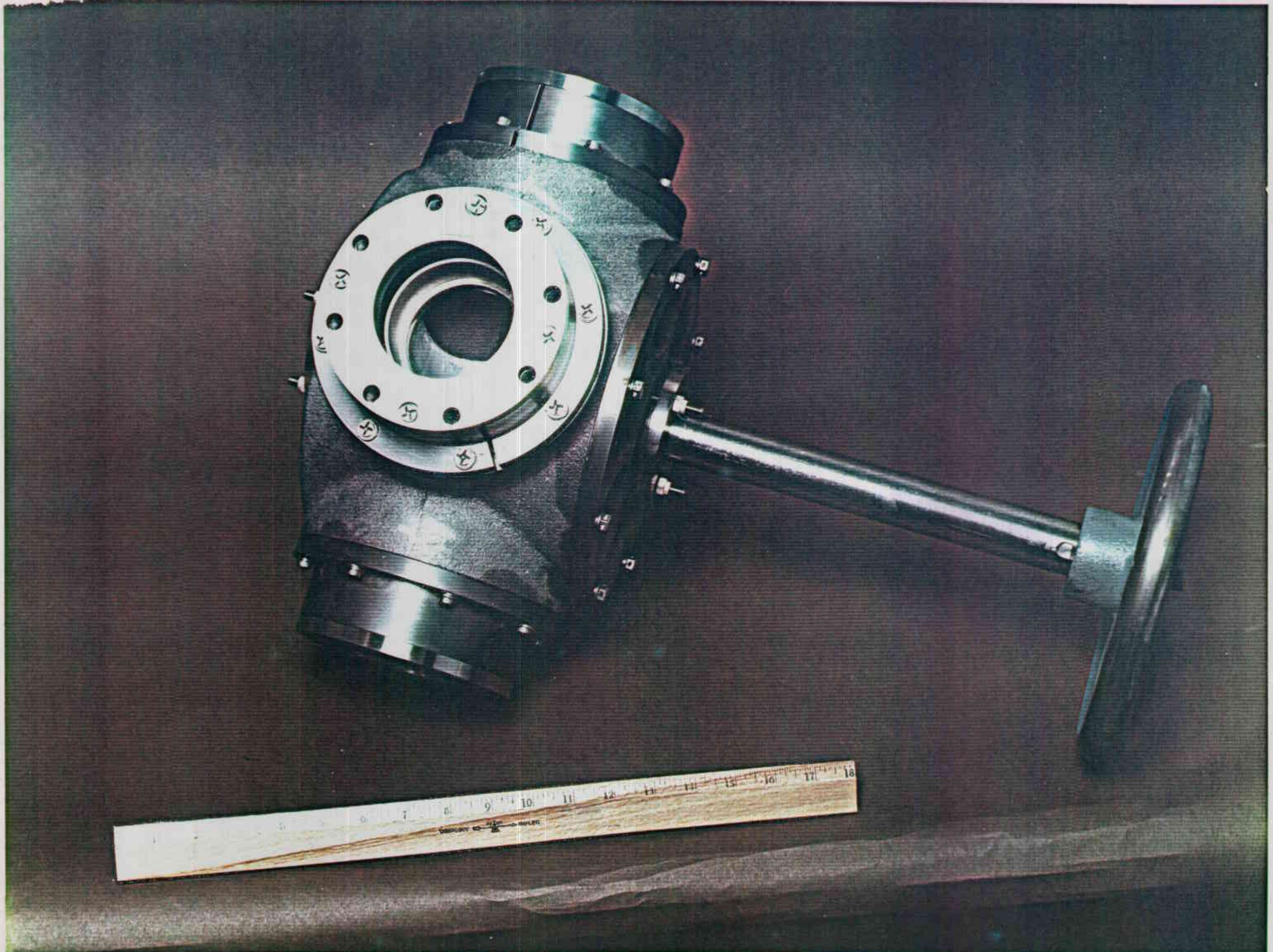

FIGURE 2-13

# SECTION 3
# TEST SYSTEM DESCRIPTION

## 3.1 TEST REQUIREMENTS

The main test objectives of the Small Solar Power System Demonstration program fall into the following categories:

- Demonstration of thermocline performance in the TSM.
- Operation of the TSM up to 1700$^{o}$F.

To accomplish the test requirements of the TSM, the test equipment had to meet the operational requirements listed in Table 3-1.

TABLE 3-1
TEST SYSTEM REQUIRED SPECS

| COMPONENT | TEMP. | PRESSURE (ATM.) | FLOW(LB/SEC.) |
|---|---|---|---|
| TSM | Ambient - 1700 | 1 - 3 | 0.2 - 0.6 |
| Burner | 300 - 1800 | 1 - 3 | 0.2 - 0.6 |
| 4-Way Valve | 1700 | 1 - 3 | 0.2 - 0.6 |
| Control Valves | 1700 | 1 - 3 | 0.2 - 0.6 |

To comply with ASME temperature and pressure limitations, the ducting exposed to high temperature air was both internally and externally insulated. The system pressure was monitored both on Magnehelic gages and electronic pressure transducers. The flow through the system was controlled manually by observing the gage readings, and at the same time the output of the pressure transducers were continuously monitored and recorded.

Thermocouple monitoring of TSM and system temperatures was of primary importance. Thermocouples were inserted in between the sections of the core at varying axial and radial distances to measure the propagation and distribution of the thermocline.

The four way valve was installed in the test setup to control the direction of airflow through the TSM over the range of mass flow, temperature and pressure defined in Table 3-1. This task was accomplished by turning the valve by $90^{\circ}$ each time it was desired to change the flow direction. Gate and Globe valves were used to control system mass flow rate. They were rated to function properly at maximum system temperature, pressure and mass flow conditions.

The instrumentation requirements for the test setup consist of thermocouples, pressure transducers, and flow meters needed by the operator to set test conditions as well as to provide a permanent record of all data needed to compute the performance characteristics of the system.

The accuracy of the instrumentation was obtained from the manufacturer and by independent calibration tests at Sanders. Table 3-2 shows the results of these tests.

TABLE 3-2
ACCURACY OF INSTRUMENTATION

| | TEMPERATURE RANGE | ERROR |
|---|---|---|
| Thermocouples | 0 - 2300 | $\pm 3.6^{\circ}F$ |
| Total Pressure Transducer | 0 - 40 psi | $\pm 0.1$ psi |
| Differential Pressure Transducer | 0 - 5 psi | $\pm 0.01$ psi |

## 3.2 TEST EQUIPMENT

The test setup schematic for the thermal storage module is shown In Figure 3-1 and Table 3-3. The major components in addition to the TSM and the 4-way valve are the burner, compressor, control valves and interconnecting ducts, see Figure 3-1.

Compressed air regulated at 30 psi is introduced into the test setup through valve V1. For atmospheric test conditions, a globe valve V2 controls system mass flow rate which is monitored on flow meter F1. Air is heated in the burner and deflected to the top or bottom of the TSM depending on the orientation of the 4-way valve. For pressurized tests, V2 is fully open and the system flow rate and back pressure are maintained by adjusting V6 with V7 closed.

The burner bypass line and the bypass dump was designed to assure low temperature tests. The burner turndown ratio proved to be greater than expected so that operation of the bypass line was not needed in these tests.

### 3.2.1 Compressor

A 125 H.P. rotary electric compressor provided the air supply necessary for the tests. The unit had a maximum volumetric flow of 590 $ft^3$/min and 125 psig discharge pressure. Two pressure regulators installed in parallel limited the test inlet pressure to 30 psig. An after cooler downstream of the compressor reduced the discharge temperature from about 120$^{o}$F to 40 - 60$^{o}$F air depending on the ambient conditions. A filter located upstream of the test setup was used to collect the condensate, so that moisture free air was introduced into the burner.

### 3.2.2 Burner

The propane burner, manufactured to the specifications of Table 3-4, was purchased from Trane Thermal Components. It is a UL approved unit with all the safety features supplied by the manufacturer. Figure 3-2 is a photograph of the burner along with the gas flow train. A set of safety valves shuts the vurner when the flow, temperature and pressure conditions deviate from the design conditions.

Table 3-4 lists the burner specifications as supplied by the vendor.

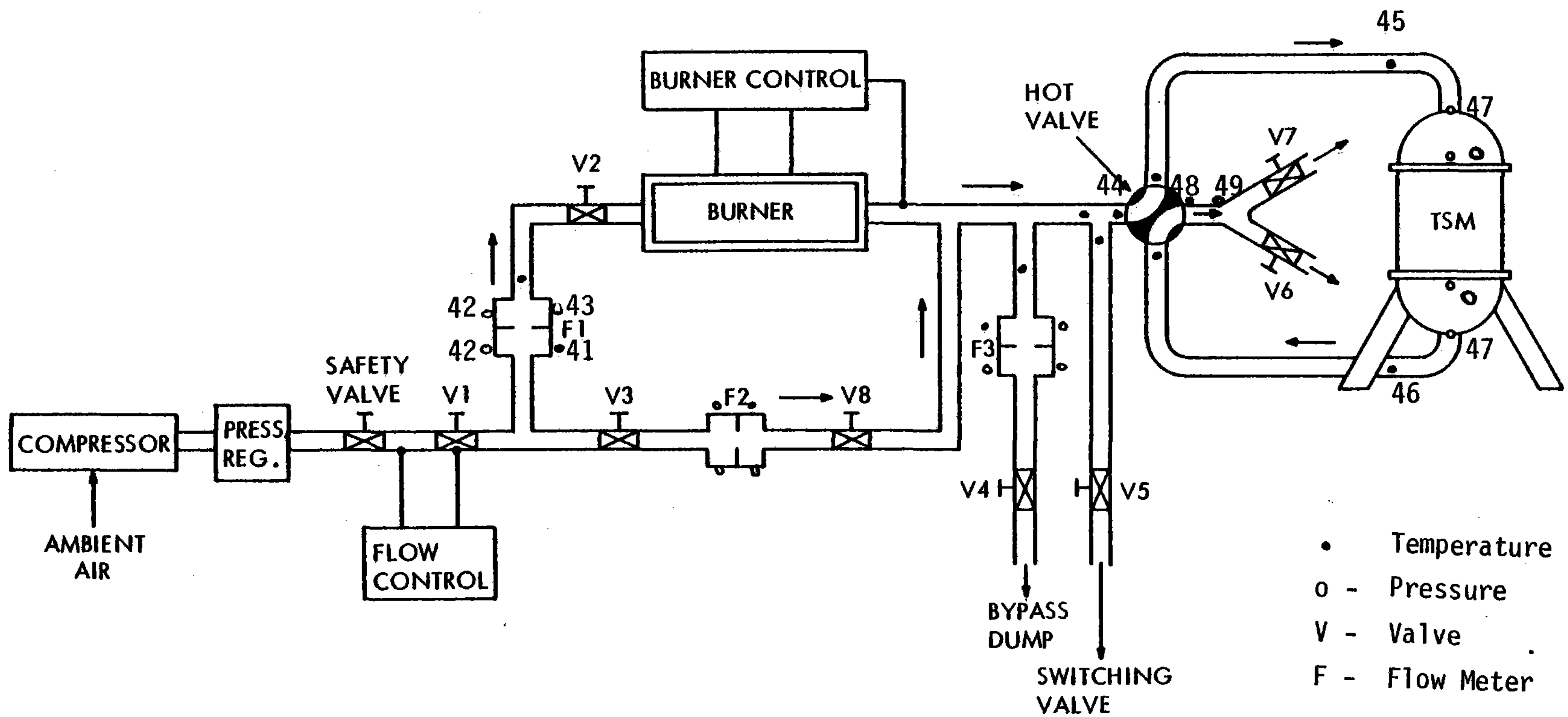


FIGURE 3-1
TEST SCHEMATIC

TABLE 3-3
DESCRIPTION OF ITEMS IN TEST SCHEMATIC

| | | |
|---|---|---|
| C | - | 125 HP Screw Type Electric Compressor (610 SCFM) |
| REG | - | Pressure Regulator Set at 30 PSIG |
| SAFETY VALVE | - | Relief Valve for Protection of Ducts |
| V1 | - | 2" S. S. Gate Valve 150 lb Rating |
| V2 | - | 2" S. S. Globe Valve with Actuator 150 Lb. Rating |
| V3 | - | 2" S. S. Globe Valve 150 Lb. Rating |
| V4 | - | 2" S. S. Globe Valve 150 Lb. Rating. |
| V5 | - | 2" S. S. Globe Valve 300 Lb. Rating |
| V6 | - | 2" S. S. Globe Valve with Actuator 300 Lb. Rating |
| V7 | - | 4" S. S. Gate Valve 300 lb. Rating |
| V8 | - | 2" S. S. Check Valve 150 Lb. Rating. |
| F1 | - | 2" Orifice Plate Flowmeter |
| F2, F3 | - | 3" Orifice Plate Flowmeter |
| Burner | - | Trane Manufacturing Company |
| 4-Way Valve | - | Sanders Design High Temperature 4-Way Valve |
| TSM | - | Thermal Storage Module |

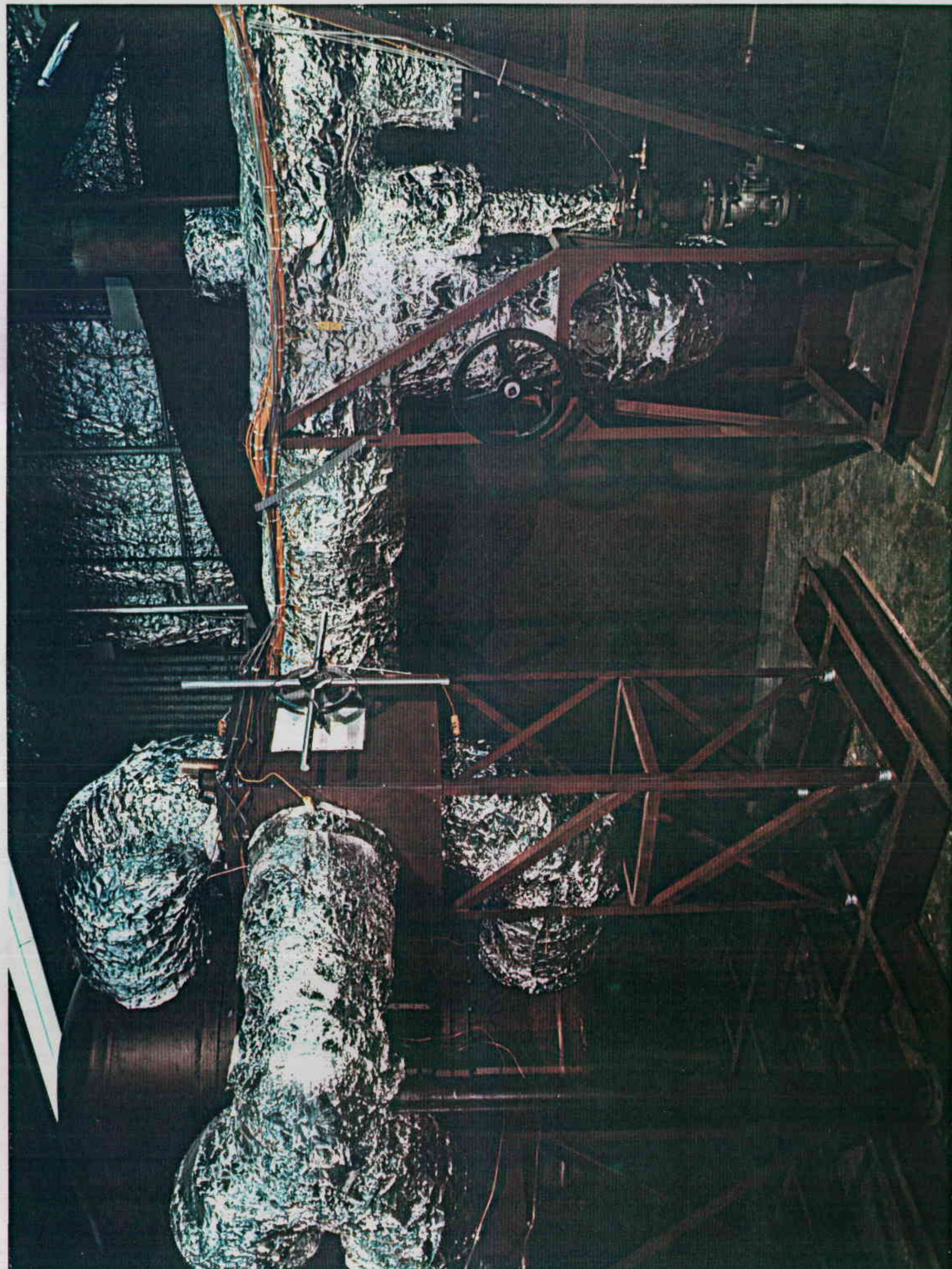

Figure 3-2a
Test Setup

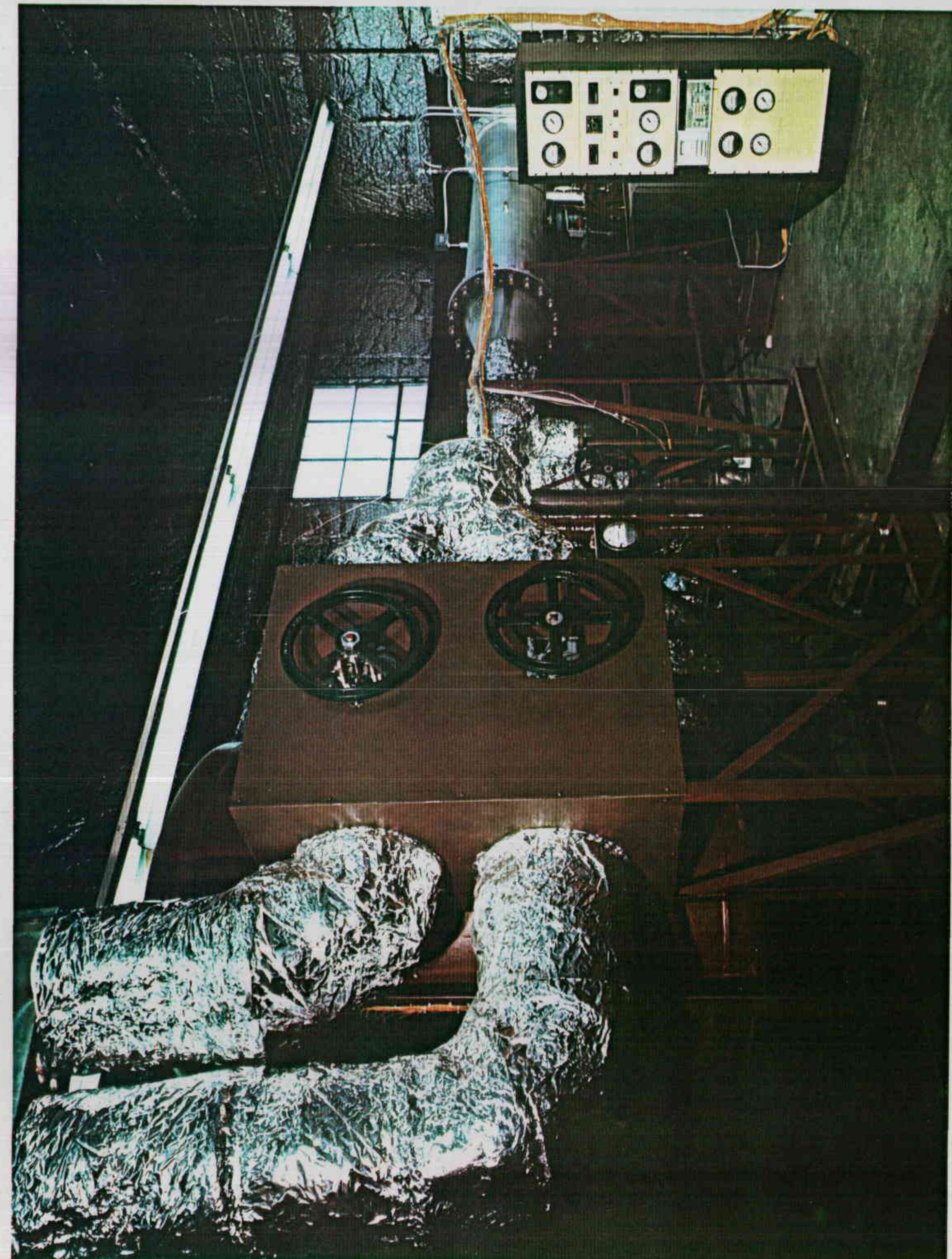

FIGURE 3-2b
TEST SET-UP

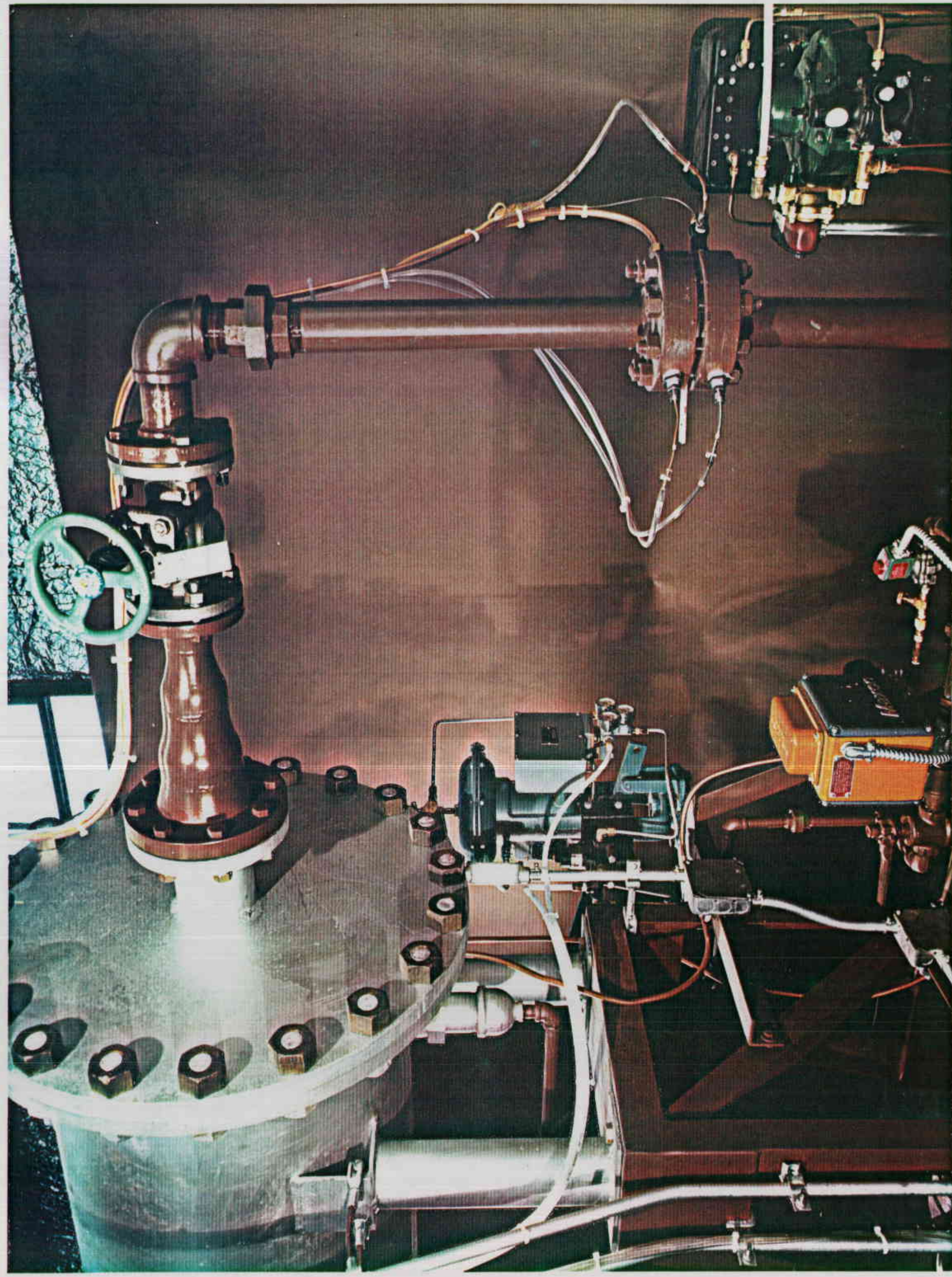

FIGURE 3-2c
TEST SET-UP

TABLE 3-4

BURNER SPECIFICATIONS

Trane Thermal Company

Conshohocken, PA 19428

PERFORMANCE CHARACTERISTICS (without bypass line)

| | |
|---|---|
| Process Air Flow | 0.6 to 0.2 lb/sec |
| Maximum Outlet Temperature | $1800^{o}F$ |
| Minimum Outlet Temperature with 0.6 lb/sec | $300^{o}F$ |
| Minimum Process Inlet Temperature | $70^{o}F$ |
| Process Air maximum back pressure | 38 psig |
| Process Air maximum pressure drop across all burner components | 2 psig |
| Heat input with no back pressure | |
| maximum | 3.5 mm BTU/hr |
| minimum | 0.35 mm BTU/hr |
| Heat input with 30 psig back pressure | |
| maximum | 1.2 mm BTU/hr |
| minimum | 0.12 mm BTU/hr |
| Turndown ratio | 10:1 |
| Fuel | Propane Gas |
| Fuel Flow Range | 416 SCFH - 56 scfh |

MECHANICAL CHARACTERISTICS

| | |
|---|---|
| Overall Length | 96" |
| Heater Body Diameter | 20" steel<br>14" insulation |
| Materials of Construction | Carbon steel |
| Supports | two short support legs at inlet end of heater |
| Process Air Inlet | 4" - 150 lb flange |
| Mixing Baffle | 309 ss |
| Approximate Total Weight | 1500 lb |

### 3.2.3 Control Valves and Ducting

Stainless steel Gate and Globe valves were used to control the flow rate through the test setup. The valves that were exposed to temperatures above 1300$^{o}$F were fitted with stellite coated seats, graphoil stem packings and inconcel o'rings.

The Gate valves were used for ON/OFF operation, while the Globe valves were used to control the flow rate. Referring to Figure 3-1, the characteristics of each valve is given in Table 3-5.

The piping in the test setup was designed according to ASME codes. All high temperature lines downstream of the burner are 8" stainless steel pipe internally insulated with 2" of cerafoam/cerablanket insulation. In addition, 2" of insulation is wrapped around the outside to keep the conduction losses low.

With an internal temperature of 1700$^{o}$F, the metal wall temperature is calculated to be 1200$^{o}$F corresponding to allowable stresses of 6.8 Kpsi, well within the ASME limit of 1500$^{o}$F or 1.5 Kpsi.

The pipes that are upstream of the burner and those that bypass it are of carbon steel construction.

TABLE 3-5
VALVE CHARACTERISTICS

| VALVE | TYPE | SIZE (IN.) |
|---|---|---|
| V1 | Gate | 2 |
| V2 | Globe | 2 |
| V3 | Globe | 3 |
| V4 | Globe | 3 |
| V5 | Globe | 2 |
| V6 | Globe | 2 |
| V7 | Gate | 4 |
| V8 | Check | 2 |

### 3.2.4 Control System

A central display control station was built to monitor the various data obtained throughout the test, as shown in Figure 3-3.

The pressure transducers shared the same line with the magnehelic gages to maintain a visual display of the test conditions. The Manual operation of setting test conditions and monitoring performance was performed directly from the control panel independent of the data logging system.

The propane flow was remotely controlled from the control panel to set the desired temperature for each test. The burner response to propane flow change was such that in 15 - 20 seconds, the burner output temperature could be changed 1000$^{o}$F for both pressurized and unpressurized conditions.

### 3.2.5 Data Logger and Recorder

Data was recorded by a Fluke Model 2240B Data Logger , as shown in the center of Figure 3-3. It is microprocessor controlled and uses common-bus architecture for greater versatility. All control, interface and data handling functions are under directions of the microprocessor. The data logger contains a printer, monitor, and front panel controls, and may be operated by and with peripheral equipment, such as CRT terminals and recorders. The printer is a 16 column digital printer providing hard-copy printout at a speed of 2.5 lines per second.

The data logger will handle 50 channels of input data. The sensors are wired directly into the chassis where the signals are scanned, conditioned, scaled, converted to equivalent digital data, and printed out automatically or on command.

During the tests, the data was recorded continuously on a Data Cartridge Recorder, Columbia Model 300C. The unit utilizes 3M tape DC-300A data cartridges, containing 300 ft. of 1/4 in. computer grade magnetic tape.

The recorder was connected in series with the Data Logger and used in the "off line" search and edit functions. The recorded data was then transferred

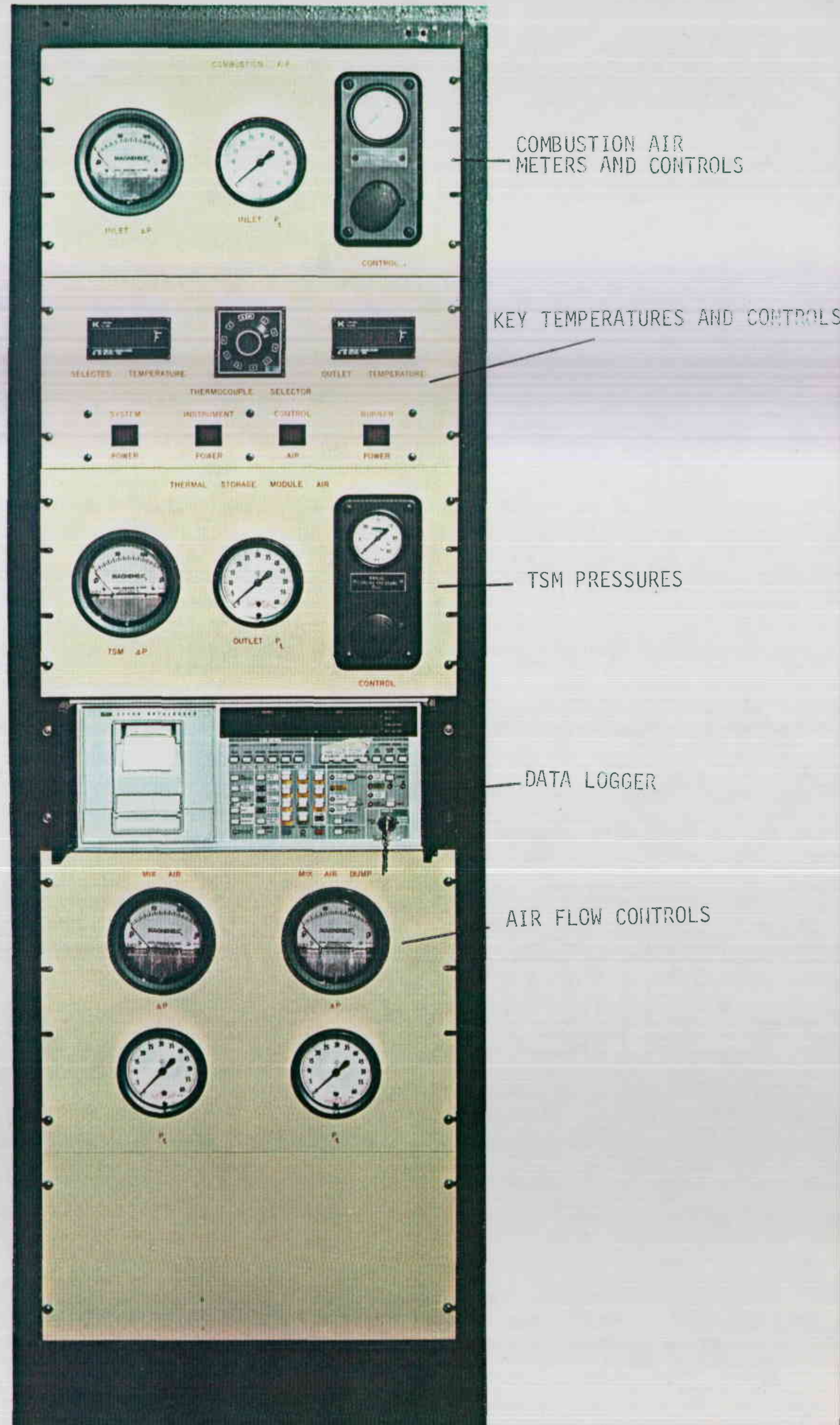


FIGURE 3-3
CONTROL PANEL - TSM TESTS

to the Sanders PDP-10 computer for computation and plotting.

## 3.3 INSTRUMENTATION

### 3.3.1 Thermocouples

The selected thermocouples were Chromel-Alumel type applicable to 2300$^{o}$F and were protected within a 0.020" diameter stainless steel sheathing material. The junctions were prepared at S/A and the thermocouples were layed in between the sections of the core assembly. Figure 3-4 shows the locations of the thermocouples and Table 3-6 describes their coordinates.

The thermocouples that monitored stream temperatures in the ducts were also Chromel-Alumel but were 1/16" thick, enclosed with 1/8" thick stainless steel sheathing material.

### 3.3.2 Pressure Transducers

Total and differential pressure transducers were used throughout the test setup to determine the flow rate, back pressure and pressure drops. The core itself was instrumented so that the pressure drop across the cordierite and across the TSM can be monitored separately and continuously.

The pressure transducers were of strain gage type with the following characteristics:

| Transducer Type | Input Voltage (VDC) | Output Voltage (VDC) | Pressure Range (psi) |
|---|---|---|---|
| Total | 8 | 1 - 6 | 0 - 40 |
| Differential | 8 | 1 - 6 | 0 - 5 |

To convert the pressure transducer data from VDC to psi or in-$H_2O$, the following linear equations are used for the total and differential pressures respectively:

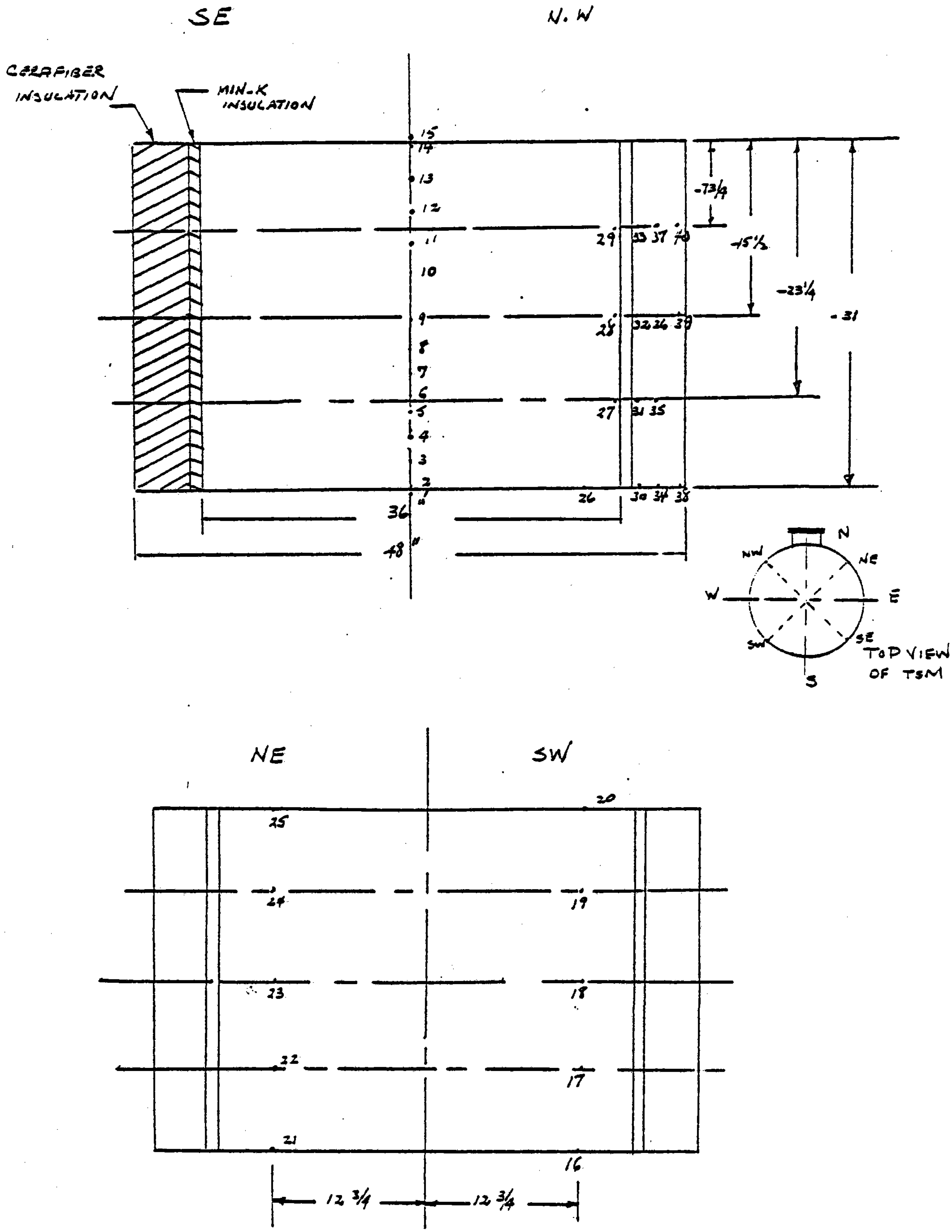


FIGURE 3-4. TSM INSTRUMENTATION (THERMOCOUPLE LOCATIONS)

TABLE 3-6

THERMOCOUPLE LOCATIONS, DATA LOGGER CHANNEL ASSIGNMENTS AND OTHER INSTRUMENTATION

| DATA LOGGER CHANNEL | THERMOCOUPLE NO. OR DEVICE | PLANE | RADIUS | DISTANCE FROM TOP (IN) | DESCRIPTION | |
|---|---|---|---|---|---|---|
| 0 | ΔP-XDCR S/N 413132 | - | - | - | TSM CORE | ΔP |
| 1 | 1 | ℄ | ℄ | - 31 1/4 | CORE | CENTER |
| 2 | 2 | " | " | - 31 | " | " |
| 3 | 3 | " | " | - 28 3/4 | " | " |
| 4 | 4 (BAD) | " | " | - 26 1/2 | " | " |
| 5 | 5 | " | " | - 24 1/2 | " | " |
| 6 | 6 | " | " | - 22 1/4 | " | " |
| 7 | 7 | " | " | - 20 | " | " |
| 8 | 8 | " | " | - 17 3/4 | " | " |
| 9 | 9 | " | " | - 15 1/2 | " | " |
| 10 | 10 | " | " | - 11 | " | " |
| 11 | 11 (BAD) | " | " | - 8 3/4 | " | " |
| 12 | 12 (BAD) | " | " | - 4 1/2 | " | " |
| 13 | 13 | " | " | - 2 1/4 | " | " |
| 14 | 14 | " | " | 0 | " | " |
| 15 | 15 (BAD) | " | " | + 1/4 | " | " |
| 16 | 16 | SW | 12 3/4 | - 31 1/4 | CORE | ANNULUS |
| 17 | 17 | SW | " | - 21 1/2 | " | " |
| 18 | 18 | SW | " | - 15 1/2 | " | " |
| 19 | 19 | SW | " | - 7 3/4 | " | " |
| 20 | 20 (BAD) | SW | " | 0 | " | " |
| 21 | 21 (BAD) | NE | " | - 31 1/4 | " | " |
| 22 | 22 (BAD) | NE | " | - 21 1/2 | " | " |
| 23 | 23 | NE | " | - 15 1/2 | " | " |
| 24 | 24 | NE | " | - 7 3/4 | " | " |
| 25 | 25 | NE | " | 0 | " | " |
| 26 | 26 (BAD) | NW | 14 3/4 | - 31 1/4 | " | " |
| 27 | 27 | NW | 18 | - 23 1/4 | CORE | EDGE |
| 28 | 28 | NW | 18 | - 15 1/2 | " | " |
| 29 | 29 | NW | 18 | - 7 3/4 | " | " |
| 30 | 30 | NW | 19 | - 31 1/4 | INNER | INSULATION |
| 31 | 31 (BAD) | NW | 19 | - 23 1/4 | " | " |
| 32 | 32 | NW | 19 | - 15 1/2 | " | " |
| 33 | 33 | NW | 19 | - 7 3/4 | " | " |
| 34 | 34 | NW | 21 | - 31 1/4 | MIDDLE | INSULATION |
| 35 | 35 | NW | 21 | - 23 1/4 | " | " |
| 36 | 36 | NW | 21 | - 15 1/2 | " | " |
| 37 | 37 | NW | 21 | - 7 3/4 | " | " |
| 38 | 38 | NW | 23 | - 31 1/4 | OUTER | INSULATION |
| 39 | 38 | NW | 23 | - 15 1/2 | " | " |
| 40 | 40 | NW | 23 | - 7 3/4 | " | " |

TABLE 3-6 (Cont'd.)

| | | | | | |
|---|---|---|---|---|---|
| 41 | 84 | - | - | - | Combustion Air Temp. |
| 42 | ΔP-XDCR S/N 413345 | - | - | - | Combustion Air ΔP |
| 43 | $P_t$-XDCR S/N 4002031 | - | - | - | Combustion Air $P_t$ |
| 44 | 80 | - | - | - | Inlet Pipe Air Temp. |
| 45 | 76 | - | - | - | TSM Top Elbow Temp. |
| 46 | 75 | - | - | - | TSM Bottom Elbow Temp. |
| 47 | ΔP-XDCR S/N 413279 | - | - | - | TSM ΔP (Elbow to Elbow) |
| 48 | 78 | - | - | - | Output Temp. |
| 49 | $P_t$-XDCR S/N 4001959 | - | - | - | Output $P_t$ |

FIXED DATA NUMBER: 40 ----

| THERMOCOUPLE SELECTOR SWITCH POSITION | THERMOCOUPLE NUMBER | THERMOCOUPLE LOCATION |
|---|---|---|
| 1 | 82 | Exhaust Dump |
| 2 | 83 | Bypass Air Dump |
| 3 | 79 | 4-Way Valve Top Elbow |
| 4 | 77 | 4-Way Valve Bottom Elbow |
| 5 | 85 | Tank Skin Temp.-Bottom Header |
| 6 | 87 | " " " -Tank Center-Bottom |
| 7 | 88 | " " " " " |
| 8 | 90 | " " " " " |
| 9 | 91 | " " " " " Top |
| 10 | 93 | " " " -Top Header |

Outlet Temperature Meter - Thermocouple 81 (Inlet Pipe Air Temp.)

<u>YLW</u> Pressure Transducer Calibration Data

<u>Differential Pressure Transducers</u>

S/N 413132 Input - 0 PSID = 1.0040 volts output
2 " = 3.0450 "
4 " = 4.0500 "
5 " = 6.0130 "

S/N 413279 Input - 0 PSID = .9820 volts - Output
2 " = 2.9930 "
4 " 3.9950 "
5 " = 5.9670 "

S/N 413345 Input - 0 PSID = .9870 volts - Output
2 " = 3.0040 "
4 " = 4.0060 "
5 " = 5.9910 "

<u>Total Pressure Transducers</u>

S/N 400 1959 Input - 0 PSI = 1.014 volts - Output
40 " = 6.0637 "

S/N 400 2031 Input - 0 PSI = .9981 volts- Output
40 " = 6.247 "

All data is for room temperature (25°C) and a supply voltage of 8.0 volts D.C.

$$P_t = P_s + P_d$$

where: $P_t$ = Total pressure (psi)

$P_s$ = Static head (psi)

$P_d$ = Dynamic head = $\frac{1}{2}\frac{\rho v^2}{g}$

$$P_s \text{ (psia)} = \left\{\left[\text{transducer output (volts)} \times \text{slope } \left(\frac{\text{psi}}{\text{volt}}\right)\right] - \text{intersection point of curve with P-axis}\right\} + 14.7 \text{ psi}$$

$$\Delta P \text{ (in-}H_2O) = \left\{\left[\text{transducer output (volts)} \times \text{slope } \left(\frac{\text{psi}}{\text{volt}}\right)\right] - \text{intersection point of curve with P-axis}\right\} \times 27.684 \frac{\text{in-}H_2O}{\text{psid}}$$

Table 3-7 lists the location, function, and calibration slope for each transducer.

## 3.4 AIR FLOW METERS

The air flow is measured by orifice plate meters. There are three flow meters in the test setup. The burner and TSM flow rate is measured by an orifice plate located in a 2" pipe upstream of the burner. Burner by-pass and by-pass dump flow meters are located in 3" pipes. Since the burner was able to give low turndown ratios, there was no need to utilize the by-pass line and mix the TSM inlet temperature. Table 3-8 describes the characteristics of the 2" and 3" flow meters.

The flow meters were designed to operate at the conditions specified in Table 3-8. Any deviation from these conditions is compensated by the following equation:

$$\dot{m} = .06\sqrt{\Delta P}\sqrt{\frac{T_D}{T_t}}\sqrt{\frac{P_t}{P_D}}$$

TABLE 3-7

PRESSURE TRANSDUCER CALIBRATION

| PRESSURE TRANSDUCER S/N | FUNCTION | DATA LOGGER CHANNEL # | SLOPE (psi/volt) | INTERSECTION POINT WITH $\Delta$P AXIS |
|---|---|---|---|---|
| Differential | | | | |
| 413132 | TSM Core $\Delta$P | 0 | 0.9982 | 0.9982 |
| 413279 | TSM $\Delta$P | 47 | 1.0030 | 1.0030 |
| 413345 | Combustion Air $\Delta$P | 42 | 0.9992 | 0.9992 |
| Total | | | | |
| 4001959 | TSM Output-P | 49 | 7.9212 | 7.9212 |
| 4002031 | Combustion Air-P | 43 | 7.6206 | 7.6206 |

TABLE 3-8

FLOW METER CHARACTERISTICS

| | SYSTEM FLOW | BY-PASS AND BY-PASS DUMP |
|---|---|---|
| Meter Pipe I.D. (in.) | 2.067 | 3.068 |
| Differential @ Max. Flow ("$H_2O$) | 100 | 100 |
| Maximum Flow (lb/hr) | 2160 | 3240 |
| Normal Flow (lb/hr) | 1512 | 2268 |
| Flowing Temperature ($^oF$) | 125 | 125 |
| Flowing Pressure (psia) | 44.7 | 44.7 |
| Orifice Type | Concentric | Concentric |
| Orifice Plate Material | 304. S.S. | 304 S. S. |
| Reynolds Number @ Normal Flow | 224605 | 247196 |

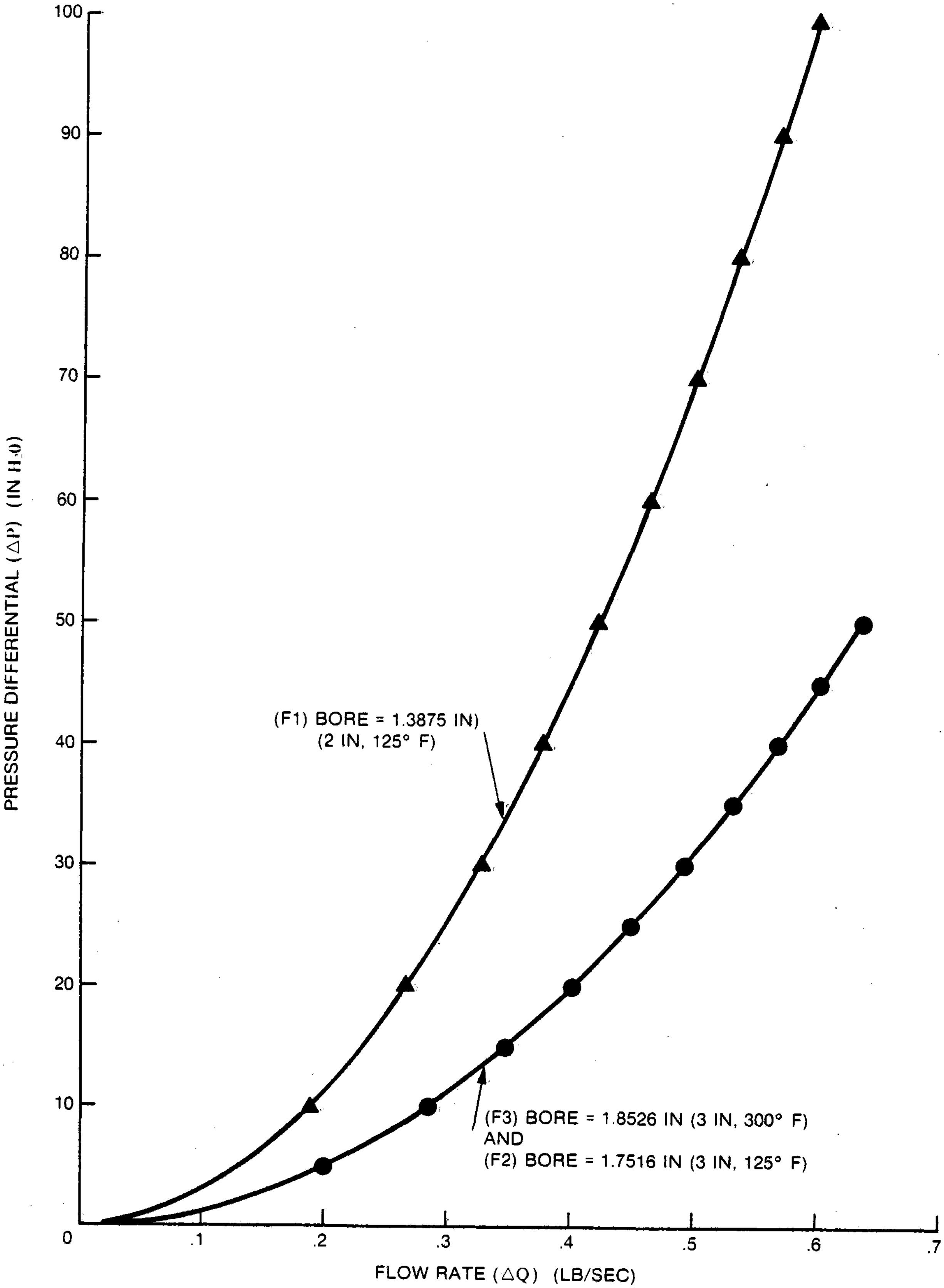


Figure 3-5.

Flow Calibration Curves for Vickery-Simms Flowmeter, 3 Jan. 1980 where:

$\dot{m}$ = Mass flow rate (lb/sec)

$\Delta P$ = Pressure drop across flow meter ("$H_2O$)

$T_D$ = Design temperature = 585$^{o}$R

$T_t$ = Test temperature ($^{o}$R)

$P_D$ = Design pressure 44.7 (psia)

$P_t$ = Test pressure (psia)

SECTION 4
EXPERIMENTAL RESULTS

## 4.1 TEST PROGRAM

### 4.1.1 Brayton Cycle

The Sanders thermal storage module performs two distinct functions in the Brayton cycle. The first function is to store the thermal energy collected by the solar receiver and reflector. In this capacity it is paired with another module where each is switched in sequence between the Brayton power loop and the solar collection loop. While in the solar collection loop it is charged with hot air from the solar collector. When fully charged it is switched into the Brayton power cycle to heat the turbine air. The test program simulated the solar collection cycle by measuring the TSM performance at temperatures up to 1700°F both under pressurized and unpressurized conditions. Under these conditions the thermocline passes completely through the TSM and the module is used to its maximum thermal storage capacity.

The second function of the TSM is to perform the recuperation function in a low pressure ratio Brayton engine. In this capacity a pair of TSM's alternately heat the compressor exhaust air and recover the heat from the turbine exhaust, Figure 4-1. To optimize recuperator effectiveness, the TSM positions are switched before the TSM has been either fully charged or discharged. Furthermore, an optimized system might well have different size storage modules for the storage of solar energy and for the Brayton recuperation function. Tests for the second function were conducted over many charge/discharge cycles simulating Brayton engine recuperation.

The test program was conducted in three series. The first series measured general thermocline characteristics as influenced by mass flow, temperature range, pressure and direction of air flow through the TSM. In the second series, the Brayton recuperation function was evaluated. Temperatures of 1700°F representing the solar collection cycle were evaluated under pressurized and unpressurized

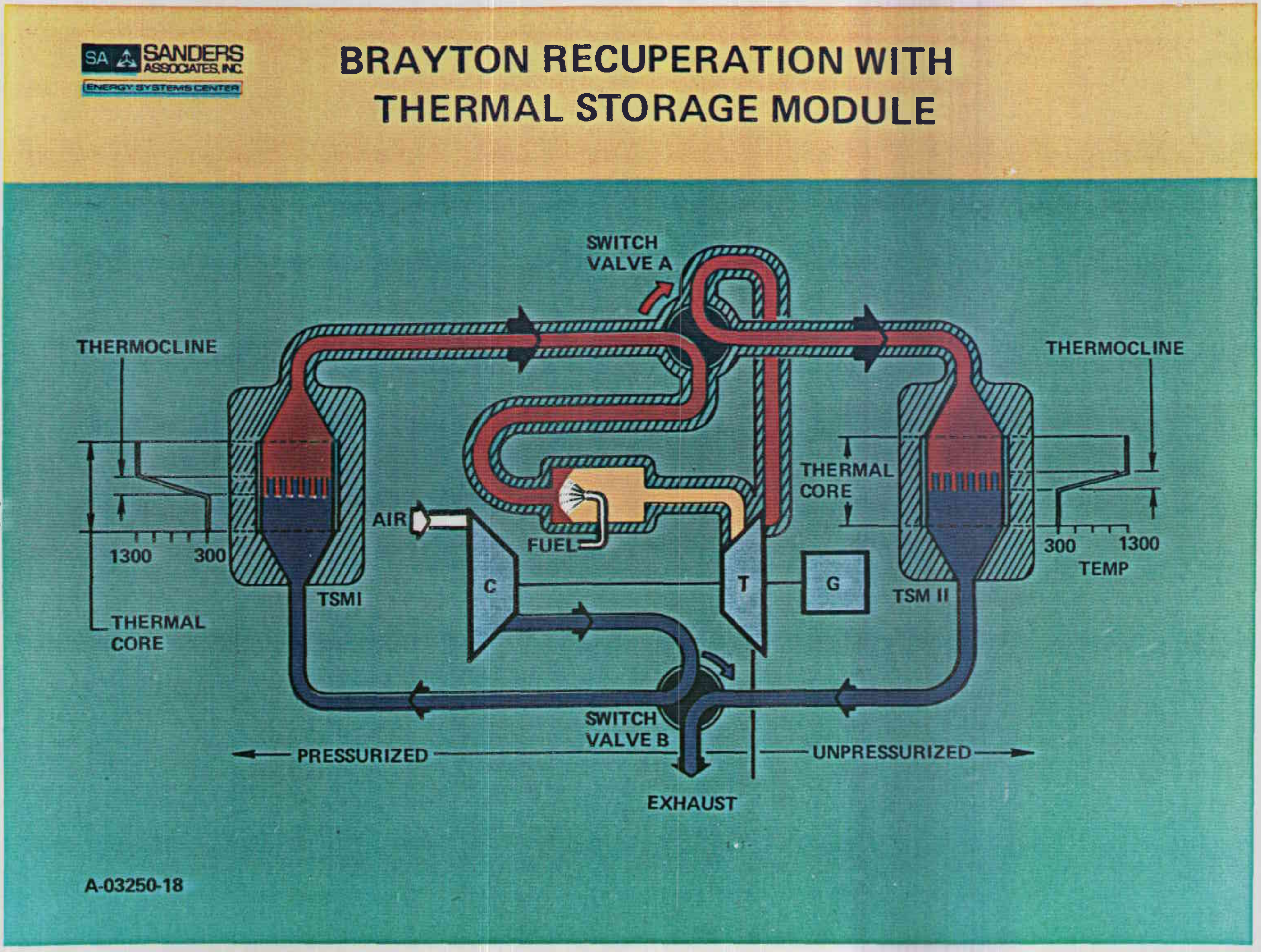
SA SANDERS ASSOCIATES, INC.
ENERGY SYSTEMS CENTER
BRAYTON RECUPERATION WITH THERMAL STORAGE MODULE
SWITCH VALVE A
THERMOCLINE
THERMOCLINE
THERMAL CORE
AIR
FUEL
1300
300
300
1300
TEMP
C
T
G
TSMI
TSM II
THERMAL CORE
SWITCH VALVE B
PRESSURIZED
UNPRESSURIZED
EXHAUST
A-03250-18

FIGURE 4-1

conditions in the third series of tests. A key to the tests conducted is presented in Table 4-1.

### 4.1.2 Equipment Operation

During a total of 100 hours of operation, there were 91 thermal cycles performed.

In beginning a test, the operator set the mass flow at high volume and adjusted fuel flow to provide the temperature for the first test. When the temperatures within the core of the TSM had equalized, test condition of temperature, pressure and flow were set signaling the beginning of a run. Generally, no further adjustment was required during a run with ambient pressure in the TSM. However, during the pressurized runs with the throttling valve downstream of the TSM, some valve adjustment was needed during the end of the run as the temperature and air density at the throttling valve began to change.

Burner outlet temperatures could be changed almost instantaneously but it took several minutes for the ducting to reach stable conditions. Consequently, the initial thermocline slope within the TSM was less than anticipated for an actual engine installation having more closely coupled components.

Several thermocouples were lost during the test program so that some of the thermal profiles presented will have missing readings.

### 4.1.3 Operation of Hot Valves

In the test configuration, the four way hot valve, manufactured by Sanders Associates, Inc., was always subjected to the same pressure in each channel but experienced large thermal gradients between the channels. For example, when the TSM was charged with 1700$^{O}$F air the exhaust air temperature was only 100$^{O}$F which created a 1600$^{O}$F gradient across the valve - a condition not expected in the cycle shown in Figure 4-1. Rather, in the proposed engine cycle, the hot valve will operate at nominally the same temperature with 30 psig across adjacent channels. In a structural sense the hot valve tests were more severe than expected in the proposed engine cycle.

TABLE 4-1 · TESTS CONDITIONS AND RUN NUMBERS

| RUN NUMBERS | $\dot{M}$ lb/sec | INITIAL CASE TEMP °F | INLET AIR TEMP °F | AIR IN TOP | AIR IN BOT | PRESSURE PSIG | COMMENTS |
|---|---|---|---|---|---|---|---|
| 4000-02 | 0.6 | Ambient | 295 | | X | 0 | Max air flow available |
| 03 | 0.6 | 295 | 1295 | X | | 0 | Max air flow available |
| 04 | 0.6 | 1295 | 295 | X | | 0 | Max air flow available |
| 05 | 0.2 | 295 | 1295 | X | | 0 | |
| 06 | 0.2 | 1295 | 295 | X | | 0 | |
| 07 | .0 | 295 | NA | | | | Overnight cool down |
| 08 | .43 | Ambient | 1295 | X | | 0 | |
| 09 | .43 | 1295 | 295 | X | | 0 | |
| 10 | .43 | Ambient | 295 | X | | 0 | |
| 11 | .41 | 295 | 1295 | X | | 0 | |
| 14 | .0 | 1295 | NA | | | | Overnight cool down |
| 14A | .43 | Overnight | 295 | | X | 0 | |
| 15 | .43 | 295 | 1295 | | X | 0 | |
| 16 | .43 | 1295 | 295 | | X | 0 | |
| 18 | .43 | Ambient | 295 | X | | 30 | |
| 19 | .43 | 295 | 1295 | X | | 30 | |
| 20 | .43 | 1295 | 295 | X | | 30 | |
| 22 | .20 | 295 | 1295 | X | | 30 | |
| 23 | .0 | 1295 | NA | | | 0 | Overnight cool down |
| 24 | .20 | Night before | 1295 | X | | 30 | |
| 25 | .2 | 1295 | 295 | X | | 30 | Flow adjustment |
| 26 | .2 | 1295 | 295 | X | | 30 | |
| 27 | .53 | 295 | 1295 | X | | 30 | |
| 28 | .53 | 1295 | 295 | X | | 30 | |
| 29 | .53 | 295 | 1295 | X | | 30 | |
| 30 | .43 | 1295 | 295 | X | | 30 | Repeat run 27 |
| 31 | .43 | 295 | 1295 | | X | 0 | Inverted -hot in bottom |
| 32 | .43 | 1295 | 295 | X | | 30 | recuperation -cool on top |
| 34 | .43 | 295 | 295 | | | 0 | Burner went out during run |
| 36 | .43 | 295 | 1295 | X | | 0 | |
| 36A | .43 | 1295 | 295 | | X | 30 | |
| 36B | .43 | 295 | 1295 | X | | 0 | |
| 36C | .43 | 1295 | 295 | | X | 30 | Simulaton of recuperation |
| 36D | .43 | 295 | 1295 | X | | 0 | cycles |
| 36E | .43 | 1295 | 295 | | X | 30 | |
| 37A | .43 | 295 | 1295 | X | | 0 | |
| 37B | .43 | 1295 | 295 | | X | 30 | |
| 37C | .43 | 295 | 1295 | X | | 0 | Simulation of recuperation |
| 37D | .43 | 1295 | 295 | | X | 30 | cycles |
| 37E | .43 | 295 | 1295 | X | | 0 | |
| 37F | .43 | 1295 | 295 | | X | 30 | |
| 37G | .43 | 295 | 1295 | X | | 0 | |
| 37H | .43 | 1295 | 295 | | X | 30 | |
| 37I | .43 | 295 | 1295 | X | | 0 | |
| 37J | .43 | 1295 | 295 | | X | 30 | |
| 38 | .43 | Ambient | 1700 | X | | 0 | |
| 39 | .43 | 1700 | Ambient | | X | 0 | |
| 40 | .53 | Ambient | 1700 | X | | 0 | |
| 41 | .53 | 1700 | Ambient | | X | 0 | |
| 42 | .2 | Ambient | 1700 | X | | 0 | |
| 43 | | | | | | | |
| 44 | .43 | 1295 | Ambient | X | | 30 | |
| 45 | .43 | 1295 | 1700 | X | | 30 | |
| 46 | .43 | 1700 | 1295 | X | | 30 | |
| 46A | .43 | 1295 | 295 | X | | 30 | |

TABLE 4-1 TESTS CONDITIONS AND RUN NUMBERS (Cont.)

| RUN NUMBERS | $\dot{m}$ lb/sec | INITIAL CASE TEMP °F | INLET AIR TEMP °F | AIR IN TOP | AIR IN BOT | PRESSURE PSIG | COMMENTS |
|---|---|---|---|---|---|---|---|
| 47 | .52 | Ambient | 1295 | X | | 30 | |
| 4000-48 | .52 | 1295 | 1700 | X | | 30 | |
| 49 | .52 | 1700 | 1295 | X | | 30 | |
| 50 | .0 | 1295 | NA | | | 0 | 1 hour cooling |
| 51 | .28 | 1295 | 1700 | X | | 30 | |
| 52 | .24 | 1295 | 1700 | X | | 30 | |
| 53 | .0 | 1700 | NA | | | 0 | Overnight cool down |
| 54 | .43 | 295 | 1295 | X | X a | 0 | 15 Minute Cycling |
| 55 | .43 | | | X | X a | 0 | Repeat 15 min. cycling |
| 56 | .43 | | | X | X a | 0 | 6 Minute Cycling |
| 57 | 0 | | | | | 0 | Overnight Cool Down |
| 58 | .43 | | | X | X a | 0 | 25 Minute Cycling |

a. In recuperation simulation runs the hot valve directed cool air in the bottom and hot air in the top for each cycle.

The initial valve spacers did not allow for thermal expansion tolerances. During the test at high temperatures the hot valve became very difficult to turn. Upon disassembly there was considerable galling of the ball and the valve seats. After grinding away the coating on the ball*, repolishing, and replacing the valve seat spacers with new spacers having proper tolerances, performance returned and no further problems were experienced.

The Globe valve, used in controlling the air flow under pressurized conditions had a special stellite seat. No throttling difficulty was experienced with this. valve even when it was operating at a bright red condition with 1700$^{o}$F air flow.

## 4.2 THERMAL STORAGE PROFILES

### 4.2.1 Temperature Distribution

Thermocouples located throughout the TSM gave vertical and horizontal profiles with time. The vertical profiles taken with a temperature difference of 1000$^{o}$F across the TSM, Figure 4-2, show uniform profiles with time at a constant slope over most of the vertical travel. Only as the thermocline reaches the end of the core is there a non-uniform slope. The uniform thermal gradient which occurs over approximately 80% of the vertical height travels at a constant rate through the TSM. For example, comparing the profiles of Figure 4-2a, with Figure 4-2b, the first representing a charge and the second of a discharge of the TSM, the time required for the thermocline to pass from one end of the cermic core to the other (31 inches) was 24 minutes in both cases. The only difference between the charge and the discharge cycles was a small change in the slope of the curve. The discharge or negative slope was slightly steeper than the charge or positive slope.

The horizontal profile as measured across the center of the core shows a uniform profile and, therefore, uniform flow in Figure 4-3a, when the air flow was downward. However, in Figure 4-3b, where the flow is upward, there is 527$^{o}$F gradient across the center plane as the thermocline passes through, indicating a non-uniform thermocline travel in the upward air flow direction. This same phenomena was observed for other mass flow and temperature conditions where the air flow entered the TSM from the bottom. This profile difference is probably caused by non-iniform flow distribution in the lower diffuser.

*Metco 443. Ni-Cr-Al Composite. Metco, Wesbury LI, N.Y.

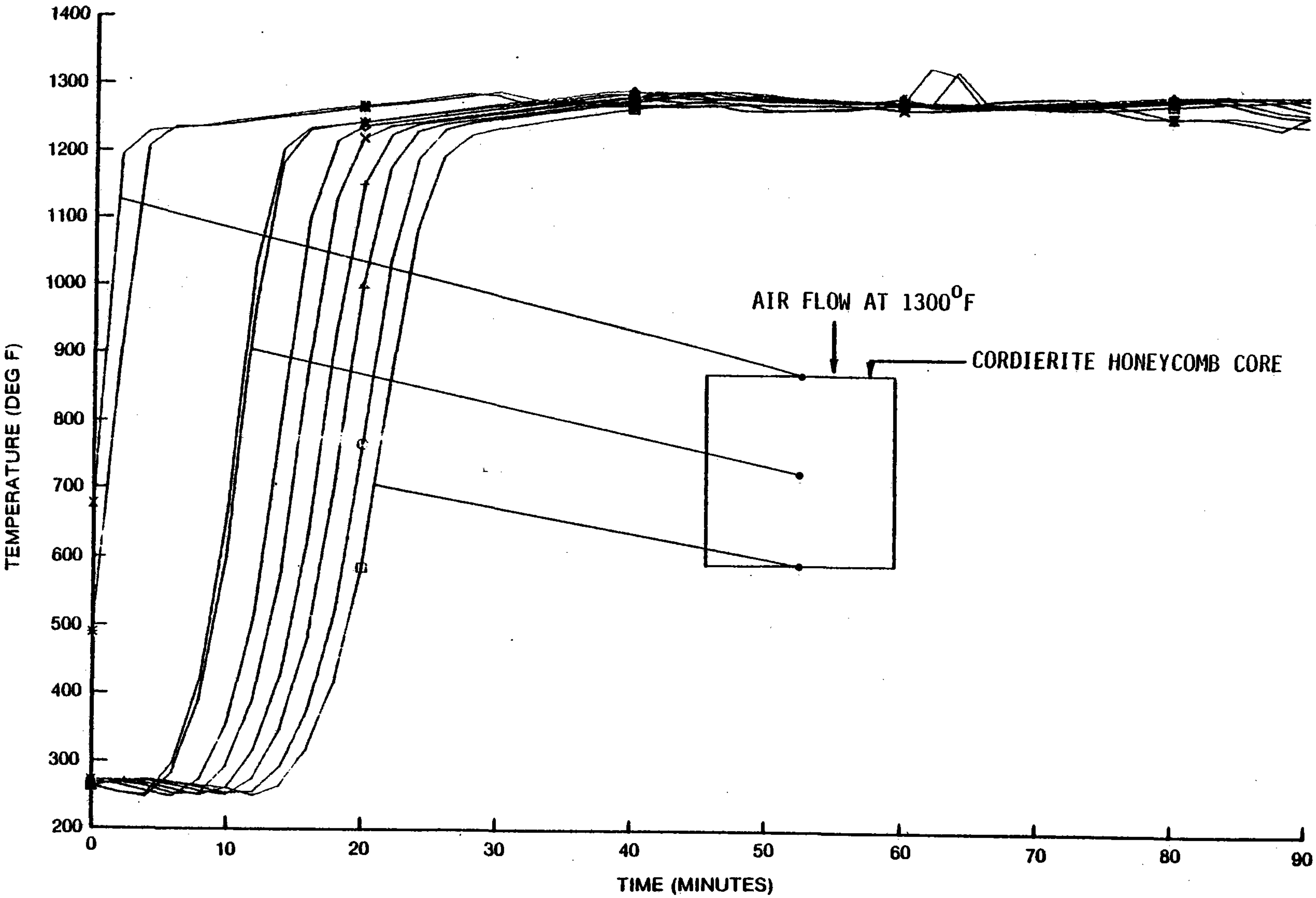


07230-19

A-05270-10

FIGURE 4-2a.

MEASURED VERTICAL PROFILES ALONG CORE CENTER LINE 0.43 LB/SEC

DOWNWARD AIRFLOW CHARGE CYCLE

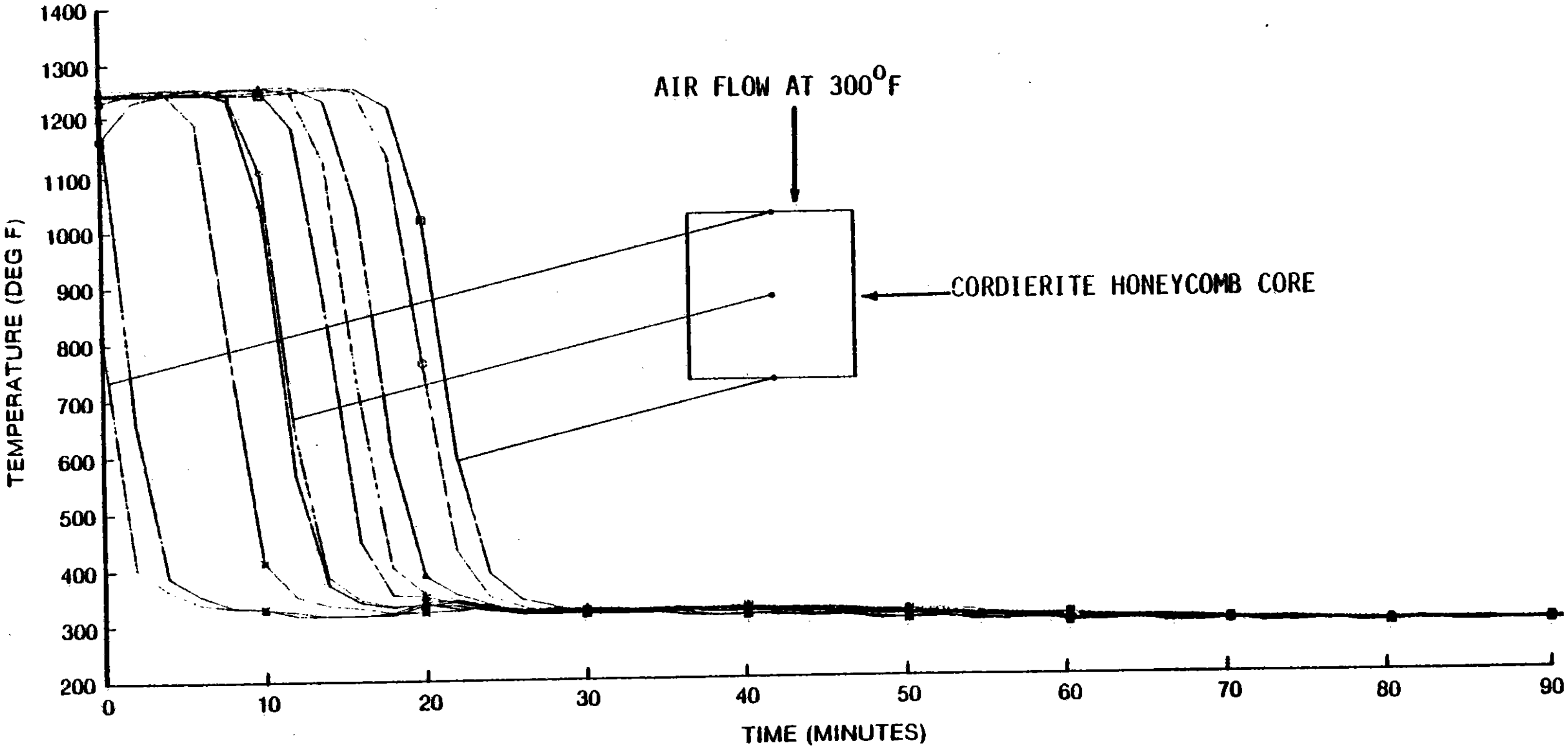


A-05270-5

07230-21

FIGURE 4-2b.

MEASURED VERTICAL PROFILES ALONG CORE CENTER LINE 0.43 LB/SEC

DOWNWARD AIRFLOW DISCHARGE CYCLE

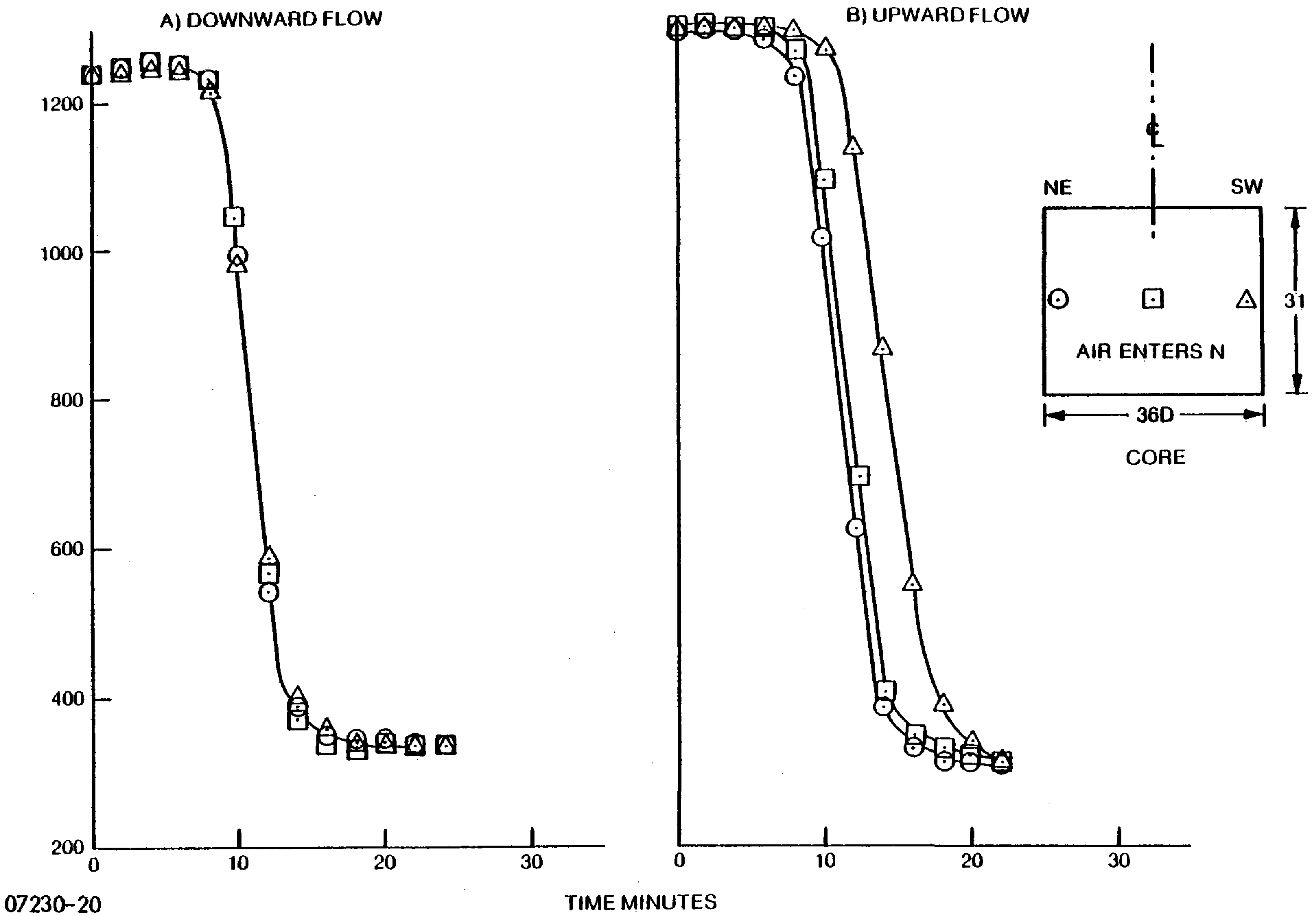


Figure 4-3a. Measured Core Horizontal Profile 0.43 Lb/Sec. 0 psig, Downward Flow

Figure 4-3b. Measured Core Horizontal Profile, 0.43 Lb/Sec. 0 psig, Upward Flow

A comparison of the centerline profiles for both the charge and discharge conditions was made between a test with air flow entering the top of the TSM, Figure 4-4a and b, and a second test with the air flow entering the bottom, Figure 4-2a and b. Since the profiles are identical, the difference in horizontal profiles noted across the centerline had a negligible effect on the travel time through the TSM and the slopes of the temperature vs time curves. Also shown on Figure 4-4 are the temperatures at the inlet and outlet elbow ahead of the four-way valve for reference. The results of this comparison show that gravity convection does not affect the thermocline propagation.

The low mass flow profiles, Figure 4-5, show the effect of time on the charging thermocline slope. For a mass flow of 0.2 lb/sec, it takes 48 minutes for the thermocline to pass through the core. During this time the thickness of the thermocline has increased from 1-3/4 inches to 11-1/2 inches which is a thermocline broadening of 0.2"/minute.

The temperature profiles discussed above represent temperatures within the ceramic honeycomb. In a real system these profiles will be degraded slightly by the losses associated with headers and valving. As a representation of these losses, thermocouples were placed in identical locations in the upper and lower elbows. These profiles, Figure 4-6a and b, indicate a continual changing slope with time on both the charge and discharge cycles. Obviously, the thermocline performance of the core is degraded by these other losses but a Brayton engine installation will have shorter couplings than this test apparatus. The curve showing the temperature variations at the inlet elbow, Figure 4-6a, and Figure 4-6b, shows the effect of delay in starting the air flow through the TSM after having been charged to 1300$^{\circ}$F. This delay is specific to the experimental apparatus and will not occur in a complete Brayton system. There was a heat loss and perhaps a very small airflow at both ends of the TSM, as indicated by the drop in inlet elbow temperature. Once the airflow was reestablished the TSM performed as though there had been no time delay.

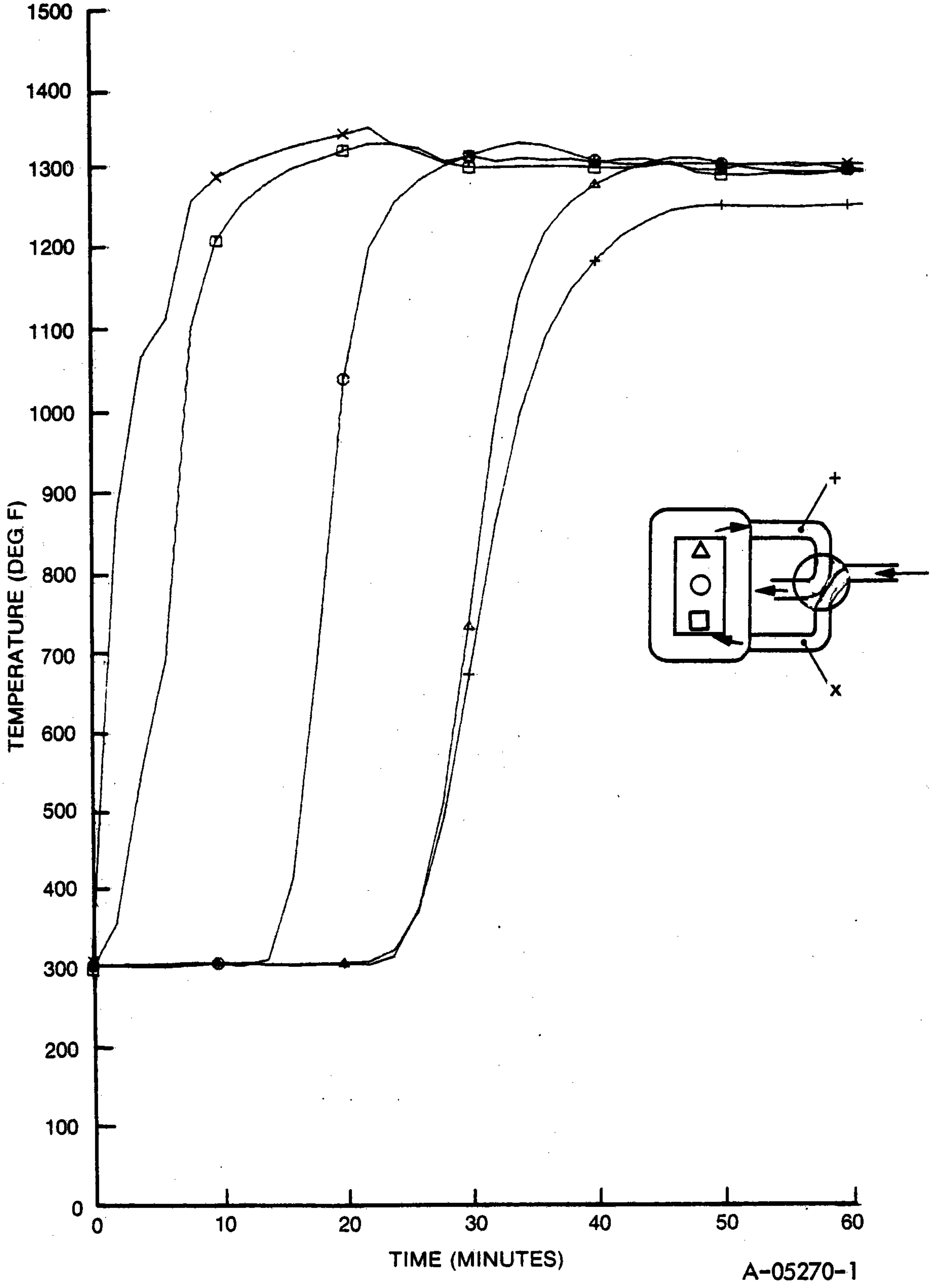


Figure 4-4a: Measured Temperature Variations Along the Core Centerline With Upward Air Flow 0.43 lb/sec. Charge Cycle

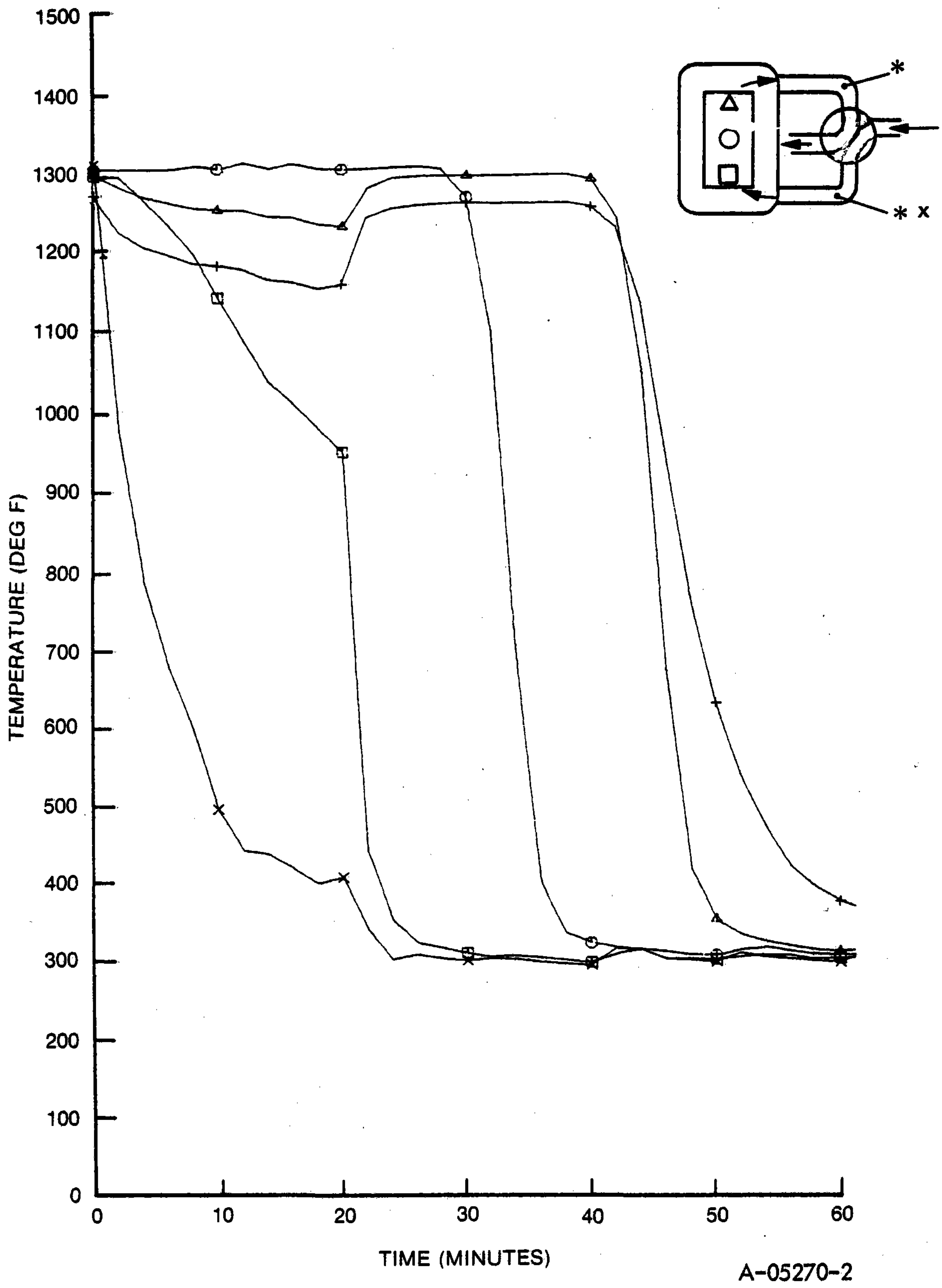


Figure 4-4b. Measured Temperature Variation Along the Core Centerline with Upward Air Flow. 0.43 lb/sec. Discharge Cycle.

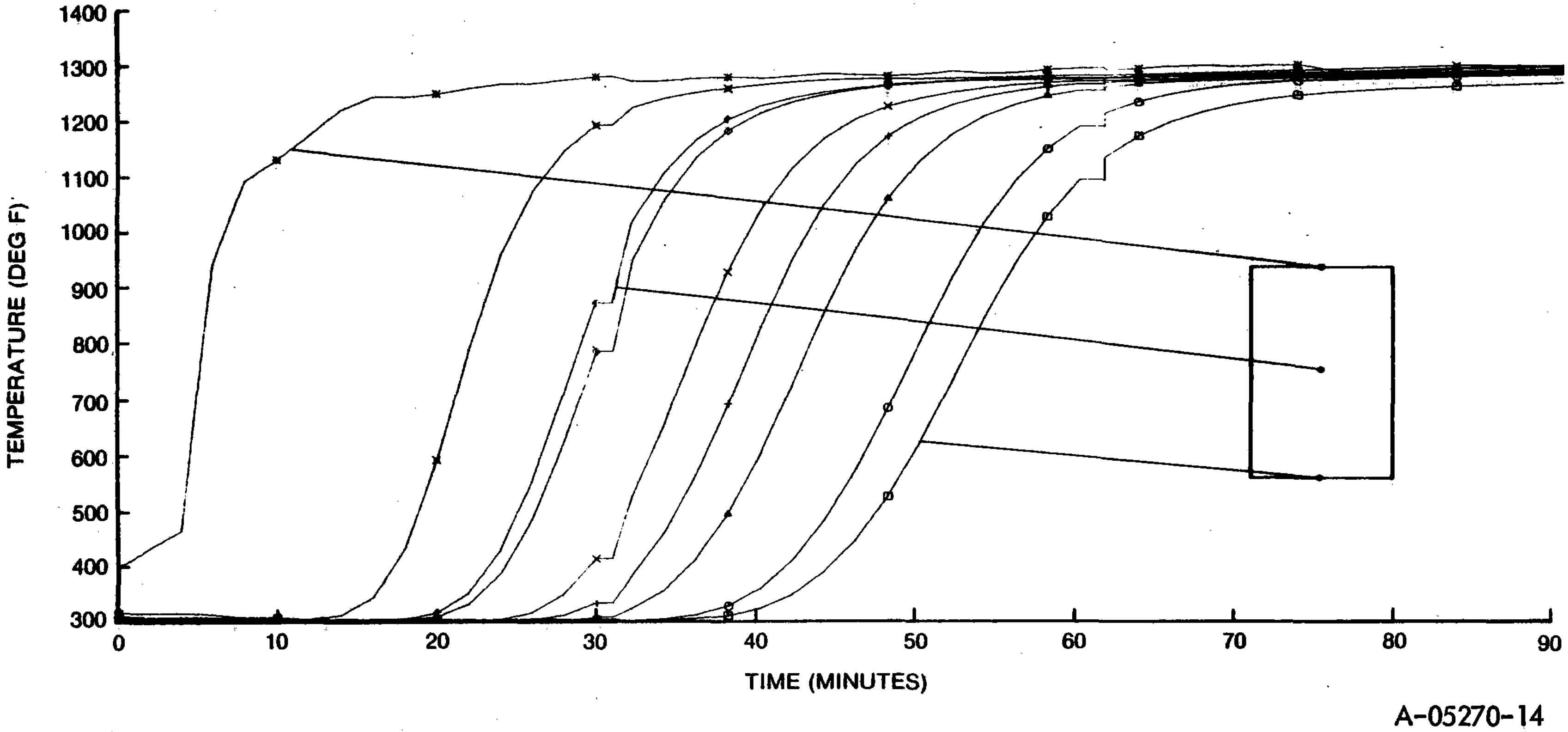


Figure 4-5. Measured Vertical Profile with Low Mass Flow
Flow Upward. 0.2 lb/sec.

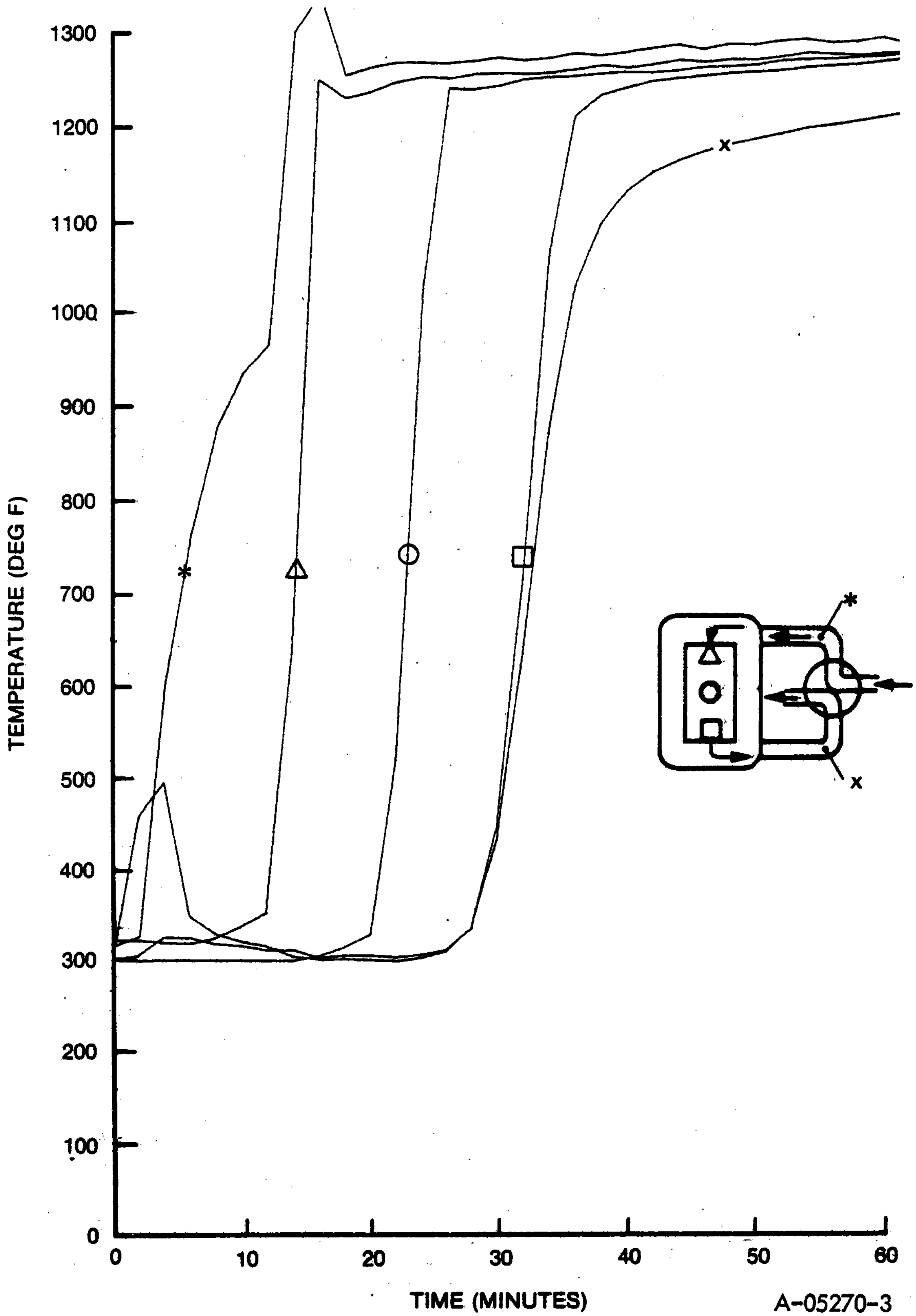


Figure 4-6A. Measured Vertical Profile with High Mass Flow, Including Ducting Effects, Downward Air Flow, 0.58 lb/sec. Charge Cycle

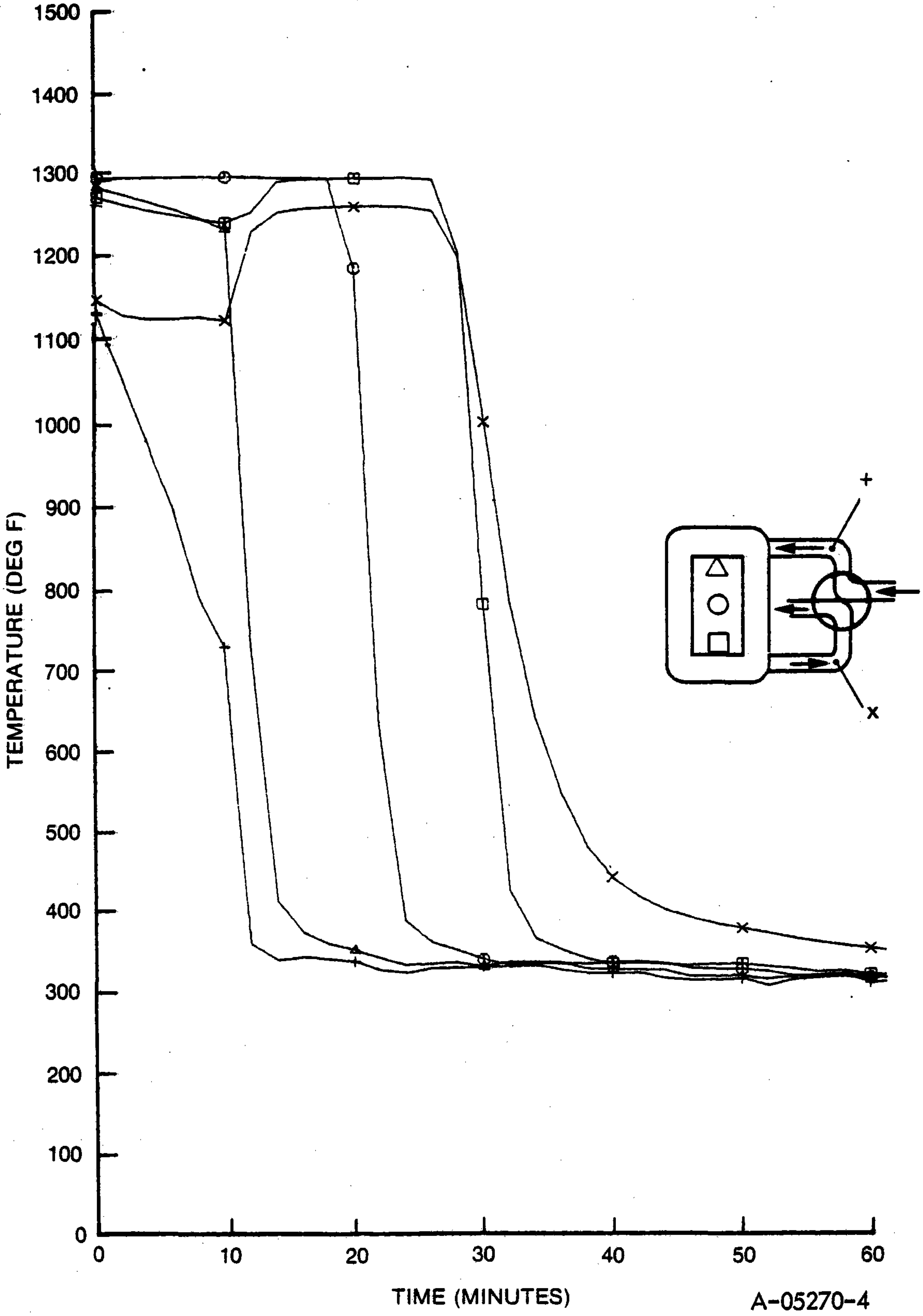


Figure 4-6b. Measured Vertical Profile with High Mass Flow, Including Ducting Effects, Downward Air Flow, 0.58 lb/sec. Discharge Cycle

### 4.2.2 Mass Flow Profiles

In order to demonstrate the effect that mass flow has on the thermoclines which develop in the TSM, three sets of curves are presented in Figures 4-7, 4-8, and 4-9 , representing mass flow of .53 lbs/sec, .43 lbs/sec, and .2 lbs/sec. respectively. The .53 lbs/sec mass flow curves represents a mass flow considerably above that expected in the 20 KWe Brayton cycle where the design mass flow is .43 lb/sec. The .2 lbs/sec curve represents a much lower flow than expected. The comparisons between runs at different mass flows are made at temperatures representing the most severe thermal gradients expected of the TSM -namely ambient to 1700$^{o}$F. The first curve, Figure 4-7, is for the high mass flow and represents the thermoclines which develop during both the charge and discharge cycles. In both instances, the cycle takes approximately 18 minutes for the thermocline to pass completely through the 31 inches of storage ceramic. This compares with the 24 minutes it takes the thermocline to pass through when the mass flow is reduced to .43 lb/sec (Figure 4-8). When the mass flow is reduced to .2 lbs/sec (Figure 4-9 ), the time is increased to 48 minutes. The travel time, t, varies directly with mass flow as is expected.

### 4.2.3 Effect of Pressure and Gravity

When used as a recuperator for the Brayton engine, a pair of TSM's is required. One recovers the heat from the turbine and operates at ambient pressure. The other adds heat to the compressed air before additional heat is added either by combustion or by solar energy. The curves shown in Figures 4-10 and 4-11 show the effect of the pressurization on the shape of the profiles. It is interesting to note that pressure has no measurable effect on the shape of the thermocline curves. Except for the possible differences in diffuser performance, there is no apparent effect of gravity on thermoclines; compare Figures 4-3 and 4-4.

### 4.2.4 Effective Temperature Range

The TSM is designed to operate over a wide range of temperatures. In order to understand whether temperature has an effect on the profiles generated, three temperature gradients are compared in Figure 4-12 at a mass flow of .43 lbs/sec. The temperatures at the top and the bottom of ceramic core are shown. The

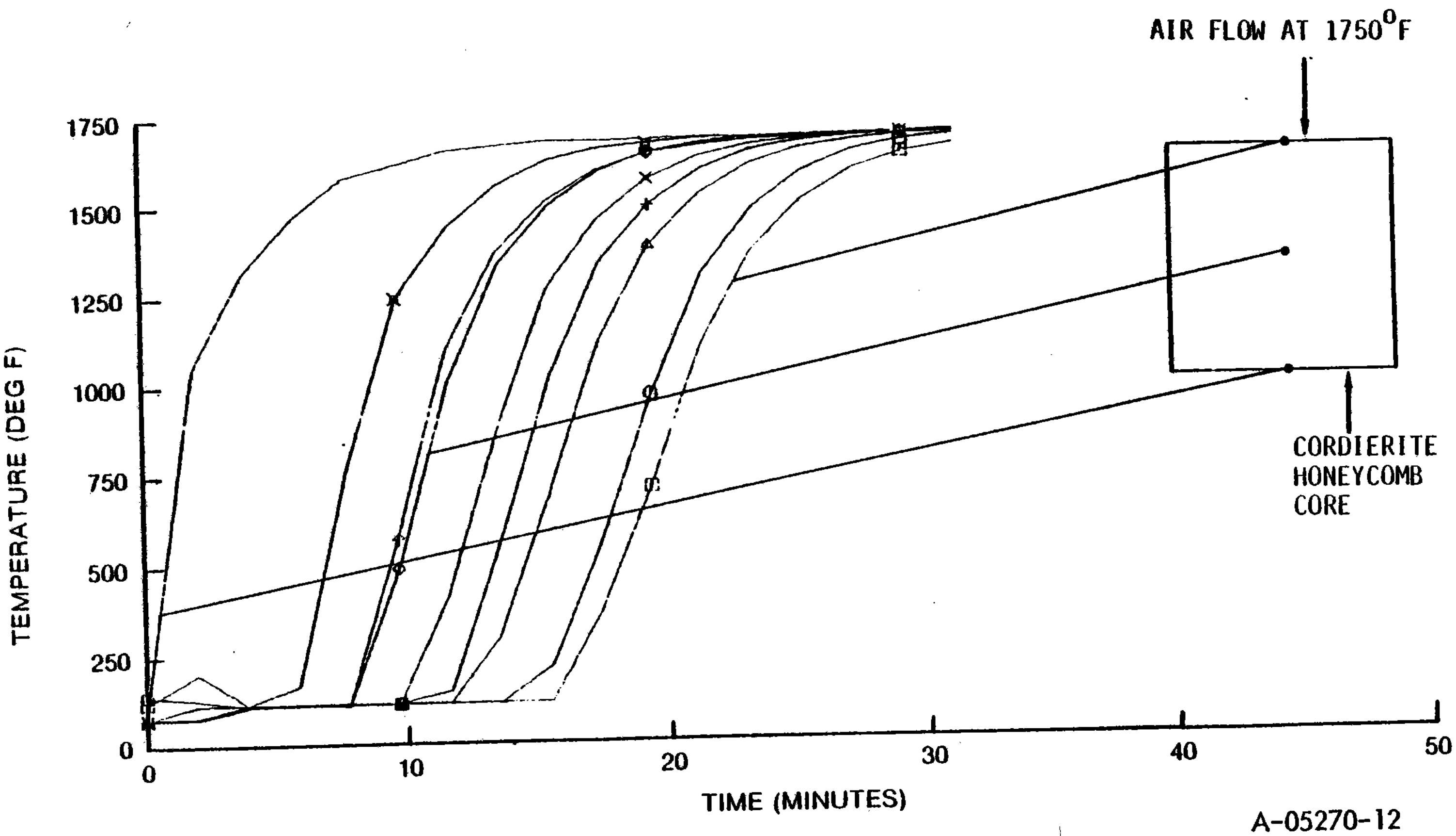


Figure 4-7a. Charge Cycle, Measured Thermocline Profile
0.53 lb/sec

SANDERS ASSOCIATES, INC.
ENERGY SYSTEMS CENTER

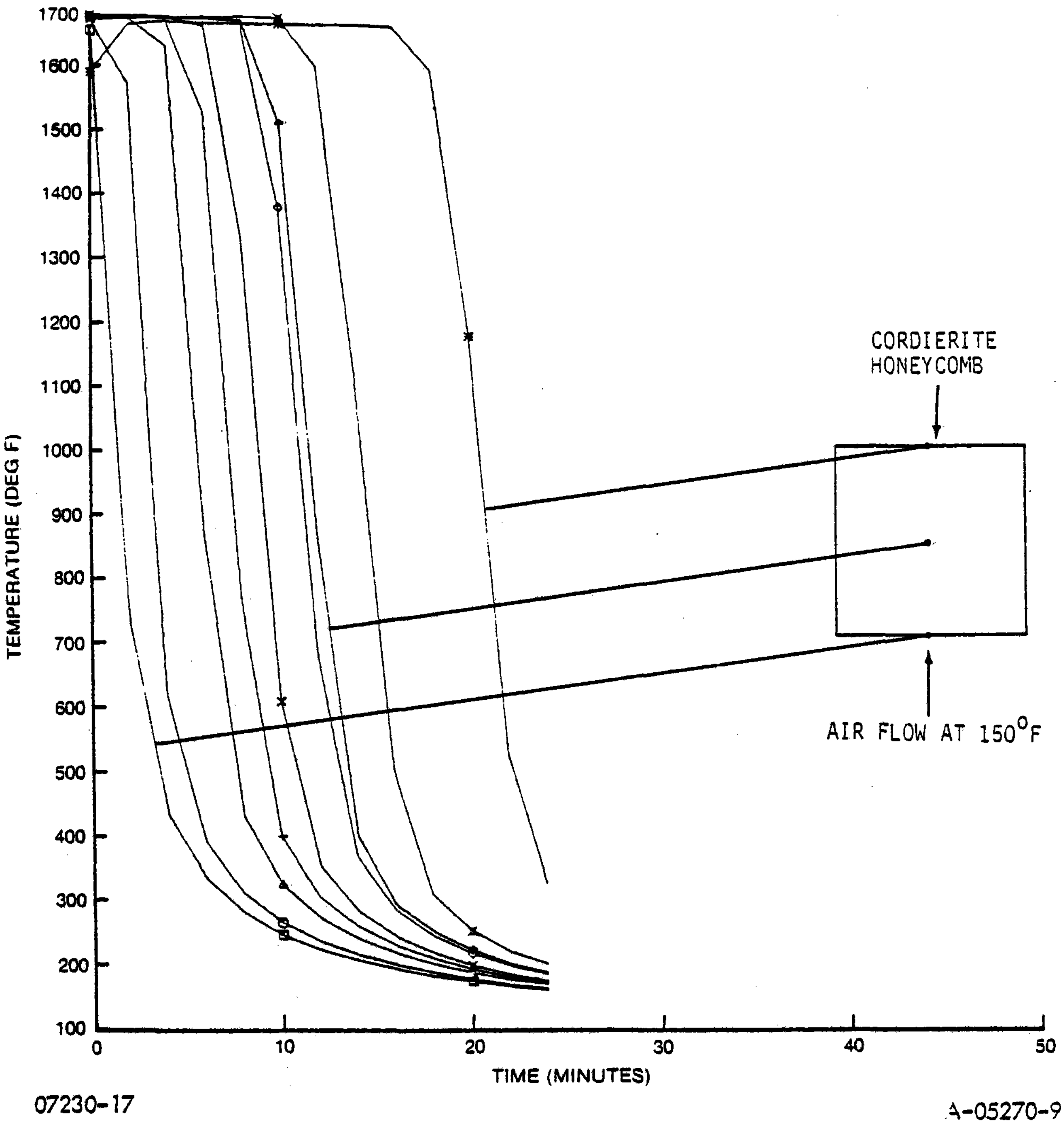


Figure 4-7b. Measured Thermocline Profile, Discharge Cycle 0.53 lb/sec.

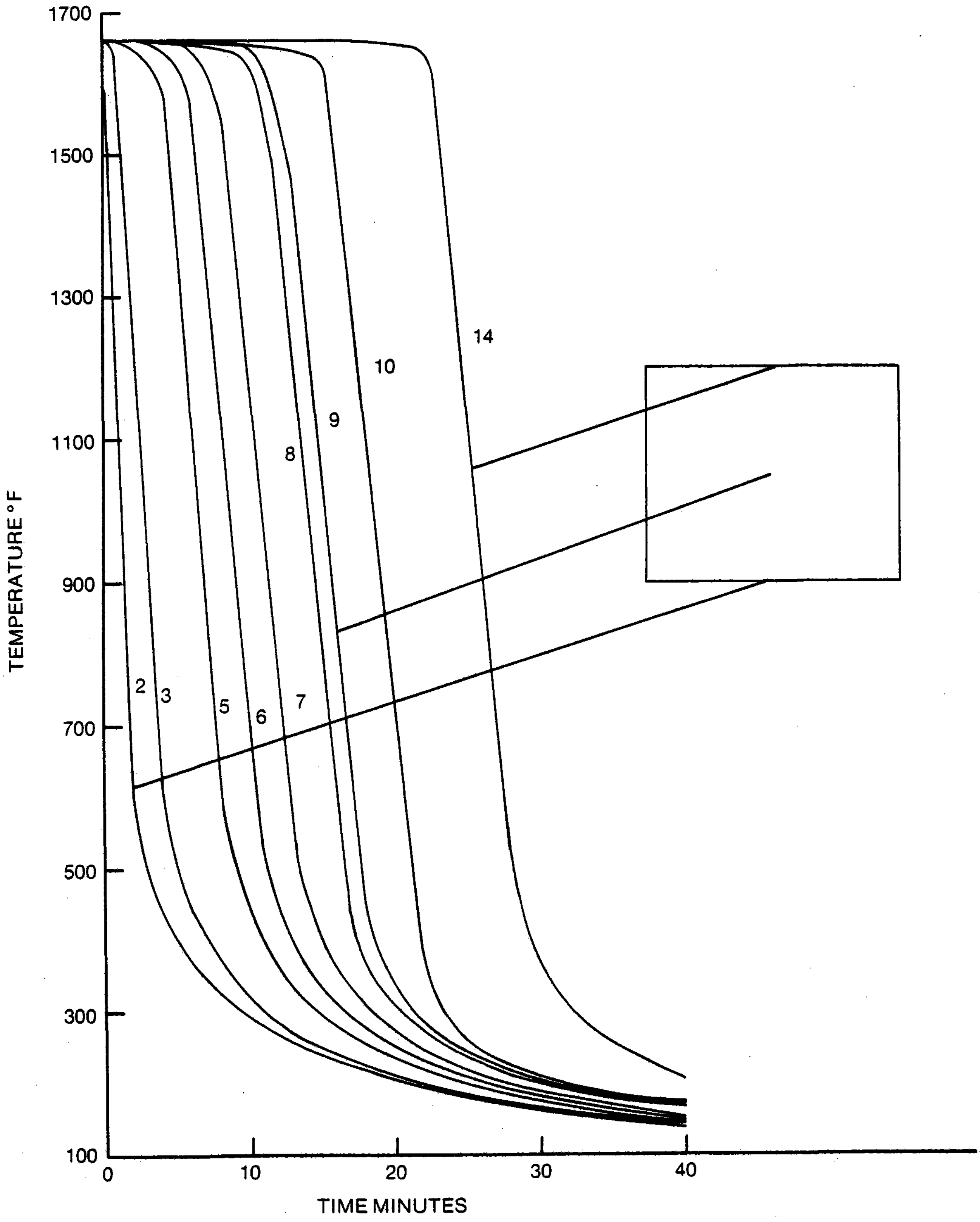


Figure 4-8. Measured Thermocline Profiles, Discharge Cycle, 0.43 lb/sec

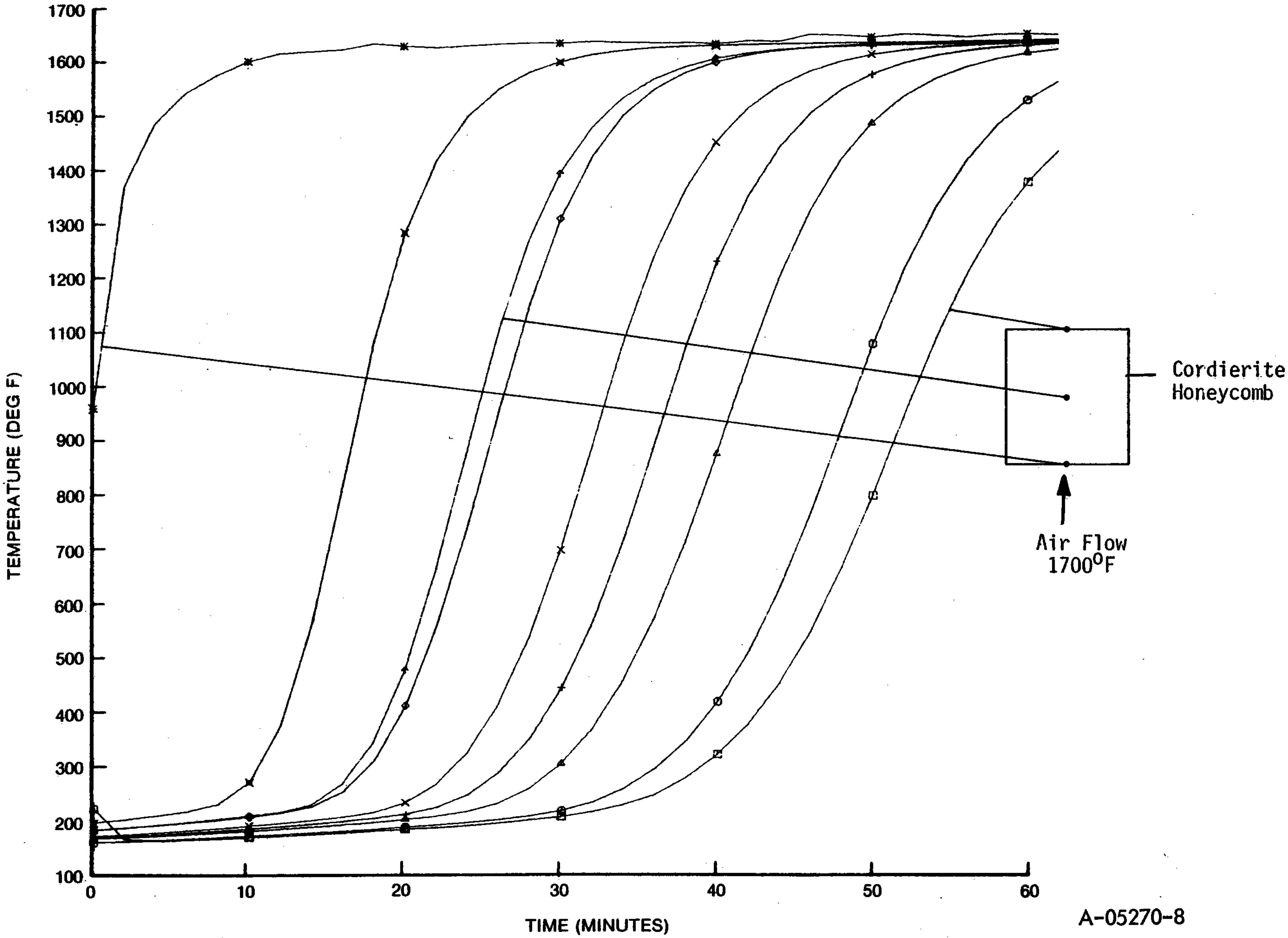


Figure 4-9. Measured Thermocline Profiles. 0.2 lb/sec

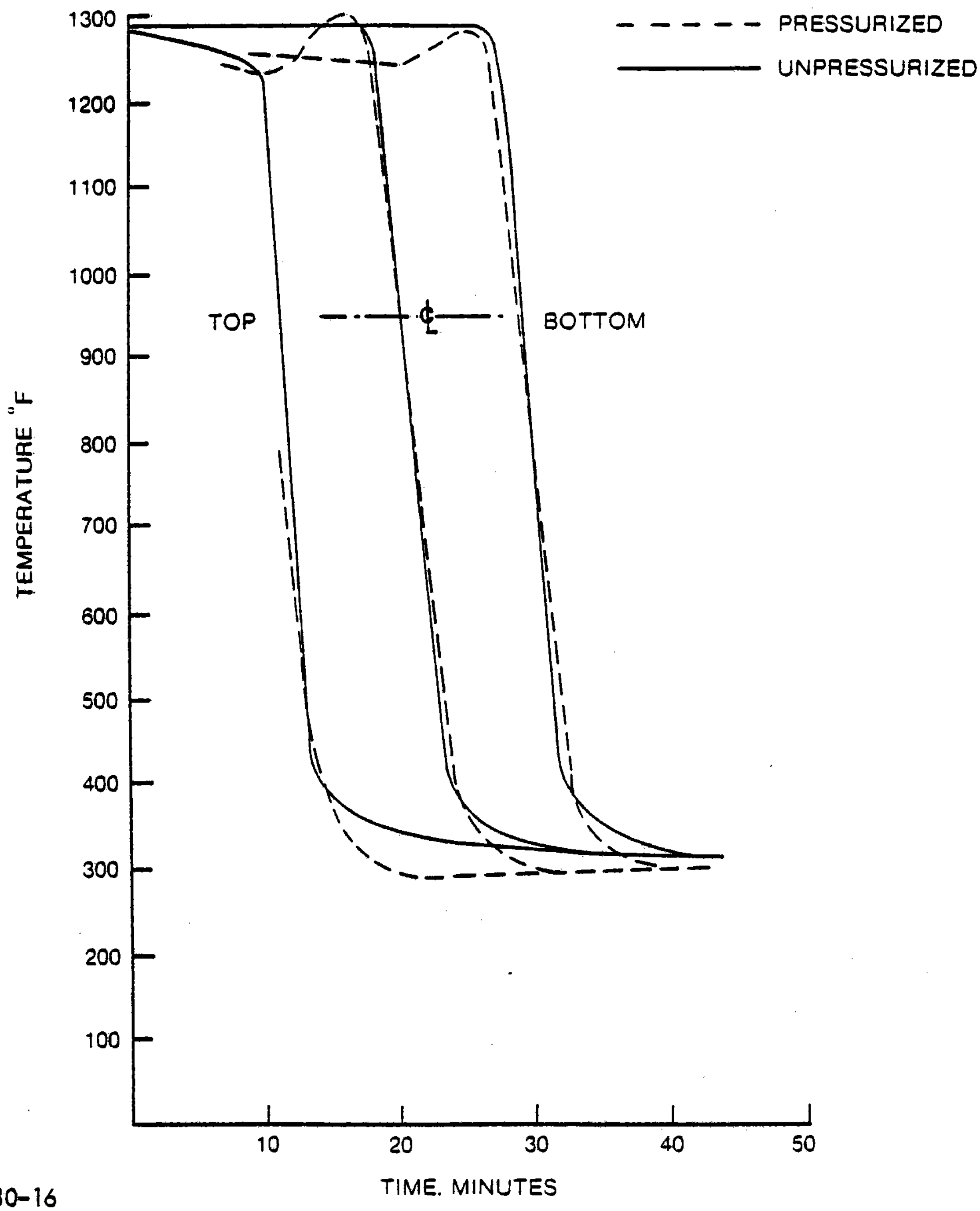


07230-16

Figure 4-10. Measured Effects of Pressure on Thermal Profiles, Discharge Cycle, 0.53 lb/sec, Downward Flow.

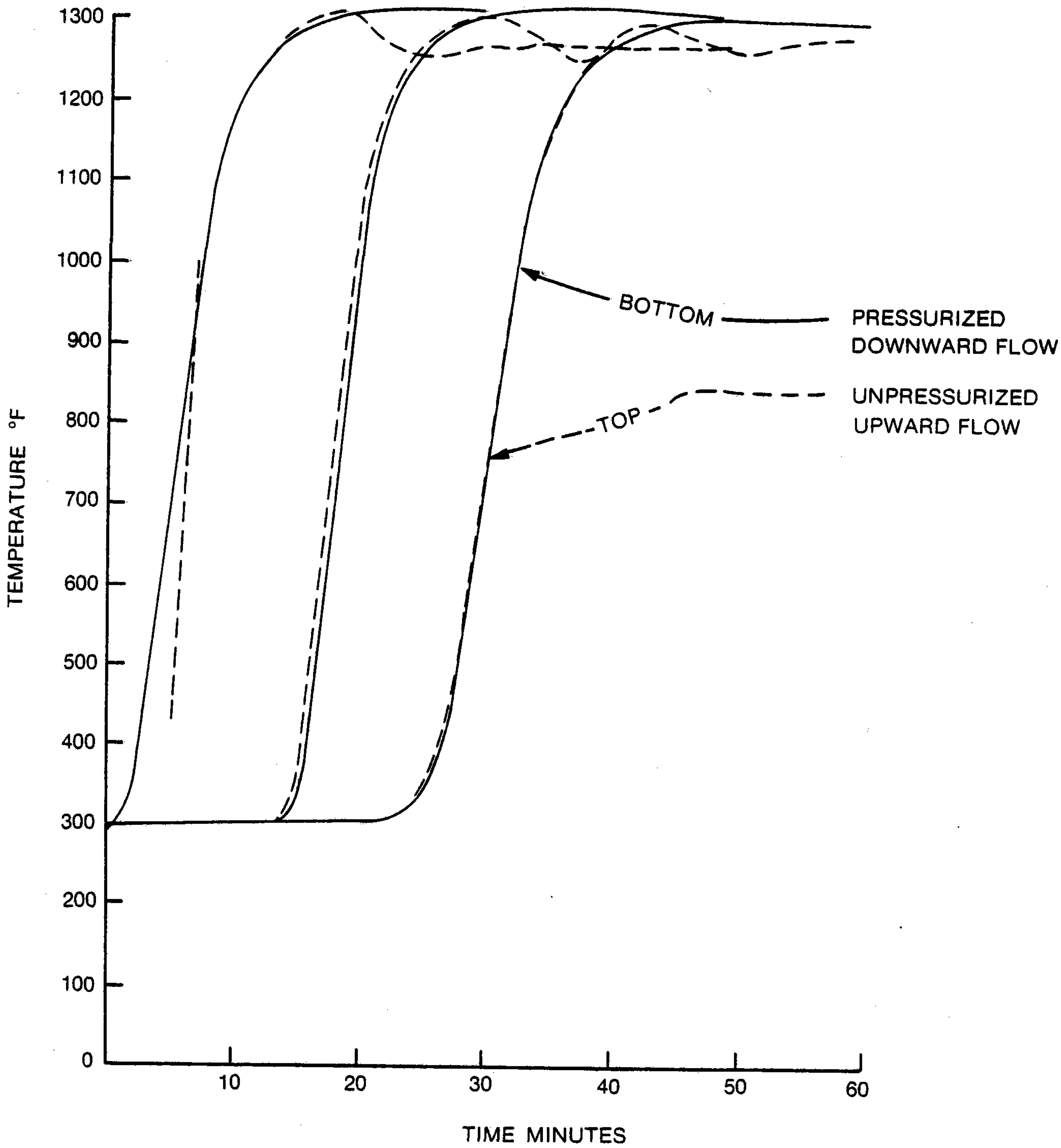


Figure 4-11. Measured Effect of Pressure on Thermal Profiles, Charge Cycle 0.43 lb/sec.

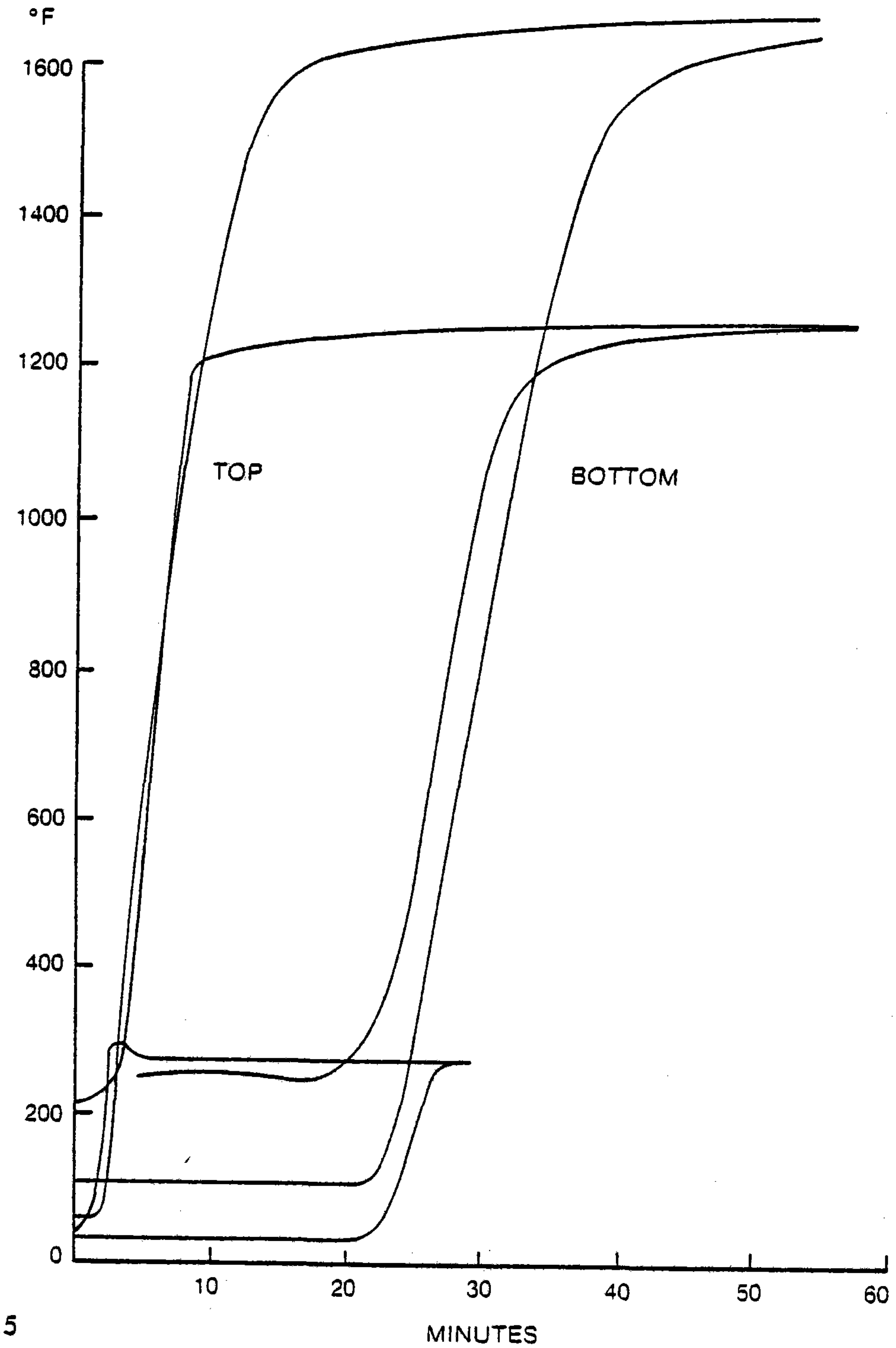


07230-15

Figure 4-12. Measured Temperature Profile at 3 Temperature Gradients, 0.43 lb/sec. 0 - psig thermoclines at the top of the core are overlayed as nearly as possible. It is interesting to note that the slopes of the curves on both the top and the bottom are parallel. The time for the thermocline to pass through the core is slightly different for the two temperature ranges. This may be due to inaccuracies in setting mass flows identical for each temperature as well as variations of heat capacity with temperature.

### 4.2.5 Cool Down

During one of the shutdowns after the days running, the experiment was left at 1700$^{O}$F with the data logger running at a slow rate. The next morning, 17 hours later, we had a record of the temperatures throughout the core during this period. Figure 4-13 shows the profiles through the centerline as a function of time. The top curve is for the thermocouple located in the center of the core. The cooling effect is initially symmetrical about the centerline. After a period of about 2 hours, the top surface is 50$^{O}$ warmer than the bottom one. Local thermal circulation patterns within the TSM are a probable cause of this gravitational effect. The uniform rate of cool down after several hours indicates that the TSM will drop in temperature to 1/e of its original temperature in 34 hours.

The horizontal losses, Figure 4-14, are symmetrical about the center.

## 4.3 PRESSURE DROP

Minimizing the pressure drop in the Brayton cycle recuperator strongly affects cycle efficiency, particularly for low pressure ratio engines. The measured core pressure drop during a charge cycle, Figure 4-15, compares closely with a theoretical curve for mass flow of 0.43 lbs/sec. As heat is added and volumetric flow increases pressure drop also increases to a maximum of 4.42 in. of $H_2O$.

BAE SANDERS ASSOCIATES, INC

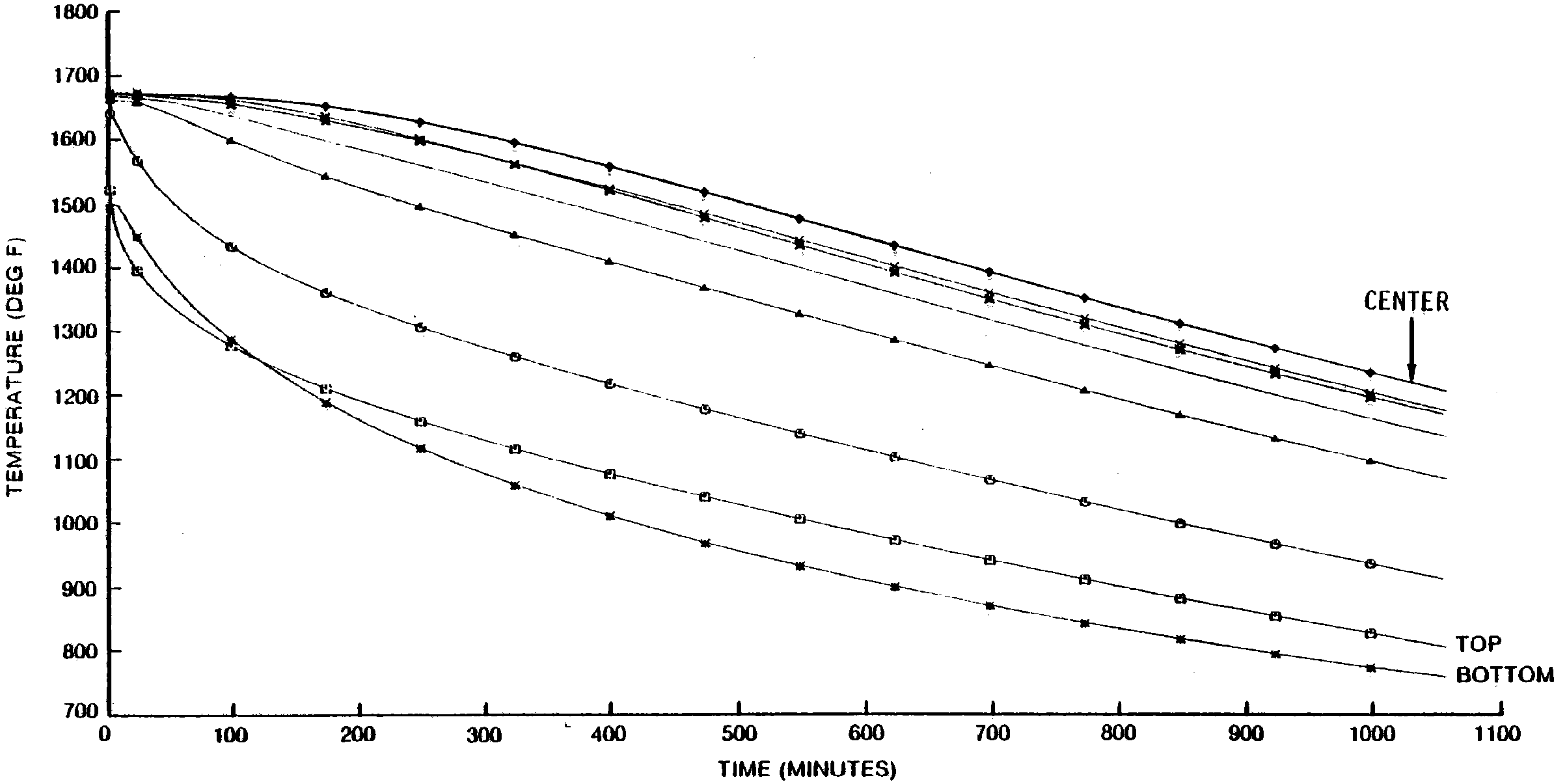


Figure 4-13. Measured Temperature Profile Through Core During Cool Down

07230-14

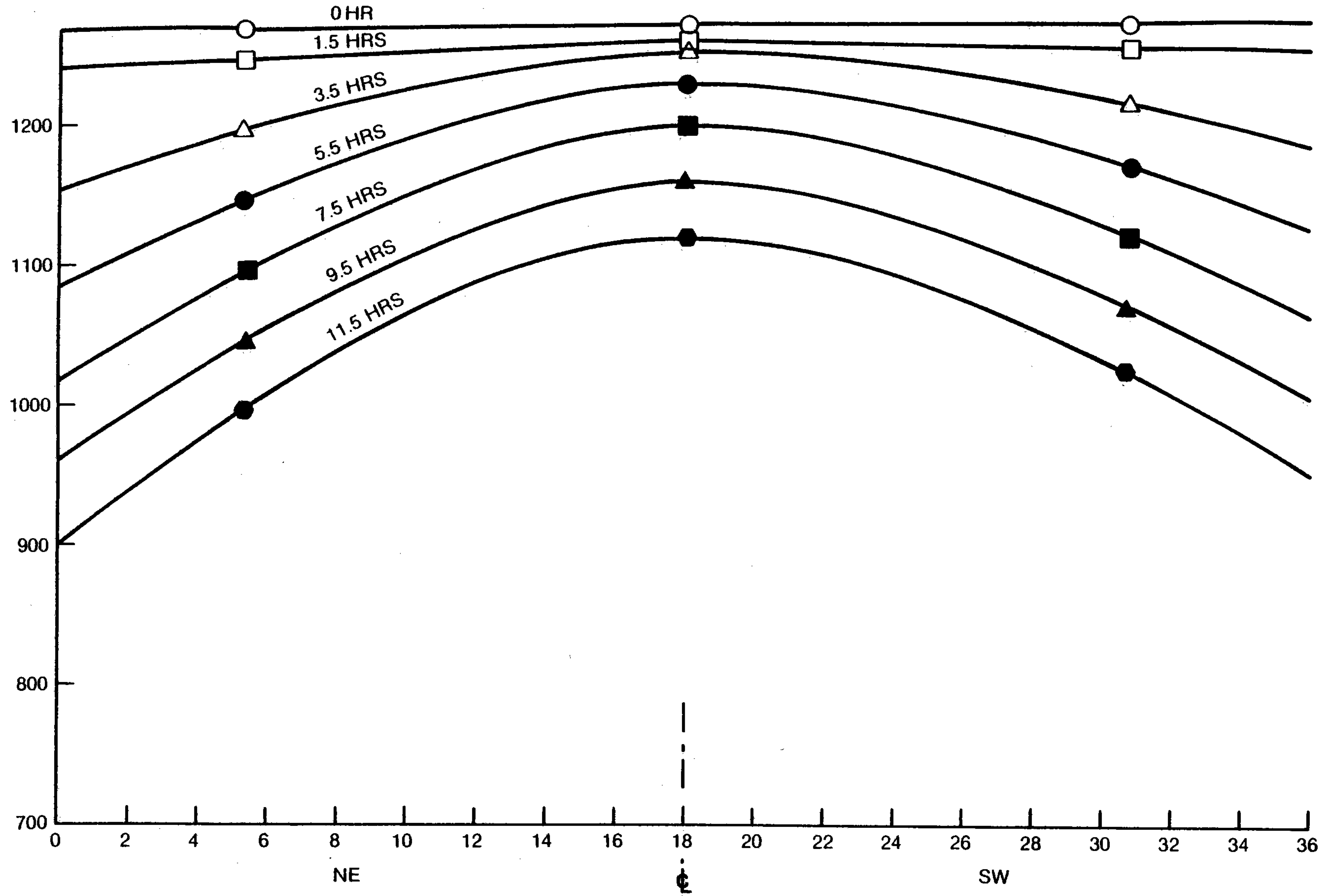


Figure 4-14. Measured Temperature Profile Across TSM During Cool Down

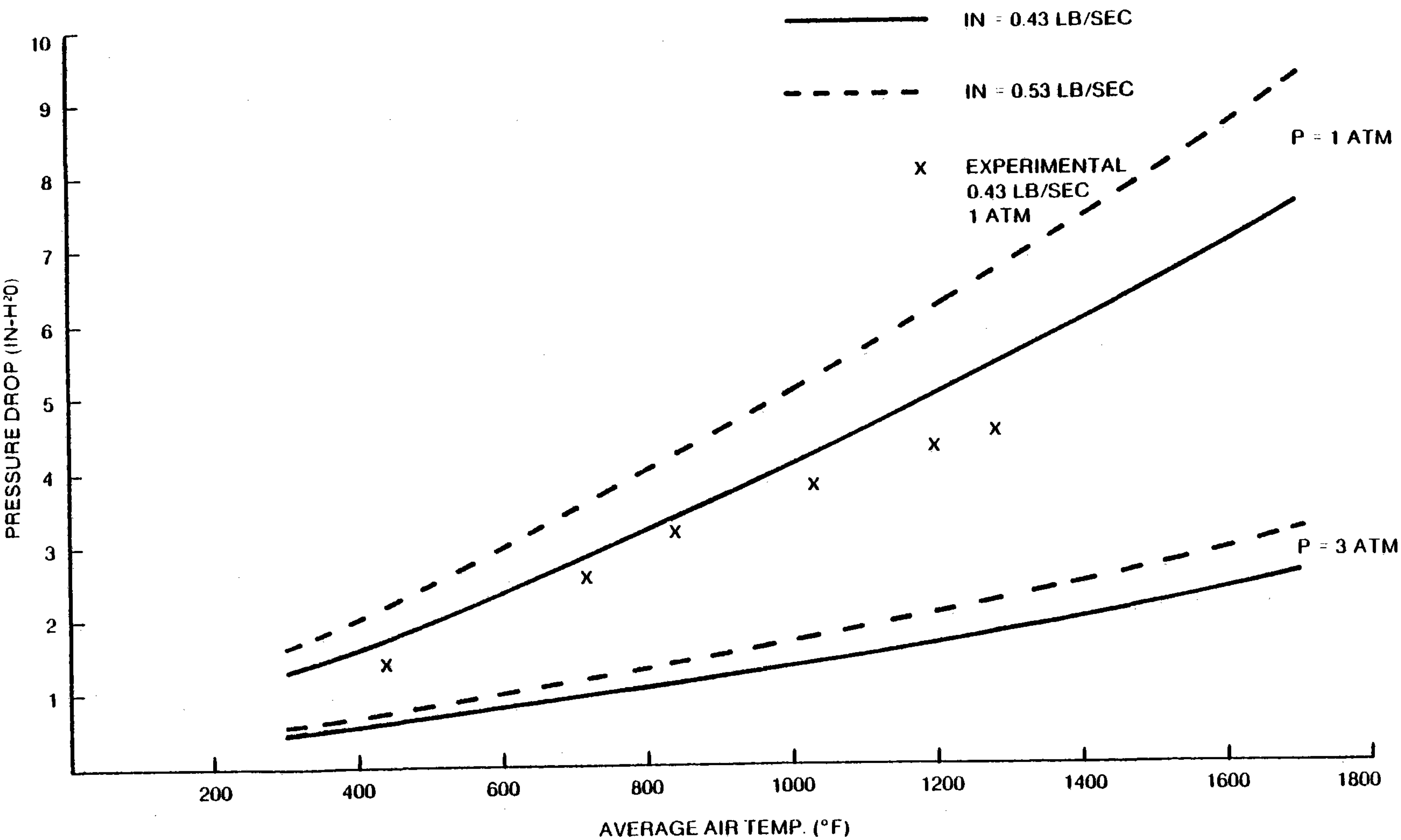


07230-13

Figure 4-15

**PRESSURE DROP THROUGH SQUARE CELL HONEYCOMB CORE**

The theoretical curves were determined as follows:

With square cell geometry, the hydraulic diameter of each cell is given by:

$$d_H = \frac{\sqrt{1 - S_f}}{\sqrt{144n}} \text{ (ft.)}$$

Where: $S_f$ = solid fraction of the core

$n$ = number of cells/in$^2$

Following the conventional definition of pressure drop in ducts:

$$\Delta P = 4f \frac{L}{d_H} \rho \frac{V^2}{2g}$$

where for laminar flow $f = \frac{16}{R_e} = \frac{16}{\rho V dH/\mu}$

The pressure drop solution is given by:

$$\Delta P = 32 \frac{L \dot{m} \mu}{g d_H{}^2 \rho A (1 - S_f)}$$

where:

$\Delta P$ = pressure drop (psf)

$L$ = duct length (ft)

$\mu$ = viscosity (lb/sec-ft)

$d_H$ = duct hydraulic diameter (ft)

$\rho$ = air density (lb/ft$^3$)

$A$ = core cross sectional area (ft$^2$)

$S_f$ = solid fraction of core (%)

$\dot{m}$ = mass flow (lb/sec)

The experimental curves in Figure 4-16 shows the pressure drop and TSM discharge temperature as a function of time at a mass flow of 0.53 lb/sec.

## 4.4 BRAYTON RECUPERATION

### 4.4.1 Simulation Tests

The data presented above describes the performance of the TSM as a sensible heat storage device applicable to the collection of solar energy or process heat. The same device can also function as a periodic heat exchanger to recuperate a low pressure ratio Brayton engine but in this application a pair of TSM's are needed (See Figure 4-1). Test conditions differ depending upon whether the function is to add heat to the compressor air, TSM-1, or recover heat from the turbine exhaust, TSM-2. Unlike the thermal storage application evaluated above, the TSMs are switched before they have been completely discharged, i.e., the direction of air flow is reversed simultaneously before the thermocline has passed completely through the core. Consequently, the thermocline performance which represents the average condition takes many cycles to be established experimentally.

The initial test duplicated as nearly as possible with one TSM the varying conditions which accompany a 15 min. switching cycle. (Computer simulations of TSM performance established the 15 min. switching time for the 31" long core.) Experimental thermocline performance was obtained by changing test conditions every 15 minutes keeping mass flow constant but reversing the direction of flow and test conditions as shown:

A. ambient pressure, 1295°F air flow downward

and, B. 30 psig, 295°F air flow upward.

Every effort was made to minimize the transient flow during the switching time. However, the pressurization and depressurization of the test chambers and the need to bypass some air flow during the hot valve switching process produced inevitable transients.

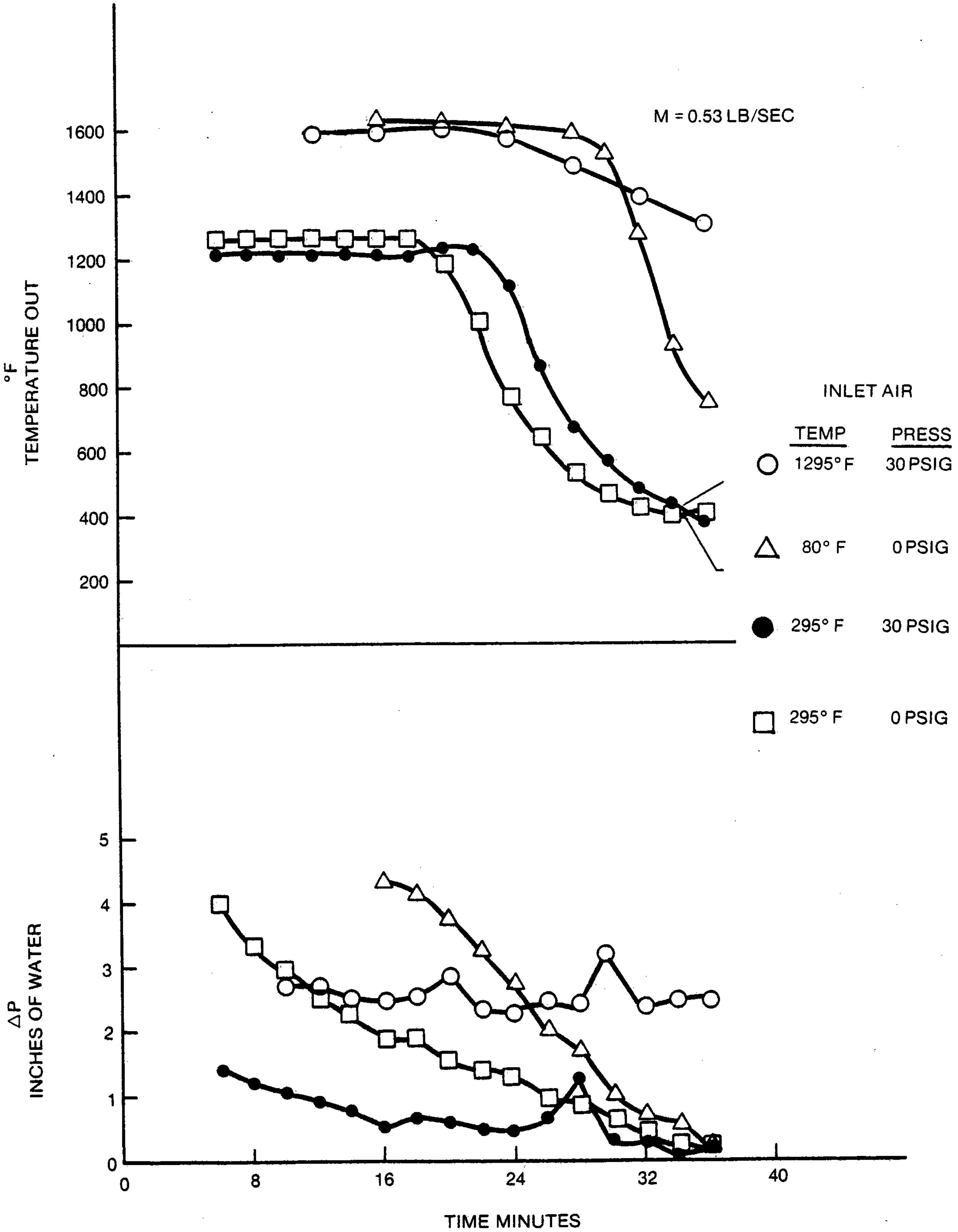


Figure 4-16. Measured Pressure Drop and Output Temperature vs Time

Two series of switching cycles were measured, the first covered 3 sequences of A and B above, the other 5 sequences. The temperature variations with time of the top, middle and bottom planes of the ceramic core are shown in Figure 4-17. Switching points for the hot valve represent starting points for a new cycle and signify a reversal in the direction of air flow through the TSM. Of importance to the efficiency of the Brayton cycle is the average temperature of the exhaust air during the A condition or exhaust. In the first, cycle, the exhaust air temperature never rises above 295$^{O}$F. As the number of sequences increases there is a rise in exhaust temperature near the end of the 15 minute cycle indicating a decrease in effectiveness and cycle efficiency. After a few cycles equilibrium is established and the data can be used to determine the effectiveness.

Experimental data from the fourth cycle of Figure 4-17, compared with the theory of Figure 2-8, is shown in Figure 4-18. The top curve is a comparison of the compressor exhaust air with time during the 14.2 minute switching interval as it leaves the TSM. Note that the drop in temperature near the switching point is from 1295$^{O}$F to 1170$^{O}$F, whereas the computed final temperature is 1090$^{O}$F. Similarly, the turbine exhaust air rises to 435$^{O}$F experimentally whereas the computed temperature is 600$^{O}$F. These differences account for an improvement in effectiveness from 90% to 93%.

Temperature and pressure drop data covering the same sequence of switching cycles are shown in Figures 4-19 and 4-20 respectively. The pressure drop across the core is 1.1 inches of water and 0.4 inches of water for cycles A and B respectively. Corresponding pressure drops from elbow to elbow which includes the diffuser and 12 inches of ducting outside the TSM tank was 5.0 inches of water and 1.1 inches of water for cycles A and B respectively.

The second series of tests was performed without pressurizing the low temperature cycle (condition B) and thereby reducing the switching transient effects. Since pressure was observed to have a negligible effect on the thermocline shape and velocity, this modification in test procedure should provide a more precise measure of effectiveness. A series of tests covering three different switching times were run until the thermocline shapes stabilized at each switching time series.

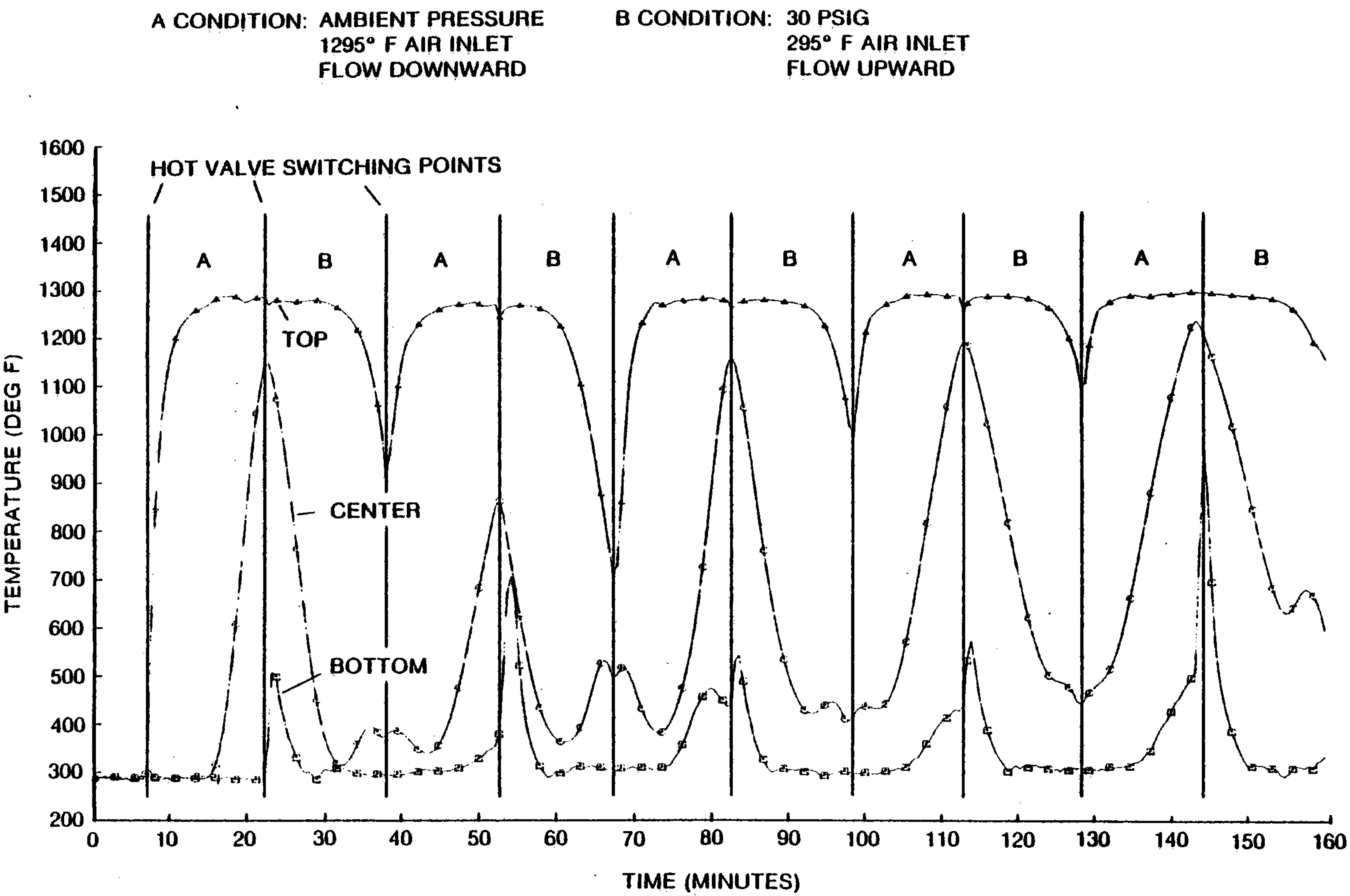


07230-12

A-05270-7

Figure 4-17. Brayton Engine Recuperation Cycle - Measured Core Temperatures

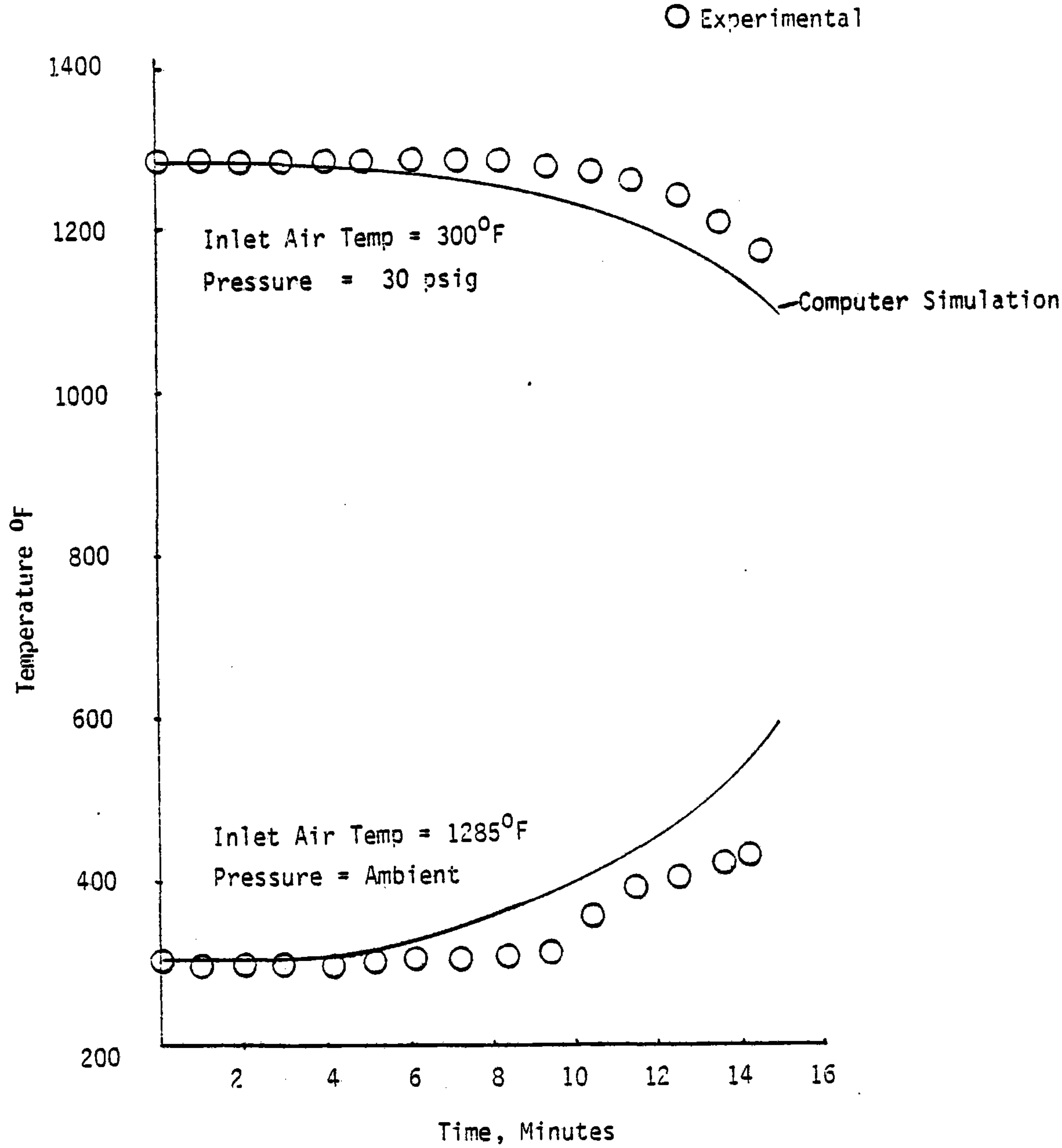


Figure 4-18. Comparison of Computed with Experimental Air Duct Temperatures for Both Recuperator TSM

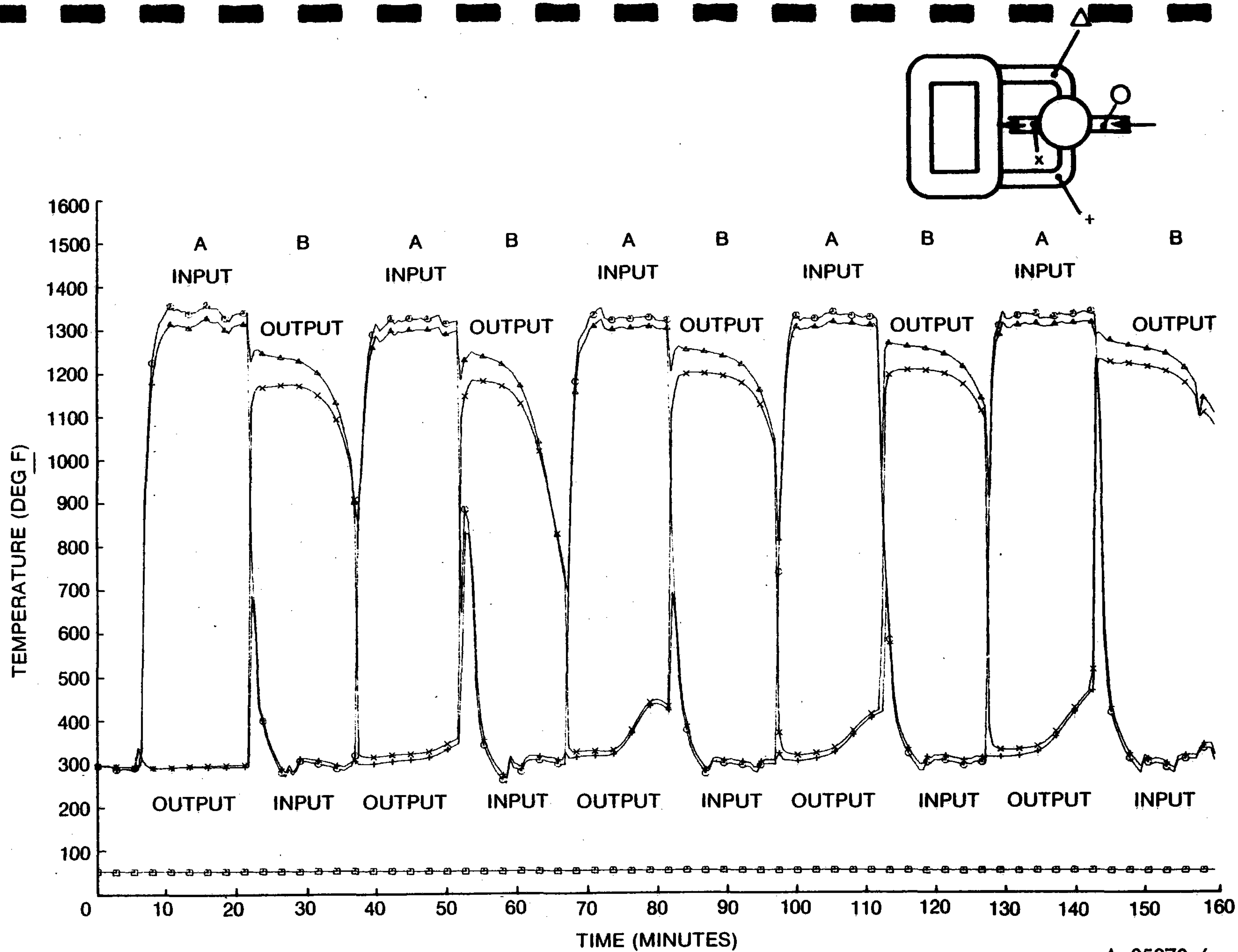


Figure 4-19. Brayton Engine Recuperation Cycle - Measured Ducting Temperatures

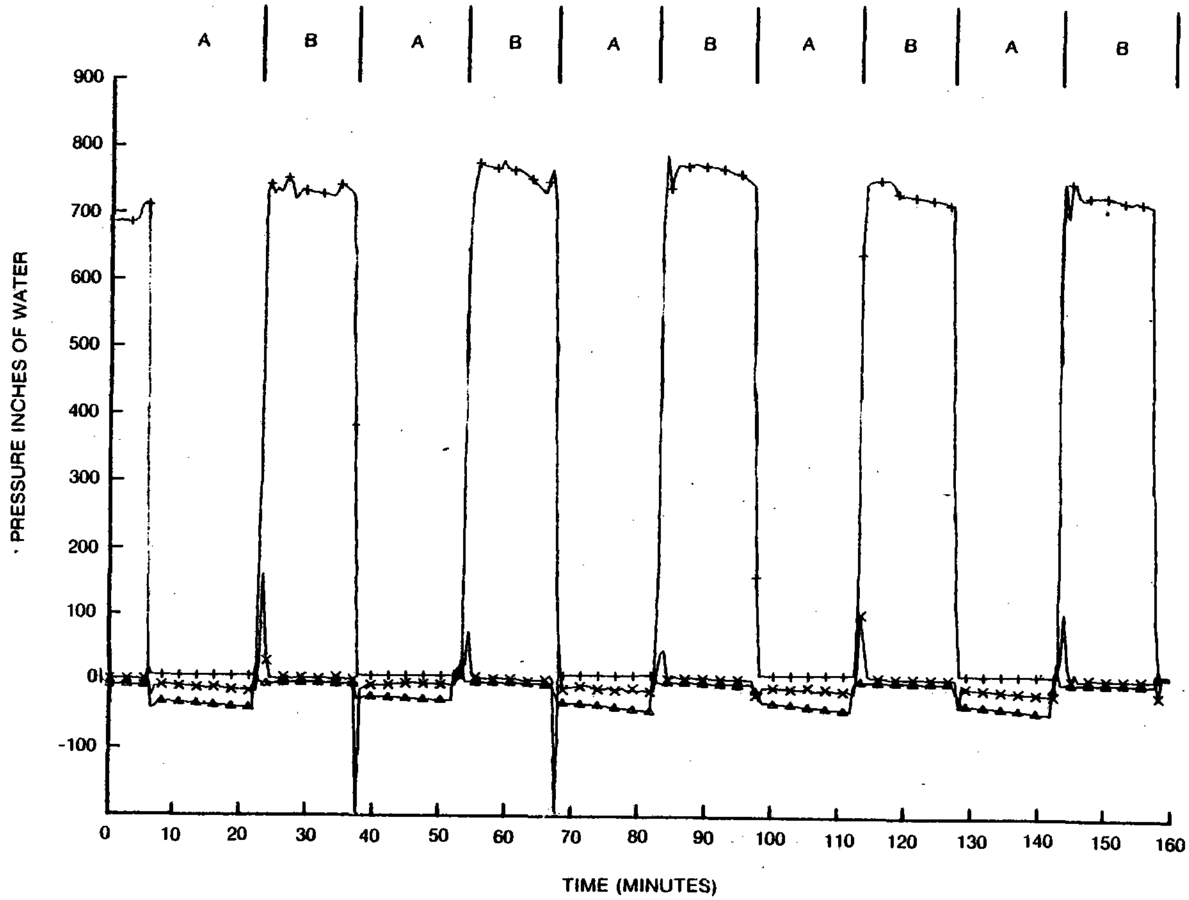


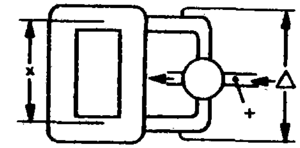


AVERAGE VALUES OF PRESSURE DROP, " $H_2O$

| CONDITION | Δ | x |
|---|---|---|
| A | 12.7 | 4.6 |
| B | 2.6 | 1.0 |

Figure 4-20. Brayton Engine Recuperation Cycle - Measured Pressures

For the low switching time, 6 min., Figure 4-21, and the standard switching time, 15 minutes, Figure 4-22, stable operation was obtained in 7 cycles. For long switching time, 25 min, Figure 4-23, stable operation was reached after 3 cycles. The short switching time had the highest effectiveness, 0.97, which compares with 93% for 15 minutes and 80% for 25 minutes, Figure 4-24.

In order to evaluate the use of a pair of TSM's as a recuperator for a Brayton engine, the set of engine performance specifications, Table 4-2, was assumed. The measured pressure drop and effectiveness for a 15 minute switching cycle was included to obtain an overall engine thermal to mechanical efficiency of 40%, see Table 4-2.

## 4.5 THERMAL STORAGE ANALYSIS

### 4.5.1 Theory vs Experiment

Prior to this experimental program, Sanders Associates developed a theoretical heat transfer simulation program for the storage of sensible heat in a ceramic honeycomb matrix. In solving the simultaneous heat transfer equations, the physical properties of air, cordierite, and insulation shown in Figure 4-25 were employed to predict thermal gradients in the core as a function of time. Subsequent small scale experimental measurements supported the calculated thermocline profiles but showed a substantial wall effect. This experiment is larger in diameter and therefore wall effects are reduced substantially.

The air and core temperatures were calculated for the instrumented nodel points in the experimental program. A typical thermal gradient profile was developed from the theory and is compared with an experimentally developed profile in Figure 4-18. Note that the thermocline slopes are steeper than predicted by theory.

The model accurately predicted the timing of the thermocline motion through the center of the core but greatly underestimated the sharpness of the thermocline, i.e., the measured thermocline width was 8 minutes compared with 17.5 minutes predicted by the model. The significance of this difference in slope is to improve the effectiveness of the core when applied as a Brayton engine recuperator was 93%. The model predicted 90% for the same 15 minute switching cycle.

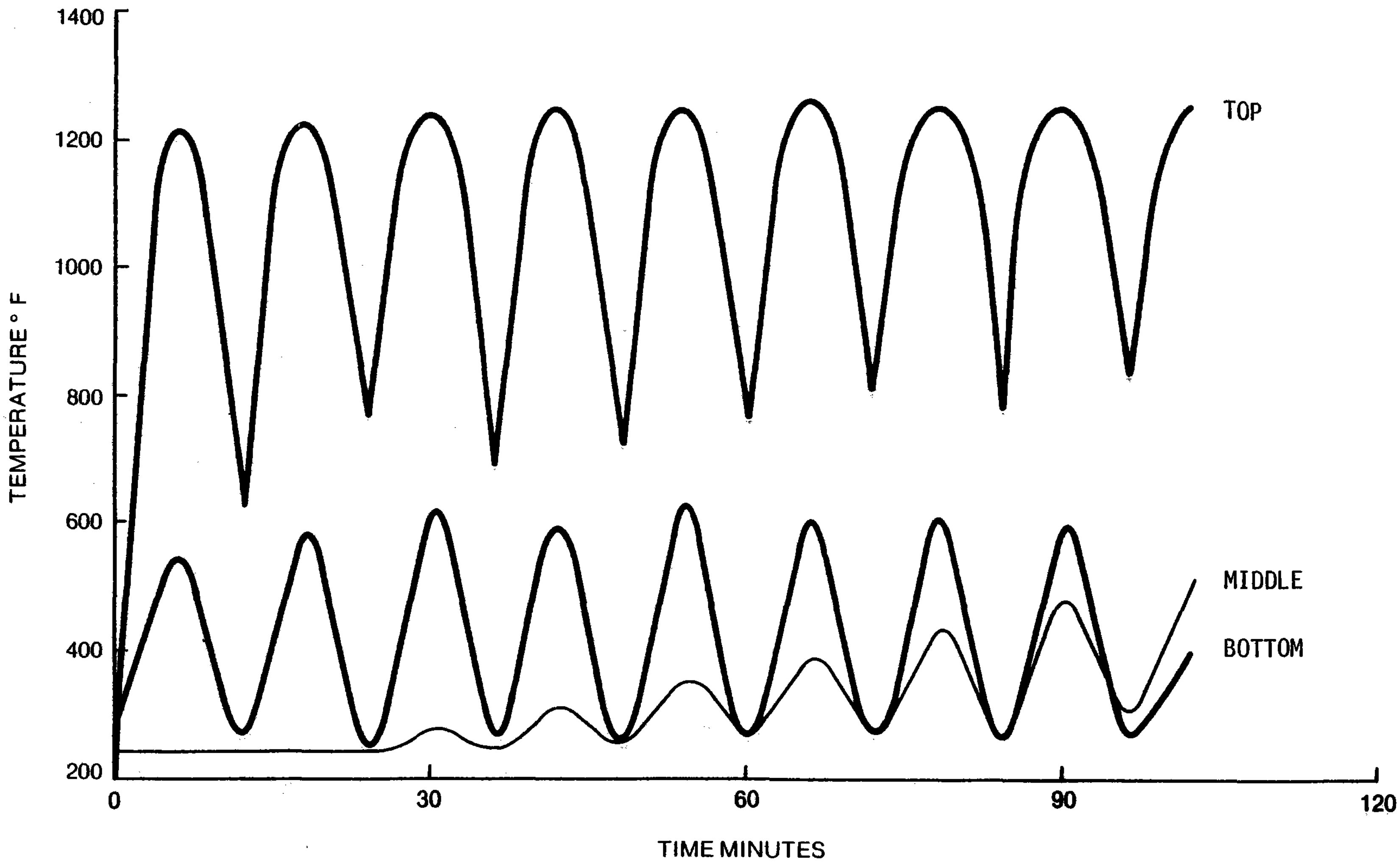


Figure 4-21. Brayton Engine Recuperation, 6 Minute Switching Cycle
0.43 lb/sec (Experimental Data)

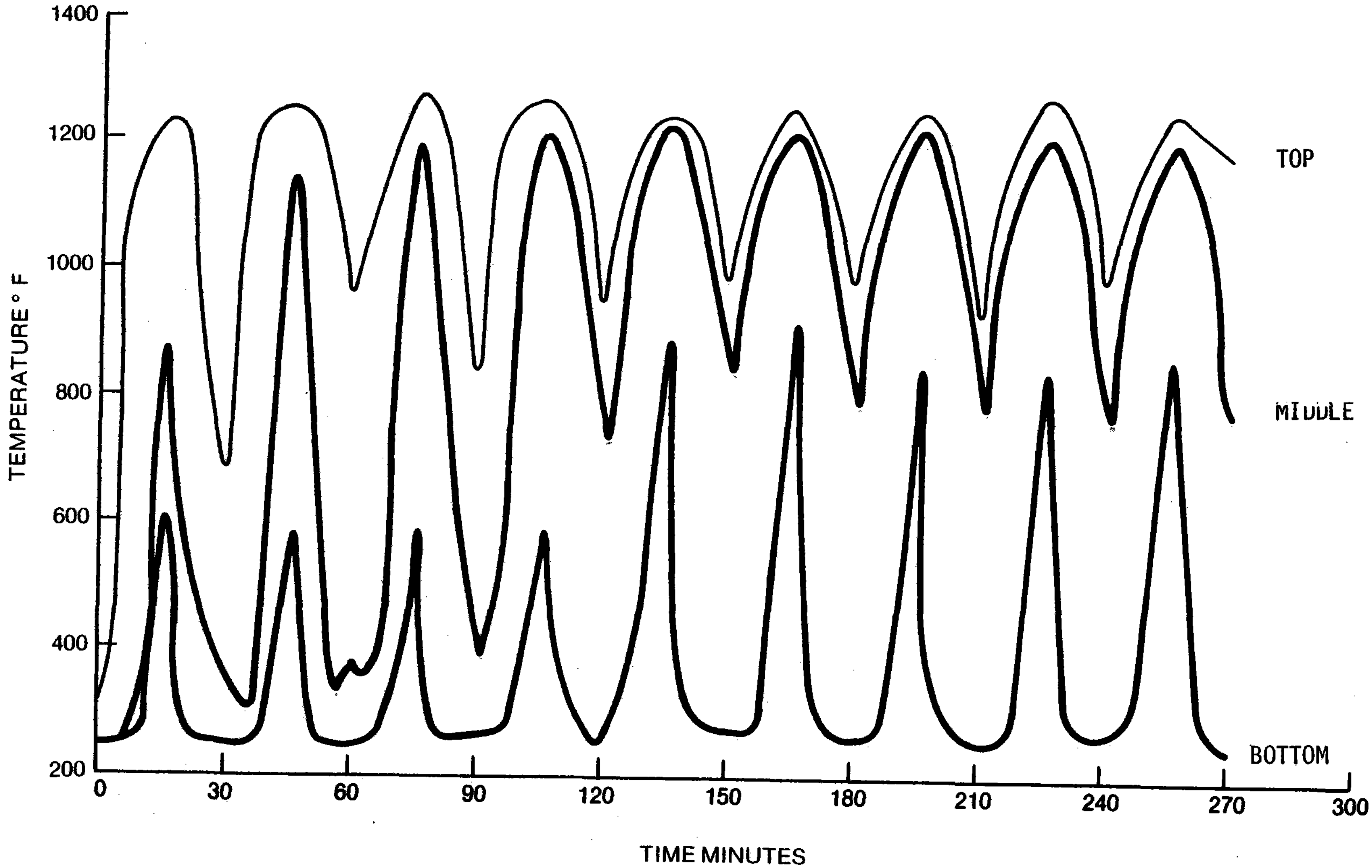


Figure 4-22. Brayton Engine Recuperation. Run 54, Core Temperature, 15 Min. Switching Cycle 0.43 lb/sec. (Experimental Data)

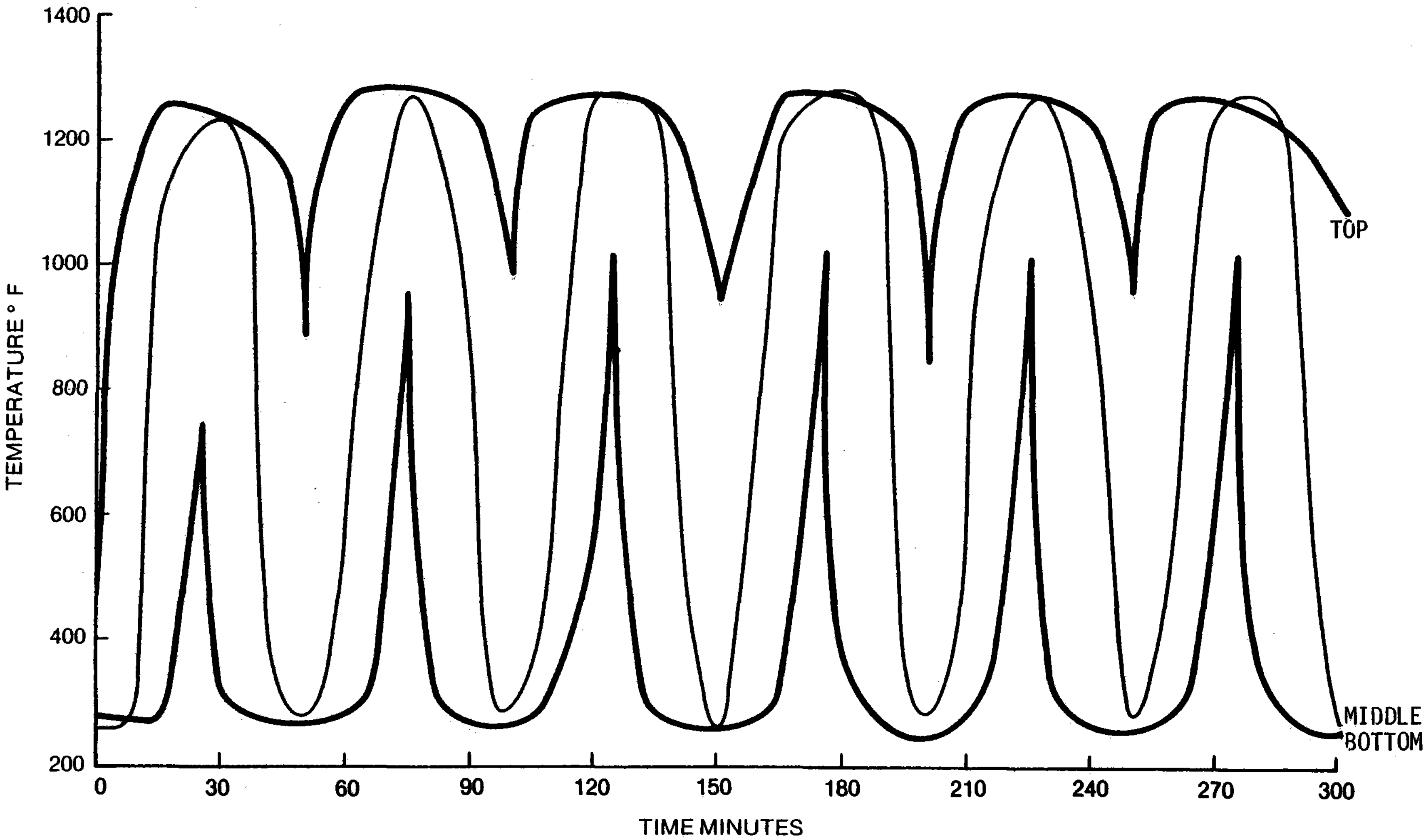


Figure 4-23. Measured Core Temperature, 25 Min. Switching Cycle

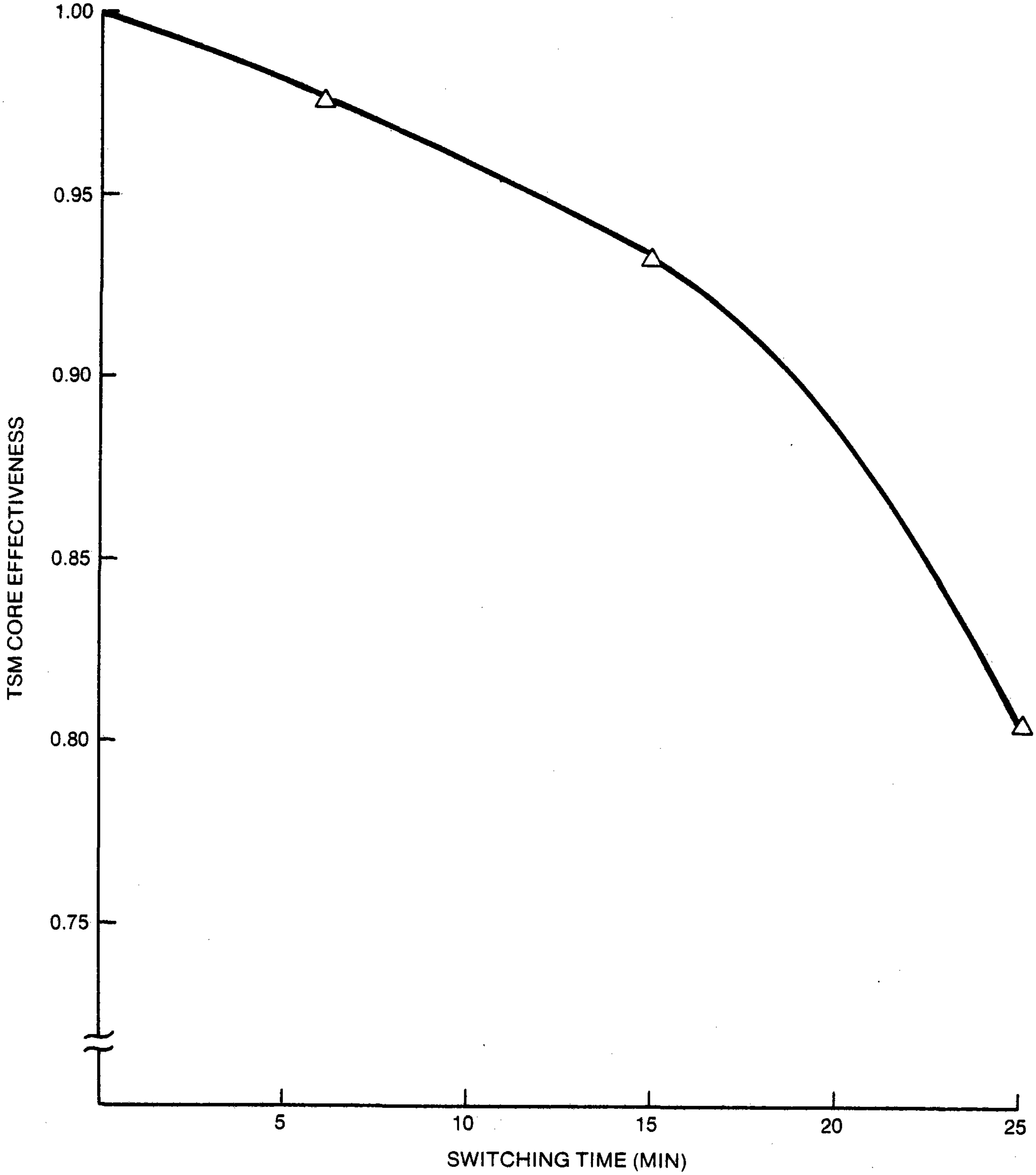


Figure 4-24. Measurements of TSM Core Effectivness vs Switching Time

TABLE 4-2

BRAYTON ENGINE PERFORMANCE SPECIFICATIONS

| | |
|---|---|
| Compressor Inlet Temperature | $50^{o}F$ |
| Turbine Inlet Temperature | $1700^{o}F$ |
| Compressor Pressure Ratio | 2.92 |
| Mass Flow Rate | 0.423 (lb/sec) |
| Compressor Adiabatic Efficiency | 0.80 |
| Turbine Adiabatic Efficiency | 0.85 |
| Enthalpy Rise Between Compressor Output and Turbine Inlet | 374.3 BTU/lbs |

BRAYTON ENGINE PERFORMANCE ESTIMATES

| Performance | Initial Estimate | Revised Estimate |
|---|---|---|
| $\sum\Delta P/P$ | .0315 | .0315 |
| Turbine Exhaust (BTU/lb) | 254.8 | 254.8 |
| Recuperator Loss (BTU/lb) Exh. + Cond. + Vent | 24.25 | 16.3 |
| Effectiveness | 0.904 | 0.93 |
| Total Heat Loss (BTU/lb) | 35.95 | 28 |
| Compression Loss (BTU/lb) | 0.64 | 0.64 |
| Compressor Work (BTU/lb) | 54.53 | 54.53 |
| Turbine Work (BTU/lb) | 115.74 | 115.74 |
| Heat Addition (BTU/lb) | 155.45 | 147.5 |
| Cycle Thermal Efficiency | .390 | .41 |

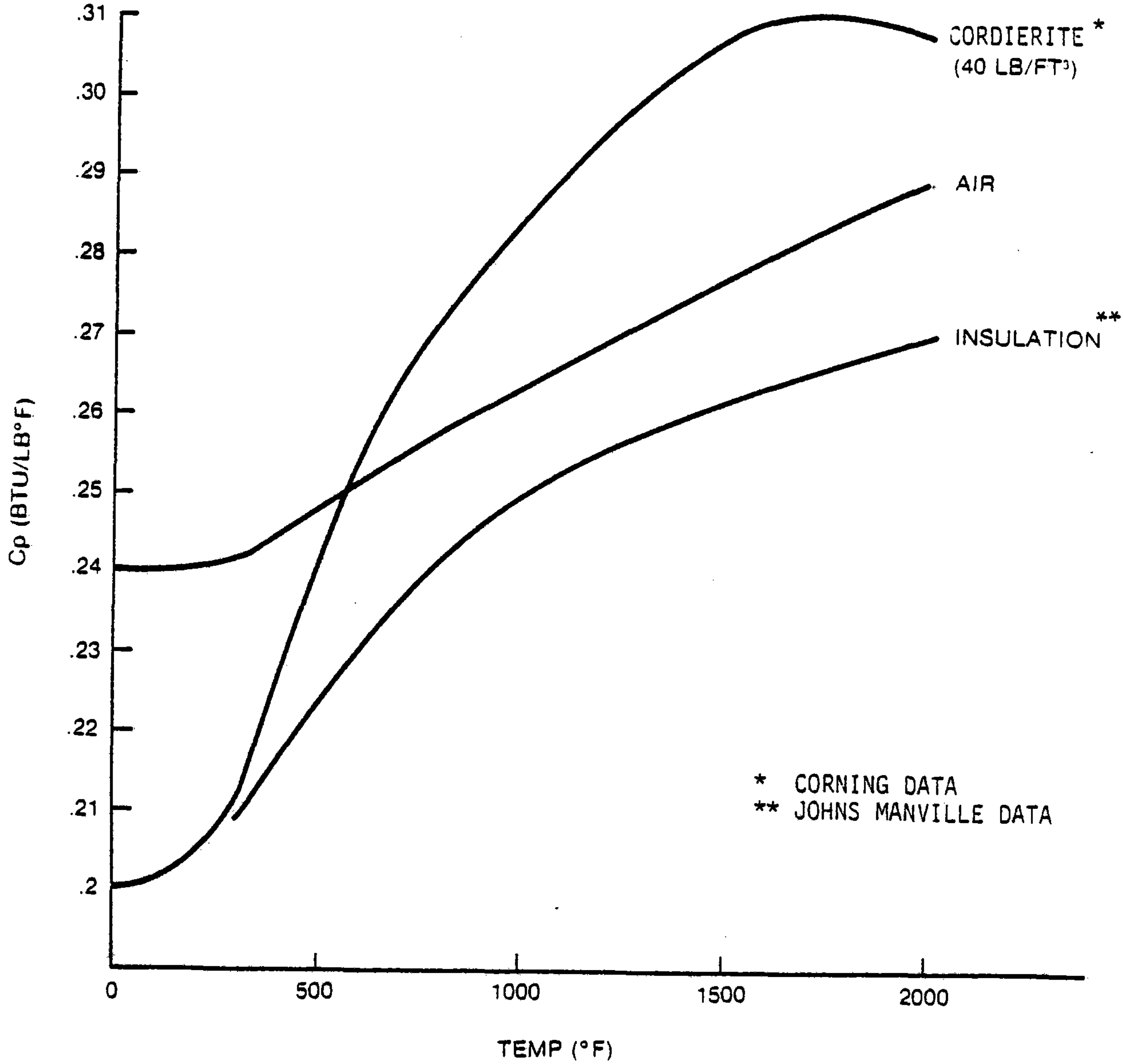


07230-7

FIGURE 4-25

## VARIATION OF $C_p$ WITH TEMPERATURE FOR TSM CONSTRUCTION MATERIALS

### 4.5.2 Generalized Performance

A simplified approach to understanding the performance of a thermal storage module is to ignore the effect of insulation. Then using the First Law Analysis:

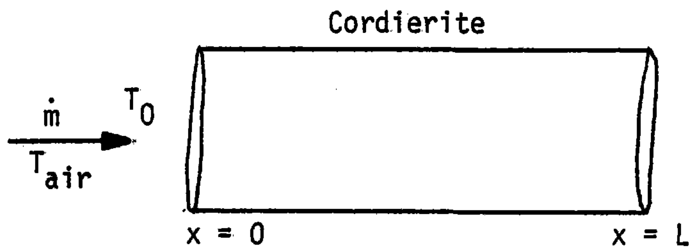


$T(x,t)$ = Temperature of Air
$\theta(x,t)$ = Temperature of Cordierite
$\dot{m}$ = Mass Flow
$T_0$ = Inlet Air Temperature

specifying boundary conditions for air and cordierite such that:

$$T(0,t) = T_0 = \theta(L,\ t_2) \text{ and } T(L,t_2) = \theta(L,0) = T_1$$

assuming all of the energy carried in the stream is absorbed in the cordierite.

$$mc_{p_a}(T_0 - T_1)t_2 = Wc_{p_c}(T_1 - T_0) \qquad \text{Eq. 4-1}$$

where $t_2$ = The time for the wall temperature at L to rise from $T_1$ to $T_0$ .
This would occur only if a normal (infinite slope) thermocline passed through the TSM and thus no energy was exhausted above the datum temperature of $T_1$.

In the actual case, the thermocline has a finite slope which varies with time and thus results in an exhaust stream enthalpy which is not ideally transferred to the cordierite. A finite slope of the thermocline indicates a finite time necessary for the heat transfer between the fluid and the cordierite to take place, an infinite slope, that which is assumed in Eq. 4-1 represents the ideal case of an infinite heat transfer rate.

In the actual case, the energy balance must be restated:

$$mc_{p_a}(T_0 - T_1)t_2 - m\int_{t_1}^{t_2}\left[\int_{T(L_1t_1)}^{T(L_1t_2)} c_{p_a} \qquad dt\right]dt$$

$$= Wc_{p_c}(T_1 - T_0) \qquad \text{Eq. 4-2}$$

The first term represents the influx energy necessary to raise the cordierite temperature to an equilibrium temperature of $T_0$, and $t_2$ is the time in which to do so.

The second term is the enthalpy of the stream which is exhausted (thus not transferred to the cordierite) in the interval defined by the time at which the cordierite temperature at $x = L$ (the last thermocline) begins to rise from its datum temperature ($T_1$) to its final equilibrium temperature of $T_0$. This interval has been illustrated in Figure 4-26 as $t_2 - t_1$.

The time interval, $\Delta t = t_2 - t_1$, has been the subject of experimental analysis. For the purposes of this analysis, the relation $T = f(t)$ will be assumed linear over this interval $\Delta t$.

A linear temperature history such that:

$$T(L,t) = T_1 + (T_0 - T_1)\left(\frac{t}{\Delta t} - t_1\right) \qquad t_1 < t < t_2 \qquad \text{Eq. 4-3}$$

will be assumed as an approximation.

Evaluating the integral equation in Equation 4-2 yields the following simplified result.

$$\dot{m}c_{p_a}\,(T_0 - T_1)t_2 - \dot{m}c_{p_a}(T_0 - T_1)\frac{\Delta t}{2} \cong Wc_p\,(T_1 - T_0)$$

or simply:

$$mc_{p_a}\left(t_2 - \frac{\Delta T}{2}\right) \cong Wc_{p_c} \qquad \text{Eq. 4-4}$$

This relation has been shown in Figure 4-27 to correlate well with experimental data for various temperature ranges. In order to account for the variation of specific heat ($c_p$) with temperature, the actual equation plotted was:

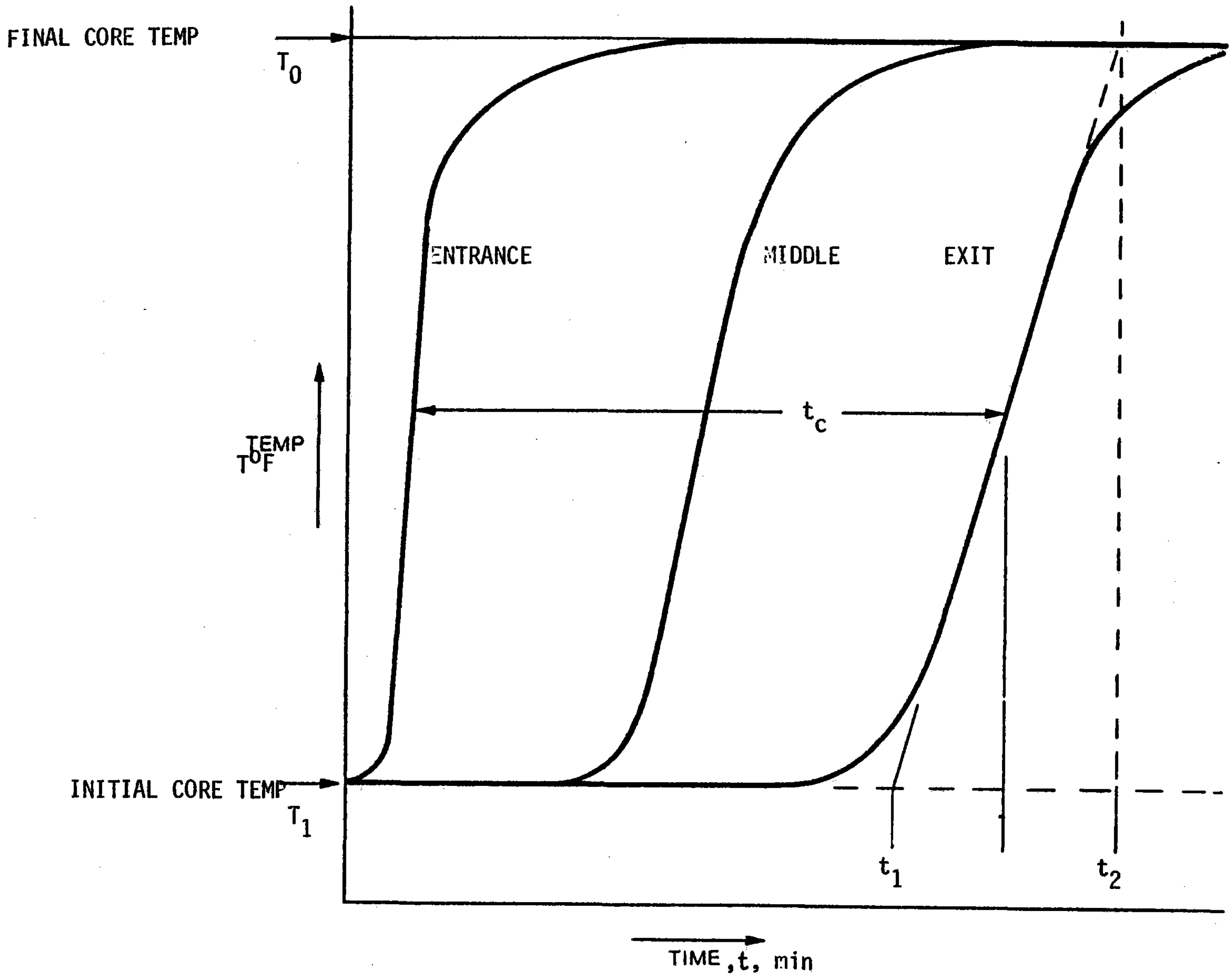


$t_c$ - TIME FOR THERMOCOUPLE TO PASS THROUGH

FIGURE 4-26
NOMENCLATURE - THERMOCLINE ANALYSIS

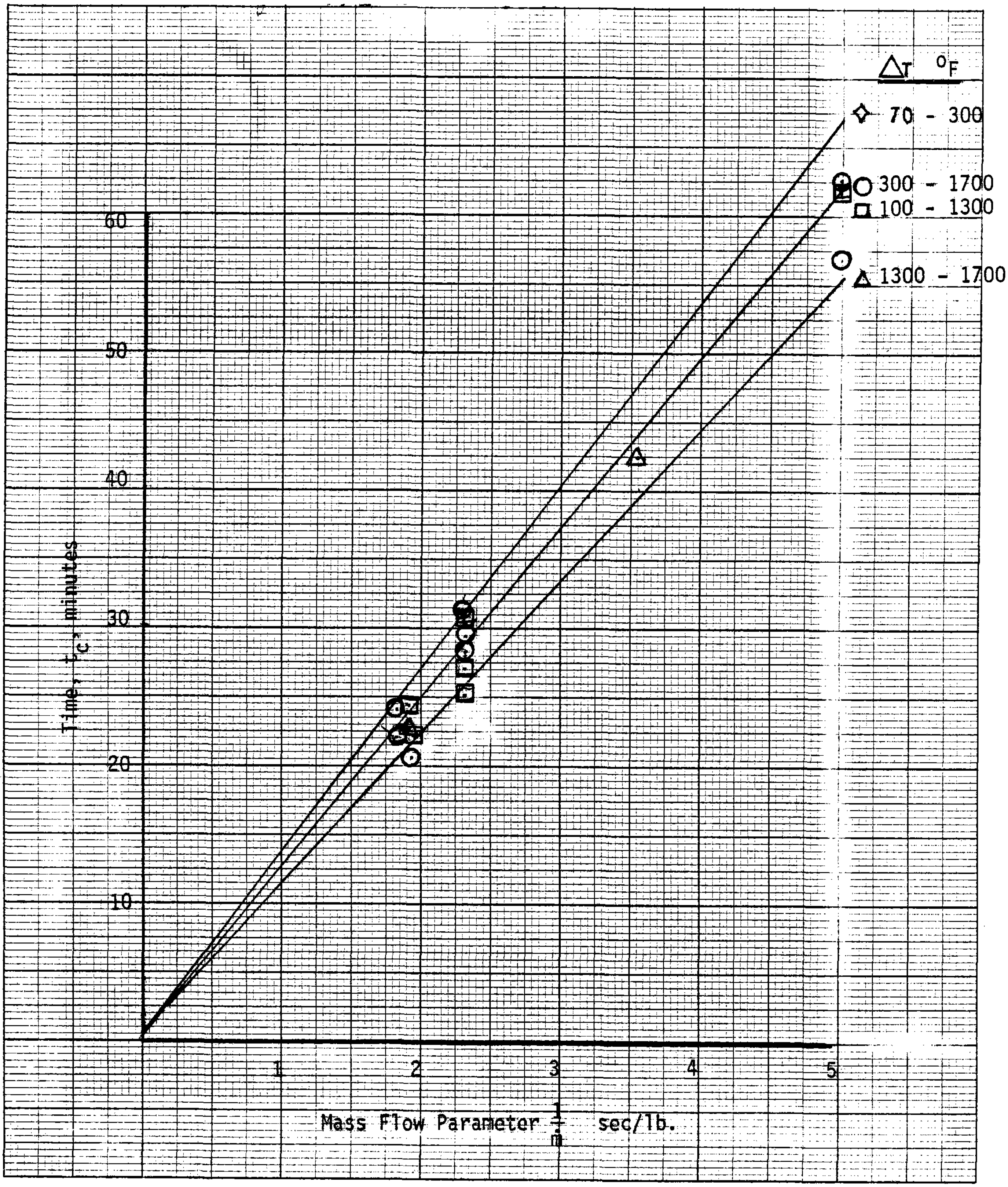


FIGURE 4-27

COMPARISON OF EXPERIMENTAL WITH THEORETICAL TIMES FOR THERMOCLINE TO PASS THROUGH CORDIERITE CORE

$$(t_2 - \frac{\Delta t}{2}) = \frac{W}{\dot{m}} \frac{\int_{T_o}^{T_1} c_{p_c} dt}{\int_{T_0}^{T_1} c_{p_a} dt} \cong t_c \qquad \text{Eq. 4.5}$$

where the integrals were evaluated graphically using the physical properties of the materials presented in Figure 4-25.

The thermocline profiles shown in Figure 4-2 to 4-12 all show a general trend towards decreasing slope, with time. Measured values of slope vs time, Figure 4-28a, b, c, compare this trend for several different runs at a mass flow of 0.43, 0.53, and and 0.2 lb/sec respectively. Note that even though the initial slope varies considerably due to experimental difficulties in setting up its initial test conditions, the change in slope with time seems predictable and not significantly influenced by either the pressure level or the temperatures over the range of variables investigated. There is a trend for the slope to be greater when the core temperatures are decreasing compared with increasing temperatures (Figure 28a). Small values of $\Delta T$ tend to develop low values of thermocline slopes (Figure 28b). Attempts have been made to correlate slopes of experimental data, but the variability of the initial conditions from run to run could not be adequately evaluated. Further experiments are needed to understand the factors which determine the slope of the thermoclines as temperatures, mass flow, and $\Delta T$ are varied.

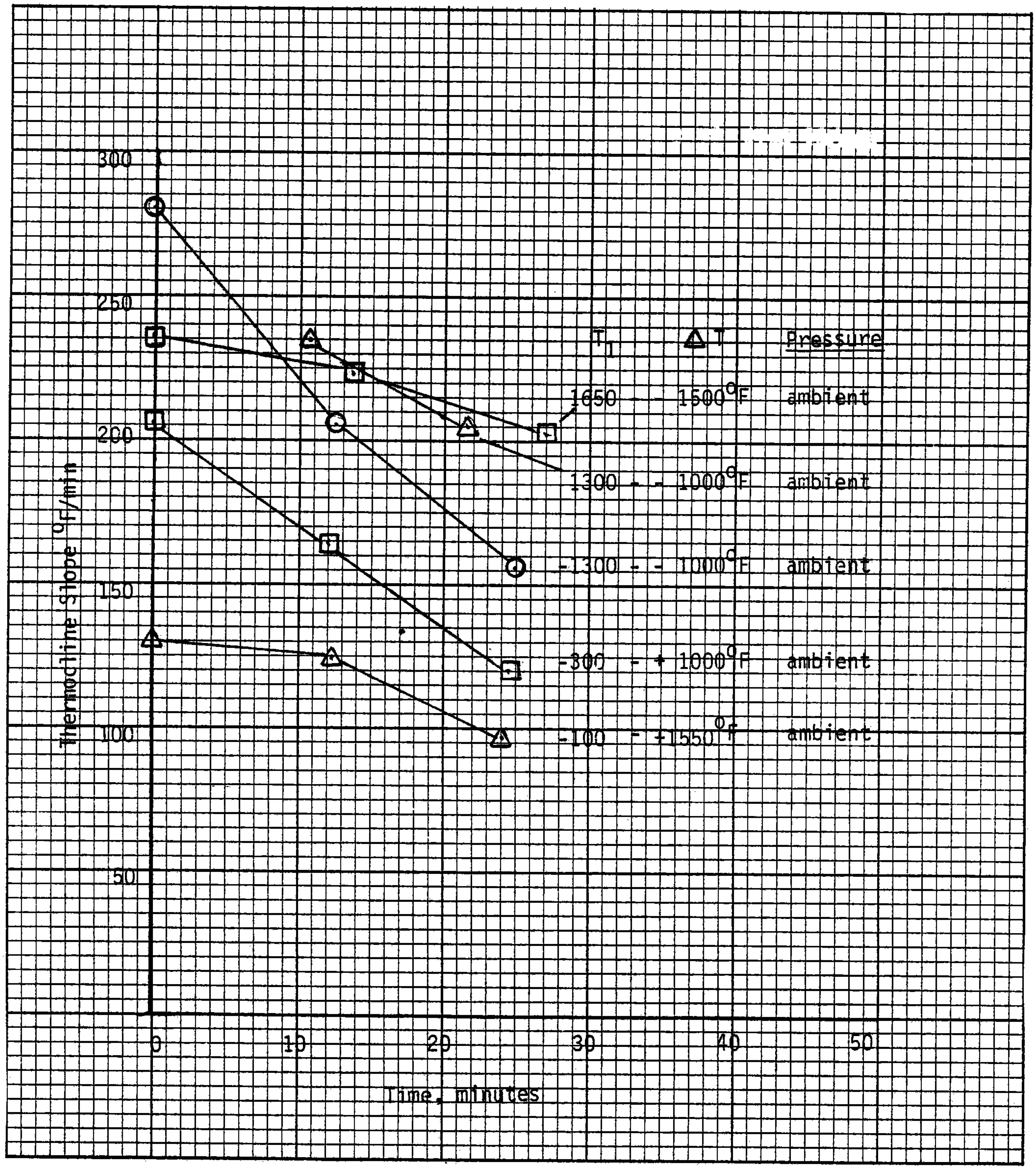


FIGURE 4-28a

EXPERIMENTAL MEASUREMENTS OF THERMOCLINE SLOPES, m = 0.43 lb/sec

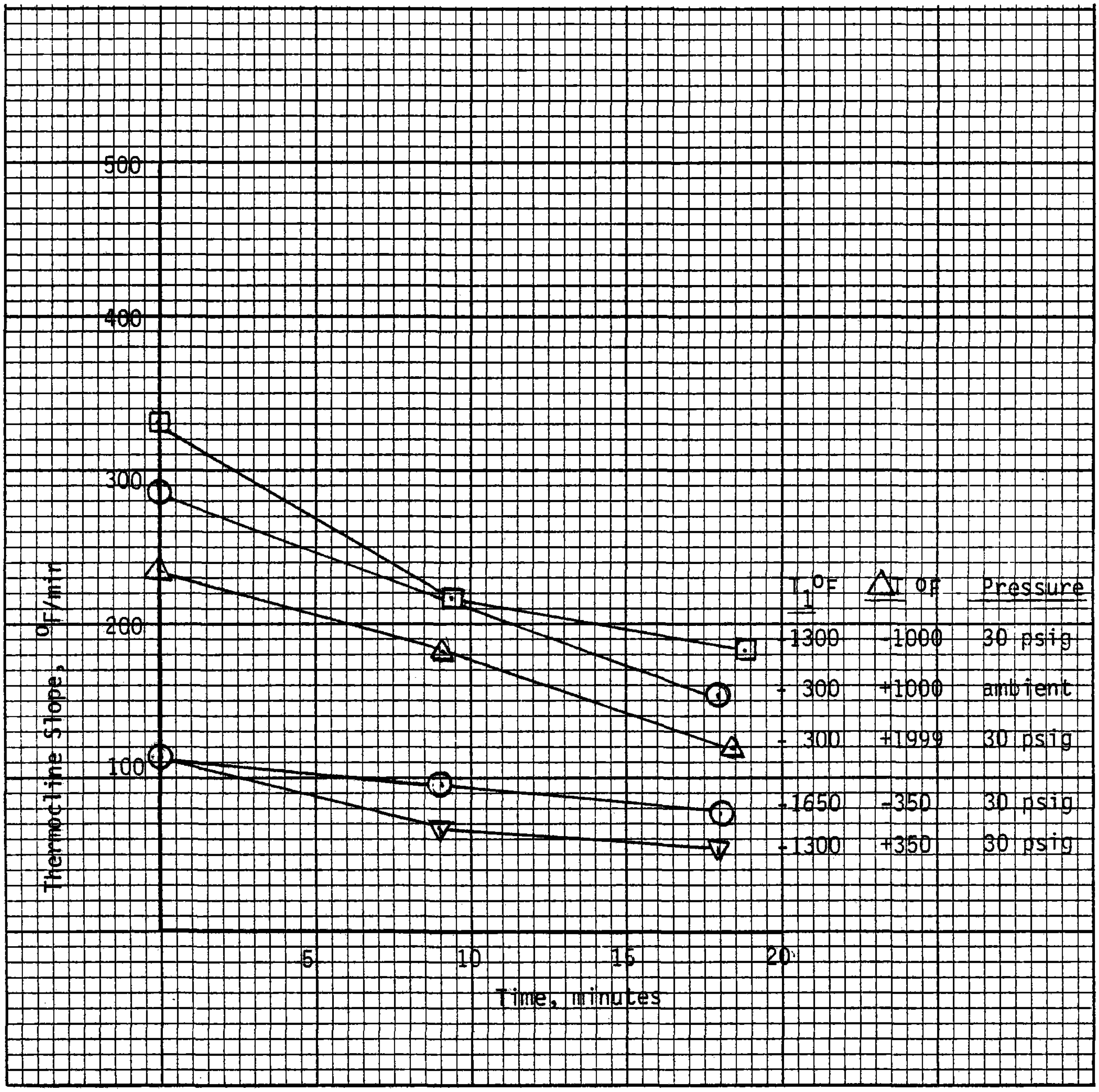


FIGURE 4-28b

EXPERIMENTAL MEASUREMENTS OF THERMOCLINE SLOPES, m = 0.53 lb/sec

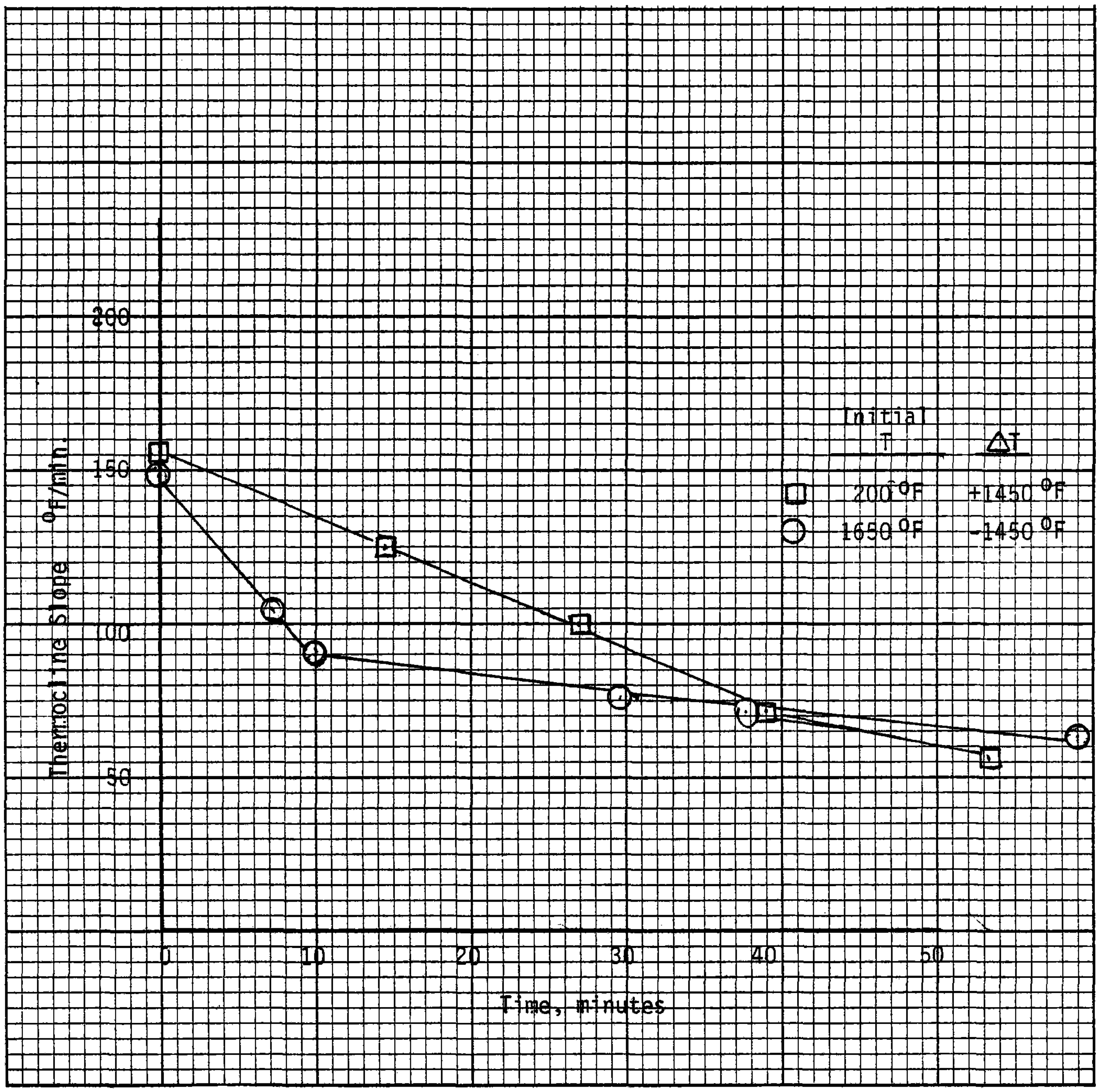


FIGURE 4-28c

EXPERIMENTAL MEASUREMENTS OF THERMOCLINE SLOPS, m = .2 lb/sec,

## SECTION 5
## SUMMARY, RECOMMENDATIONS AND CONCLUSIONS

### 5.1 SUMMARY

The first full scale measurements of thermocline in the Sanders ceramic honeycomb sensible heat storage module were made in a unit designed to operate with a 20 KWe Brayton power plant. The measurements were made by passing temperature controlled air through 730 lb of porous cordierite 36" dia. x 31" long. Air flow conditions were varied to cover all aspects of the Brayton power cycle as follows:

| | | |
|---|---|---|
| Air Temperature | - | Ambient to $1700^{o}F$ |
| Air Pressure | - | Ambient to 3 atmospheres |
| Air Flow | - | 0.2 to 0.5 lb/sec |

Thermoclines which developed in the ceramic were sharper than had been predicted by the computer model. The low pressure drop $\frac{\Delta P}{P} < 2\%$ and high effectiveness (93%) indicates that the low pressure ratio Brayton engine with a pair of thermal storage modules used as a recuperator should have a thermal to mechanical conversion efficiency of 40% or greater.

An analysis of the experimental performance data indicates that the thermocline slopes were influenced by the initial temperature profiles which were difficult to replicate from run to run. By discounting the initial slope, the time to fill or empty the core was predictable from the material physical properties evaluated at prevailing temperatures.

As part of the experimental program a new four-way valve for use in switching the storage modules was designed, built and tested at temperatures of $1700^{o}F$.

## 5.2 CONCLUSIONS

The Sanders high temperature thermal storage module has wide application for reliable, efficient, low pressure drop gaseous heat transfer for temperatures as high as 1700$^{o}$F. Design criteria are available to scale the TSMs to meet solar and industrial thermal storage application. As a recuperator for a Brayton engine, the TSM has an effectiveness of 93% and makes thermal to mechanical conversion efficiencies in excess of 40% feasible and practical.

## 5.3 RECOMMENDATIONS

Additional work is recommended to resolve issues regarding off design performance and valve cycling. The recommended program includes the following tasks:

- Parked Thermocline Experiments

  Propagate a sharp thermocline to the center of the ceramic core. Shut off all air flow and monitor the diffusion of the thermocline. Repeat the experiment for three different temperatures, 900$^{o}$F, 1300$^{o}$F, 1700$^{o}$F, to determine the role of radiation in the thermocline diffusion.

- High Mass Flow Tests

  Rerun the thermocline propagation tests with very high mass flows, 2 to 3 times the design mass flow, to determine the flow rate at which the thermocline performance begins to degrade.

- Valve Cycling Tests

  Operate the high temperature valve in a cycling mode at 1300$^{o}$F and at 1700$^{o}$F. Determine the number of cycles (1/4 turn) which the valve can sustain without damage. The cycling experiment will be configured to soak the valve at the test temperature and pressure and to rotate the valve 1/4 turn every 5 minutes. At the end of the test, or at failure, disassemble the valve and inspect for dimensional stability, cracking and galling.

- Update TSM Design

  Based on the results of Items 2 to 5, update the TSM design and estimate its effectiveness as a recuperator and the performance of a 20 KWe fossil fired recuperated Brayton system.

- Update TSM Model

  Update the mathematical model describing the thermocline propagation. Include the effects observed during testing. Include radiation effects if these are determined to be significant.

This program has demonstrated unique potential for using TSM's in solar Brayton systems. The additional tasks recommended above will resolve the few remaining questions. The next step is to demonstrate a fully integrated system.